View metadata, citation and similar papers at core.ac.uk
brought to you by CORE
provided by Universidade do Minho: RepositoriUM

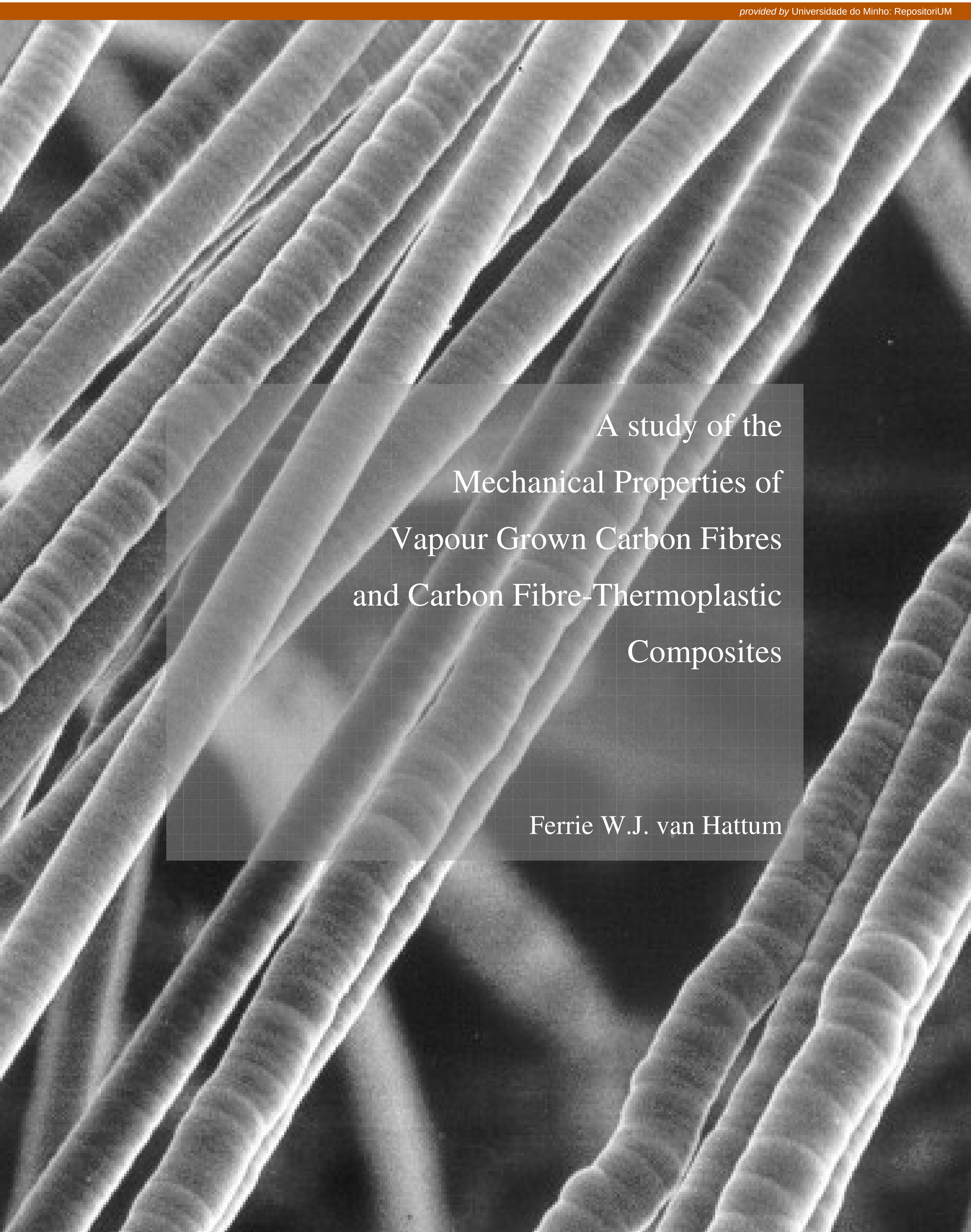

# A study of the Mechanical Properties of Vapour Grown Carbon Fibres and Carbon Fibre-Thermoplastic Composites

Ferrie W.J. van Hattum

Ferrie Wander Joseph van Hattum

# A STUDY OF THE MECHANICAL PROPERTIES OF VAPOUR GROWN CARBON FIBRES AND CARBON FIBRE-THERMOPLASTIC COMPOSITES

Tese submetida à Universidade do Minho para a obtenção do Grau de Doutor em Ciência e Engenharia de Polímeros

**Universidade do Minho**

**1999**

**Cover.** Scanning electron micrograph of vapour grwon carbon fibres, grown on a substrate (with acknowlegements to Prof. Figueiredo, University of Porto).

# PREFACE

The thesis lying before you, is the result of an interesting mixture of Portuguese and Dutch elements, both in a cultural as well as in a scientific way. Being Dutch, living and working in Portugal, gave me the opportunity to benefit from a wide range of different viewpoints and new experiences. This inspired me to conduct my research in a way that combined the best of both cultures, in a perhaps somewhat uncommon way. I am convinced that this work reflects the true spirit of the ancient Chinese proverb:

团结就是力量

*-It is not the separate spices, but the right mixture that makes the taste-*

# ABSTRACT

Vapour Grown Carbon Fibres (VGCFs) combine potentially low production costs with encouraging mechanical, thermal and electrical properties. This makes them of specific interest for applications where ex-pitch- and ex-polyacrylonitrile (PAN) carbon fibres (designated by ‘conventional’ fibres) are too expensive, and glass fibres cannot provide the required properties.

A research was carried out with three goals. First, to study systematically the different morphologies in which VGCFs can be produced and to evaluate their effect on the mechanical properties. Second, to develop know-how on the production of thermoplastic-VGCF composites. The determination of the mechanical properties of the composites allows the assessment of VGCFs as reinforcements of thermoplastics. Finally, to develop micromechanical models to predict the more relevant mechanical properties of the materials produced. By using these models inversely, it is possible to derive the properties of the fibres. In the case of VGCFs with diameters below 1 μm (submicron VGCFs) this is the only way to determine these properties.

The different morphologies in which VGCFs can be grown were studied systematically and the effect of the shape on the mechanical properties of the fibres evaluated. It was concluded that the shape of the VGCFs has a small influence on the value of the tensile modulus. However, fibres with shapes different from perfect cylinders, have a lower tensile strength. Overall, both the tensile modulus and strength were significantly lower than those of commercially available ex-pitch- or ex-PAN carbon fibres. Furthermore, it was shown that the fragmentation method cannot be used to assess the quality of the interface of these fibres in polymeric matrix composites, irrespective of the morphology. This is due to the failure mode, which is inherent to the inner structure of the VGCFs.

The production and processing of submicron VGCF-reinforced thermoplastic composites was done with commercial technologies, without major difficulties, provided the appropriate equipment was used. To evaluate the performance of the fibres, the properties of the composites were determined and compared to those reinforced with conventional ones. It was found that VGCF-composites can be produced with comparable strength and coefficient of thermal expansion (CTE) but with lower stiffness.

Micromechanical models available in the literature and a newly developed model were used to predict stiffness, CTE and strength of short fibre reinforced composites from the fibre and matrix properties. The models were validated experimentally and then applied inversely to calculate the submicron VGCFs properties. It was concluded that VGCFs have an apparent CTE that is higher than that of ex-PAN carbon fibres and a lower stiffness. Although the fibre strength could not be calculated, as most of the fibres are well below the critical length, the inverse modelling methodology allows the determination of the interfacial shear strength. It was shown that the interfacial adhesion between VGCFs and the thermoplastic matrix is comparable to that of conventional carbon fibres. The differences in properties between VGCF- and ex-PAN carbon fibre composites, can be attributed to the differences in fibre properties. Furthermore, it was concluded that the apparent stiffness and CTE of submicron VGCFs are, at least, as good as those of glass fibres.

# RESUMO

As fibras de carbono produzidas na fase de vapor (VGCFs) combinam custos de produção potencialmente baixos com propriedades mecânicas, térmicas e eléctricas favoráveis. Isto torna-as de especial interesse para as aplicações onde as fibras de carbono, baseadas no pitch ou no poliacrilonitrilo (PAN) (designadas por fibras 'convencionais') são demasiado caras e as fibras de vidro não apresentam as propriedades necessárias.

O presente projecto de investigação visou três objectivos. Em primeiro lugar, estudar sistematicamente as diferentes morfologias em que as VGCFs podem ser produzidas e avaliar o seu efeito nas propriedades mecânicas. Em segundo lugar, obter conhecimentos sobre a produção de compósitos de VGCF e matriz termoplástica. A determinação das propriedades mecânicas dos compósitos permite avaliar o desempenho das VGCFs como reforço de termoplásticos. Finalmente, pretende-se desenvolver modelos micromecânicos para prever as propriedades mecânicas mais relevantes dos materiais produzidos. Usando estes modelos inversamente, é possível derivar as propriedades das fibras. No caso de VGCFs com diâmetros menores que 1 μm (VGCFs sub-micrométricas), é esta a unica maneira para determinar estas propriedades.

Estudaram-se sistemáticamente as diferentes morfologias em que as VGCFs podem ser produzidas e avaliou-se o efeito da forma sobre as propriedades mecânicas das fibras. Concluiu-se que a forma não influencia significativamente o valor do módulo à tracção. No entanto, as fibras com forma diferente de cilindros perfeitos têm uma resistência de ruptura à tracção mais baixa. Globalmente, o módulo e a resistência à tracção são significativamente mais baixos do que os das fibras de carbono, ex-pitch ou ex-PAN, comercialmente disponíveis. Mostrou-se também que o método da fragmentação não pode ser usado para avaliar a qualidade da interface destas fibras em compósitos de matriz polimérica, qualquer que seja a morfologia. Isto deve-se ao tipo de rotura, que é inerente à estrutura interna das VGCFs.

Produziam-se e processaram-se compósitos termoplásticos reforçados com VGCFs sub-micrométricas usando tecnologias commerciais, sem problemas significativos, sempre que se utilizou o equipamento apropriado. Para avaliar o desempenho das VGCFs, as propriedades dos compósitos foram determinadas e comparadas com as dos reforçados com fibras convencionais. Verificou-se que os compósitos de VGCFs podem ser produzidos com resistência à ruptura e coeficiente de expansão térmica (CTE) comparáveis, embora com rigidez mais baixa, do que as daqueles compósitos.

Usaram-se modelos micromecânicos disponíveis na literatura e um novo modelo para prever a rigidez, o CTE e a resistência à ruptura de compósitos reforçados com fibras curtas, a partir das propriedades da fibra e da matriz. Os modelos foram verificados experimentalmente e aplicados inversamente para calcular as propriedades das VGCFs sub-micrométricas. Concluiu-se que as VGCFs têm um CTE aparente mais alto do que o das fibras de carbono ex-PAN e rigidez mais baixa. Embora a resistência à ruptura das fibras não possa ser calculada, dado que o comprimento da maioria das fibras é inferior ao comprimento crítico, a metodologia de modelação inversa permite determinar a resistência ao corte interfacial. Mostra-se que a adesão interfacial entre as VGCFs e a matriz termoplástica é comparável à das fibras de carbono convencionais. As diferenças de propriedades entre os compósitos de VGCF e os reforçados com fibras de carbono ex-PAN, podem ser atribuídas à diferença de propriedades das fibras. Além disso, concluiu-se que a rigidez e o CTE aparentes das VGCFs sub-micrométricas são, pelo menos, tão boas como as das fibras de vidro.

# SAMENVATTING

Vapour Grown Carbon Fibres (VGCFs) combineren een potentieel lage kostprijs met veelbelovende mechanische, thermische en electrische eigenschappen. Dit maakt hen bijzonder geschikt voor toepassingen waar ex-pitch en ex-polyacrylonitriel (PAN) koolstofvezels (hier ‘conventionele’ vezels genoemd) te duur voor zijn en glasvezels de vereiste eigenschappen niet kunnen bieden.

Een onderzoek is uitgevoerd, gericht op drie doelen. Ten eerste het systematisch bestuderen van de verschillende morphologieën waarin VGCFs geproduceerd kunnen worden en hun invloed op de mechanische eigenschappen. Ten tweede het ontwikkelen van kennis op het gebied van de vervaardiging van VGCF-thermoplastische composieten. Door de mechanische eigenschappen van de composieten te bepalen, kan de de rol van VGCFs als versterking voor thermoplasten vastgesteld worden. Tenslotte het ontwikkelen van micromechanische modellen die de relevantere eigenschappen van de geproduceerde materialen kunnen voorspellen. Door deze modellen omgekeerd te gebruiken, kunnen de eigenschappen van de vezels afgeleid worden. Dit is de enige manier om deze eigenschappen te bepalen voor VGCFs met diameters kleiner dan 1 μm (submicron VGCFs).

De verschillende morphologieën waarin VGCFs geproduceerd kunnen worden, zijn systematisch bestudeerd en het effect van de vorm van de vezel op de mechanische eigenschappen is geëvalueerd. De vorm van de VGCFs blijkt weinig invloed te hebben op de hoogte van de trekstijfheid. Vezels met een andere dan een perfecte cylinder-vorm, hebben echter een lagere treksterkte. In het algemeen waren zowel de trekstijfheid als de treksterkte van de VGCFs significant lager dan die van commercieel beschikbare ex-pitch of ex-PAN koolstofvezels. Daarnaast is aangetoond dat de fragmentatie-test niet gebruikt kan worden om de kwaliteit van de interface van deze vezel in composieten met een polymeer-matrix te bepalen, ongeacht hun morphologie. Dit komt door hun bezwijkgedrag, dat inherent is aan de interne structuur van de VGCFs.

Submicron VGCF-versterkte thermoplastiche composieten zijn zonder noemenswaardige problemen geproduceerd en verwerkt met behulp van commerciele technologieën, onder voorwaarde dat de geschikte apparatuur gebruikt werd. Om de prestaties van de vezels te evalueren, zijn de eigenschappen van de composieten bestudeerd en vergeleken met die van composieten versterkt met conventionele vezels. Het bleek dat VGCF-composieten geproduceerd kunnen worden met een vergelijkbare sterkte en thermische uitzettingscoefficient (CTE) maar met een lagere stijfheid.

Micromechanische modellen beschikbaar uit de literatuur en een nieuw ontwikkeld model zijn gebruikt om de stijfheid, CTE en sterkte van korte-vezel versterkte composieten te voorspellen vanuit de vezel- en matrixeigenschappen. De modellen zijn experimenteel gevalideerd en vervolgens omgekeerd toegepast om de submicron VGCF-eigenschappen te berekenen. Geconcludeerd kan worden dat submicron VGCFs een schijnbare CTE hebben die hoger is dan die van ex-PAN koolstofvezels en een lagere stijfheid. Hoewel de sterkte van de vezels niet direct berekend kon worden, omdat de meeste vezels ruim beneden de kritische lengte zijn, maakt invers modelleren wel de afleiding mogelijk van de afschuifsterkte van de interface tussen matrix en vezel. De hechting tussen VGCFs en de thermoplastische matrix blijkt vergelijkbaar met die van conventionele koolstofvezels. De verschillen in eigenschappen tussen VGCF- en ex-PAN koolstofvezel versterkte composieten kunnen worden toegeschreven aan de verschillen in vezeleigenschappen. Daarnaast is geconcludeerd dat de schijnbare stijfheid en CTE van submicron VGCFs zeker zo goed zijn als die van glasvezels.

# ACKNOWLEDGEMENTS

The work presented in this thesis would not have been possible without the support of many people, institutions and companies.

First and most of all, I wish to express my gratitude to Prof. Carlos Bernardo for offering me the possibility to start my PhD at the University of Minho. His vision and continuous support and guidance throughout my PhD has helped this work to become what it is and made my stay and work in Portugal a great and pleasant experience.

Many thanks to all the members of the Department of Polymer Engineering at the University of Minho, who kindly received and accepted me as their colleague and greatly supported me in the different aspects of the work. Special thanks go to my colleagues Dr. Conceição Paiva, Dr. Pedro Nunes and Dr. Nuno Neves for the many fruitful discussions and co-operation that contributed greatly to this work. I would also like to thank Dr. Olga Carneiro and Eng. Guilherme Caldeira for their indispensable help in the processing and rheological part of this work.

I am indebted to the members of the European Research Network “Vapour Grown Carbon and Other Ceramic Fibres”, in co-operation with whom this work was completed. Especially, I would like to thank Dr. Antonio Madroñero from CENIM, Madrid, Spain and Prof. Luís Figueiredo and Dr. Philippe Serp, from the University of Porto, Portugal, for the co-operation in growing and investigating the VGCFs and Prof. Jean-Paul Issi and Dr. Eusebiu Grivei, from the University of Louvain-la Neuve, Belgium, for allowing me to stay and work in their laboratories.

Many thanks also to Dr. Gary Tibbetts and Dr. Joana Finegan for their support, co-operation and discussions during this work and for giving me the opportunity to stay and work at GM Research, Detroit, USA. Furthermore, I would like to acknowledge the support of Bob Alig

and Max Lake from Applied Sciences, Inc., Cedarville, Ohio, USA, for their co-operation and advice and their generous production and supply of the submicron VGCFs used in this work.

I am grateful to the members of the Chair Design in Plastics of the University of Twente, Netherlands, especially Prof. Peter Powell and Dr. Kaspar Jansen, for receiving me in their laboratories and let me work on and learn from their experience in short fibre composites. I have also greatly benefited from the many discussions on this subject with Ir. Rik Voerman.

Next, I would like to address many thanks to Dr. John O'Gara of GM Research, for his valuable comments on the modelling work presented in this thesis.

Special thanks also to Amélia Alonso, from the Instituto Nacional del Carbon, Oviedo, Spain, who performed the cold-oxygen-plasma treatment of the VGCFs, and to my colleague Eng. Rui Reis for injection moulding the SCORIM samples during his stay at the University of Brunel in England.

The support of Tenax Fibers, who kindly supplied the PAN-fibres, and Carbogal, who kindly offered the Carbon Black used in this work, is also thankfully acknowledged.

This work was supported by the European Economic Community, through the Human Capital and Mobility Programme, under Grant Number CHCRXCT940457. I acknowledge the personal grant received under the same contract.

# TABLE OF CONTENTS

**Preface** iii

**Abstract** v

**Resumo** vii

**Samenvatting** ix

**Acknowledgements** xi

**Table of contents** xiii

**List of tables** xix

**List of figures** xxi

**Introduction** 1

- Vapour Grown Carbon Fibres 1
  - Introduction 1
  - Fibre growth 1
  - Fibre morphology 4
  - Fibre properties 5
- Vapour grown carbon fibre composites 7
- Micromechanical modelling 8
  - Introduction 8
  - Fibre orientation 9
  - Property prediction 10

Matrix morphology and internal stresses 12

Aim of the investigation 14

References 15

---

**Part I** *Vapour Grown Carbon Fibres*

---

**1 Morphological, mechanical and interfacial analysis of Vapour Grown Carbon Fibres** 21

1.1 Introduction 21

1.2 Theory 22

1.2.1 Mechanical characterisation 22

1.2.2 Fragmentation tests 23

1.3 Experimental 23

1.3.1 Fibre production 23

1.3.2 Fibre shape characterisation 24

1.3.3 Mechanical and interfacial characterisation 24

1.4 Results and discussion 25

1.4.1 Fibre shape characterisation 25

1.4.2 Mechanical characterisation 26

1.4.3 Fragmentation test 31

1.5 Conclusion 32

1.6 References 33

**2 The effect of the morphology on the properties of Vapour-Grown Carbon Fibres** 35

2.1 Introduction 35

2.2 Results and discussion 36

2.3 Conclusion 41

2.4 References 41

## Part II *Vapour Grown Carbon Fibre Thermoplastic Composites*

**3 Production and assessment of Vapour Grown Carbon Fibre-polycarbonate composites** 45

3.1 Introduction 45

3.2 Experimental 47

3.2.1 Materials 47

3.2.2 Manufacture of the composites 48

3.2.3 Injection moulding of the composites 48

3.2.4 Mechanical and rheological characterisation 49

3.3 Results and discussion 50

3.3.1 Characterisation of the fibres 50

3.3.2 Properties of composites made with as-grown VGCF 51

3.3.3 Properties of composites made with plasma treated VGCF 56

3.3.4 Properties of composites made with as-grown VGCF and processed by SCORIM 57

3.4 Conclusion 58

3.5 References 58

**4 A study of the thermomechanical properties of carbon fibre-polypropylene composites** 61

4.1 Introduction 61

4.2 Experimental 62

4.2.1 Materials and sample preparation 62

4.2.2 Material characterisation 63

4.3 Results and discussion 63

4.4 Conclusion 66

4.5 References 66

## Part III *Micromechanical modelling*

**5 A model to predict the strength of short fibre composites** 69
5.1 Introduction 69
5.2 Theory 70
5.2.1 Strength of unidirectional composites 70
5.2.2 Single fibre strength 71
5.2.3 Fibre length distribution 72
5.2.4 Failure criterion 73
5.2.5 Fibre orientation distribution 75
5.3 Experimental 77
5.3.1 Material preparation 77
5.3.2 Material characterisation 77
5.4 Results and discussion 78
5.4.1 Material characterisation 78
5.4.2 Predictions versus experiment 80
5.4.3 The role of the fibre length in the model 83
5.4.4 The role of the fibre strength in the model 85
5.4.5 The role of the interfacial shear strength in the model 85
5.5 Conclusion 86
5.6 References 86

**6 Modelling the thermomechanical properties of carbon fibre-polypropylene composites** 89
6.1 Introduction 89
6.2 Experimental 89
6.2.1 Material characterisation 89
6.2.2 Micromechanical modelling 90
6.3 Results and discussion 91

6.3.1 Validating the models 91

6.3.2 Inverse modelling 93

6.4 Conclusion 94

6.5 References 95

**7 General discussion** 97

7.1 Vapour grown carbon fibres 97

7.2 Vapour grown carbon fibre thermoplastic composites 98

7.3 Micromechanical modelling 99

7.4 References 100

**8 Conclusions** 103

**9 Recommendations** 105

---

**Appendices**

---

**Appendix A Specimen geometry**

**Appendix B Characteristic test curves**

**Appendix C Halpin-Tsai and Halpin-Schapery Equations**

**Appendix D Orientation averaging**

# LIST OF TABLES

Table 1-1. Diameters determined on ‘perfect cylinder’ VGCF. 27

Table 1-2. Diameters determined on 2 sets of ‘perfect cylinder’ VGCF. 28

Table 1-3. Parameters of the Weibull distribution. 28

Table 2-1. Diameters of 2 batches of VGCF with different shapes. 37

Table 2-2. Calculated tensile strength for the 2 batches of VGCF. 38

Table 3-1. Operational parameters determined in the extrusion experiments. 48

Table 3-2. Geometrical characteristics and density of VGCF. 50

Table 3-3. Elemental composition of the carbon fibre surface. 50

Table 3-4. Relative differences (%) in tensile and impact properties, resulting from fibre treatment. 56

Table 3-5. Relative differences (%) in tensile and impact properties as a result of SCORIM. 57

Table 4-1. Operational conditions used in the injection moulding. 62

Table 4-2. Composite’s test results. 63

Table 5-1. Composite’s test results. 79

Table 5-2. Parameters of the Weibull distribution. 79

Table 5-3. Fibre properties. 80

Table 5-4. Material parameters used for the evaluation of the model. 81

Table 5-5. Experimental and predicted values of the mechanical properties. 83

Table 6-1. Experimental and predicted values of the composite properties 91

Table 6-2. Apparent submicron VGCF fibre properties, compared with other fibres 94

# LIST OF FIGURES

Figure I-1. VGCF growth model 2

Figure I-2. Apparatus for growing VGCF on a substrate. 2

Figure I-3. Apparatus for growing VGCF in a continuous process. 3

Figure I-4. Molecular orientation through the thickness of an injection moulded part. 13

Figure I-5. Pressure induced stresses through the thickness of an injection moulded part. 13

Figure 1-1. Schematic representation of the laser diffraction system. 24

Figure 1-2. Different morphologies in which VGCF can be produced. (a)“Perfect cylinder”; (b)“Quasi-perfect cylinder”; (c)“Cylinder with debris”; (d)“Finely-screwed thread”. 25

Figure 1-3. (Continued) Different morphologies in which VGCF can be produced. (e)“Palm tree trunk”; (f)“Lathe shaped”; (g)“Crenulated”. 26

Figure 1-4. Total compliance $C_t$ as a function of l/A. 27

Figure 1-5. Fibre strength data and Weibull confidence limits. 29

Figure 1-6. Fibre strength versus average fibre diameter (legend refers to fibre length). 30

Figure 1-7. Three-dimensional plot of fibre strength as a function of gauge length and average fibre diameter. 30

Figure 1-8. SEM micrographs of VGCF fragments after dissolution of the matrix of monofilament composites. 31

Figure 2-1. Different shapes of VGCFs. (a)’Perfect cylinder’; (b)’Quasi-perfect cylinder’; (c) ‘Crenulated’. 36

Figure 2-2. Fibre strength data and Weibull confidence limits for ‘quasi-perfect cylinder / crenulated’ fibres. 38

Figure 2-3. Three-dimensional plot of the fibre strength as a function of gauge length and average fibre diameter for both ‘Perfect cylinder’ and ‘Quasi-perfect cylinder / crenulated’ fibres. 39

Figure 3-1. SEM micrograph of the Pyrograf III®. 50

Figure 3-2. Relative mechanical properties of PC-VGCF composites. (a) Yield stress; (b) Modulus at 1% strain; (c) Impact properties. 52
Figure 3-3. SEM micrograph of a fractured surface. 53
Figure 3-4. Comparison of the relative properties of PC-VGCF and PC-CB composites: (a) Modulus at 1% strain; (b) Impact properties. 53
Figure 3-5. Shear viscosity of the PC and the PC-VGCF composites. 54
Figure 3-6. Shear viscosity of the PC and the PC-20%VGCF composite after extrusion and after injection. 55
Figure 3-7. Time sweep for PC-20%VGCF composite after extrusion and after injection. 55
Figure 3-8. Shear viscosity of PC and PC-20%VGCF composites made with treated fibres, after extrusion and after injection. 57
Figure 4-1. Normalised experimental modulus at 1% strain. 65
Figure 4-2. Normalised experimental strength. 65
Figure 4-3. Normalised experimental CTE. 66
Figure 5-1. Definition of the fibre angles $\phi$ and $\theta$ and the unit vector **p**. 75
Figure 5-2. Fibre strength data and Weibull confidence limits. 79
Figure 5-3. Typical fibre length-distribution (a), and fibre orientation through-thickness (b), for PP-PAN 15%. 82
Figure 5-4. Longitudinal strength (a), and modulus (b) of unidirectional composite as a function of fibre length, for PP-PAN 15%. 85
Figure 6-1. Experimental and predicted modulus for the PP-PAN composites. 92
Figure 6-2. Experimental and predicted strength for the PP-PAN composites. 92
Figure 6-3. Experimental and predicted CTE for the PP-PAN composites. 93

# INTRODUCTION

## VAPOUR GROWN CARBON FIBRES

### Introduction

Carbon fibres are increasingly used in thermoplastic composites by virtue of their favourable mechanical, thermal and electrical properties. However, their relative high price compared to other reinforcements, such as glass fibres, is keeping carbon fibres from being widely utilised. Recently, a new type of carbon fibres, Vapour Grown Carbon Fibres (VGCFs), has gained interest. As a result of their production method, VGCFs combine potentially low production costs with encouraging mechanical, thermal and electrical properties compared to conventional ex-pitch or ex-PAN carbon fibres. This makes them of specific interest for applications where currently the conventional fibres are too expensive and glass fibres cannot provide the required thermal and electrical properties.

### Fibre growth

VGCFs are prepared via the catalytic decomposition of a gaseous carbon source. In the original work of Koyama and Endo, the growth of VGCF by thermal decomposition of benzene (I-1,I-2) is described. Endo and co-workers continued this work with a series of publications describing the structure of these fibres and the catalyst particles which cause growth (I-3) and published some growth procedures (I-4). A large number of publications have since been published, describing the VGCF growth methods and properties. These works have been the subject of two comprehensive reviews (I-5,I-6).

When describing the production of VGCF, two different methods can be distinguished. In the first method, the fibres are produced on catalyst-seeded substrates, in two independent sequential stages. In Figure I-1 a scheme is shown of the growth model for VGCF as described by Tibbetts (I-6). However, it should be noted that different growth models have been reported and can coexist (I-7). In the first stage, the catalyst particle, generally with iron being the predominant constituent, originates a long, slender, partially graphitic filament when exposed to a hydrocarbon gas near and above 1000°C. A small fraction of these fibres grows to macroscopic lengths when exposed to a low carburising potential gas, while maintaining the outside diameter of the initial catalytic particle (see Figure I-1). The sizes of these particles, and hence the filament diameter, have been reported to range from 10 to 200 nanometres (I-4,I-7,I-8). The filament growth may go as rapidly as 1 mm/min and last for several minutes until the catalytic particle is deactivated (I-8). At this stage filament lengths of several centimetres may be obtained.

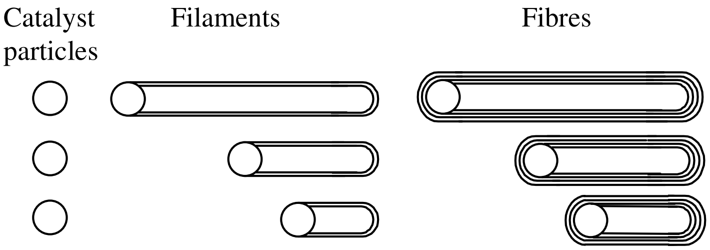

*Figure I-1. VGCF growth model (I-6).*

In the second stage, the gas potential is increased, and the filament thickens due to the deposition of pyrolytic carbon. In this way, fibres with diameters up to 100 μm have been produced in batch conditions (I-9). As pyrolytic carbon is deposited with the basal planes preferentially oriented parallel to the surface, the properties of the fibre are partially graphitic (I-6). A schematic of an apparatus for producing fibres in this way is shown in Figure I-2.

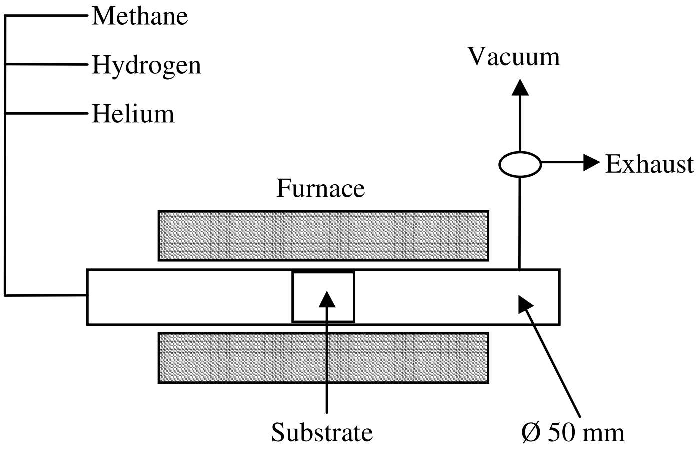

*Figure I-2. Apparatus for growing VGCF on a substrate (I-6).*

Methane, hydrogen and an inert gas are used to grow the fibres at atmospheric pressures on nesting cylindrical substrates within a growth tube. Lower concentrations of the methane-hydrogen mixtures are used for fibre lengthening, whereas higher concentrations are used for thickening. As methane is a low-cost feedstock in some parts of the world, the production of VGCFs can become very economic compared to other carbon fibres.

An alternative method of preparing VGCF uses a gas phase catalyst that stays unsupported inside a continuous flow reactor (I-10). In this method, the fibres are produced in just one stage that incorporates both lengthening and thickening. The catalytic particles are incorporated in the feedstock where the carbon potential may be adjusted to compromise between lengthening and thickening. The fibres move through the reactor with the gas stream and are collected as they exit. In Figure I-3 a schematic of this continuous process is given. As the residence times are short, the lengths of the fibres are usually below 100 µm and their diameters below 200 nm. Because of this, they are sometimes called submicron (diameter) fibres. Whereas the former method is merely a batch process, the latter method allows continuous fibre growth at a much higher rate and lower costs, which makes its commercial implementation more attractive. For both methods, the effect of addition of sulphur to the gas phase, to increase the yield of fibres has been investigated by several authors (I-6,I-11,I-12).

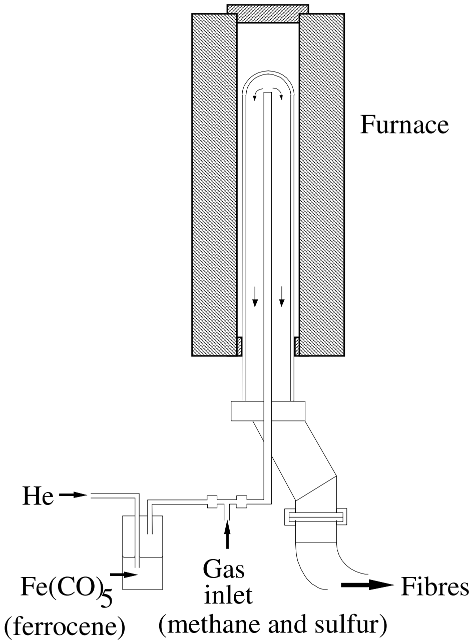

*Figure I-3. Apparatus for growing VGCF in a continuous process (I-11).*

## Fibre morphology

Due to their production method, VGCFs come in a variety of morphologies that are central to understanding their properties. Several different morphologies have been reported in the literature (I-6,I-13). To a certain extent, these morphologies reflect the fibres' internal structure. The structure of VGCFs resembles that of a tree trunk, with concentric annular rings. At the centre, along the axis of symmetry, lies the original filament. The layers are partially aligned turbostratic carbon, with the average basal plane misaligned from the fibre's axis by about 10-15° (I-3, I-6). In thinner fibres, or in fibres submitted to high temperature heat-treatments, cracks are observed between consecutive rings, and the external surfaces are often crenulated. An explanation for this crenulation has even been advanced, based on the work of Chen and Diefendorf (I-6,I-14). On cooling down, the pyrolytic carbon contracts more rapidly in the radial than in the tangential direction. The resulting radial stress (tension) will be diminished if circumferential cracking between the rings occurs. On the other hand, the contraction in the tangential direction leads to a high compressive stress that can be partially relieved by the formation of the crenulations.

The uniform geometry and the essentially carbon structure of the VGCFs makes the fibres extremely graphitisable. Endo et al. (I-15) observed rapid graphitisation with increased temperatures. At temperatures over 2600°C they showed that the structure approaches that observed in single crystal graphite. Obviously, this property will allow improvement and, to a certain level, tailoring of the fibre properties to desired values.

Recently, a growing interest has been shown in the surface properties of VGCFs, as this can be related to the interfacial properties of the fibre in composites. Darmstadt et al. showed that the surface reactivity of VGCFs is lower than that of ex-pitch or ex-PAN carbon fibres (I-16). However, it can be increased by oxidation treatment to become closer to that of the other carbon fibres. The effect of different oxidative surface treatments (nitric acid, plasma, air and carbon dioxide) on the fibres surface reactivity has been investigated by Serp et al. (I-17). They concluded that, although surface oxidation of carbon fibres is the standard technology to improve adhesion between fibre and matrix, air and carbon dioxide treatments do not significantly increase the fibre's surface reactivity, despite considerable weight loss. This was attributed to the presence of traces of iron left on the VGCF from the growth stages, that may have catalysed carbon gasification by a pitting mechanism, which had been reported by Serp and Figueiredo previously (I-18). Cleansing of the VGCFs with HCl to remove the iron can prevent this behaviour. Although nitric acid and plasma treatments were found to increase surface reactivity without altering significantly the morphology of the fibres, the latter appeared to be more favourable in improving the adhesion of VGCFs to a matrix.

## Fibre properties

### *Mechanical properties*

Although the mechanical testing of fibres is a tedious task to perform, values of the modulus and the tensile strength of VGCFs can be found without difficulty in the literature (I-6,I-8,I-12,I-19,I-20). The reported modulus values range from ca. 100 to above 1000 GPa. Tibbetts and Beetz showed that the stiffness of VGCF depends on their diameters. In a given set of fibres, produced in the same experiment, when the diameters increased from 6 to 32 µm, the moduli decreased from about 300 to 120 GPa (I-6,I-8). The stiffness of pyrolitic carbon is known to be related to the degree of preferred orientation of the graphitic basal planes. The Ruland-model (I-6) gives a relation of the stiffness of a graphite fibre as a function of the orientation angle of the graphitic planes. Tibbetts has successfully fitted this model to the stiffness-data of VGCFs by measuring their orientation parameter (I-6). As the only fitting parameter used in the Ruland model is independent of fibre diameter, the author attributed the decrease in the stiffness of thicker fibres to a decrease in their graphitic ordering. This again is due to a quicker deposition of pyrolytic carbon during the thickening period. This is in accordance with the finding that increasing the graphitisation of VGCF by heat-treatment also increases their modulus significantly. In one example, the modulus of as-grown fibres more than doubled to about 500 GPa when they were heated at 2200°C (I-6). Heat-treated fibres also fail more frequently in the “sword-in-sheath” mode. In this mode, a sequence of circumferential cracks along the inner rings allows consecutive cylinders to slide telescopically inside each other, gradually decreasing the load bearing capacity of the fibre (I-6). It is clear from these results that the modulus and failure mode of vapour grown carbon fibres are linked to their structure.

Recently, Jacobsen and co-workers (I-19), using a low-strain vibrating-reed technique, reported Young’s moduli of as-grown VGCF from 566 to 1017 GPa, with an average of 680 GPa. These values are much higher than the highest ones previously reported, 600 GPa (I-20). They attributed this difference to the high-strain (and rough handling) inherent to tensile testing, that can have a deleterious effect on brittle fibres and, thus, on the results of previous researchers. This is not necessarily true, as Tibbetts and Beetz observed that some fibres could be stressed repeatedly, with little hysteresis, leading to modulus' values around 200 GPa (I-8). Hence, it is also clear that the stiffness data of VGCFs depend on the test method used to obtain them.

Reported values of the tensile strength of VGCF are more consistent, varying from 2.5 to 3.5 GPa for fibres with diameters just below 10 μm. The dependence on the diameter, however, is very strong (I-6,I-8,I-13). Tibbetts and Beetz explained this by assuming that thicker fibres have a larger flaws' population, and a greater probability of failure, than thinner ones (I-6). Accordingly, they were able to fit a Weibull distribution function to the strength versus diameter data. The hypothesis is supported by the presence of cracks between consecutive cylindrical inner layers that may act as failure initiators.

### *Electrical and thermal properties*

The carbon structure and potential graphitisation of VGCFs by heat-treatment makes them an interesting candidate for thermal and electrical applications. VGCFs are known to have the highest electrical and thermal conductivities among carbon fibres due to their possible high structural perfection (I-21). Heremans (I-22) has measured the electrical resistivity of VGCFs that were heat-treated at temperatures ranging from 1400°C to 3000°C. Electrical resistivity measurements were done for temperatures between 10K and 370K. It was shown that VGCFs heat-treated at lower temperature have a resistivity that is almost constant with temperature. The resistivity of fibres heat-treated at higher temperatures decreases with the treatment temperature. At the highest temperatures, the resistivity of the VGCFs approaches that of a single crystal graphite, with a resistivity of about $5*10^{-7}$ Ω.m at 300K. Similar values were also obtained in the work of Tahar, Dresselhaus and Endo (I-23) on heat-treated benzene-derived VGCFs. Furthermore, they observed a decrease in resistivity with fibre diameter. This decrease was attributed to the increased ordered graphite regions as the diameter increases.

The thermal conductivity of VGCFs is remarkably high (I-6, I-21). Heremans and Beetz (I-24) measured the thermal conductivity of both as-grown VGCFs and VGCFs heat-treated to 3000°C. Conductivities were measured through a temperature range of 10K to 300K. It was shown that the heat treatment increases the fibre conductivity by a factor of 50. At room temperature the heat-treated fibres rank among the best thermal conductors available. Experiments on benzene-derived VGCFs by Nysten et al. (I-25) again revealed the high thermal conductivity of this type of fibres. Furthermore, as a remarkable result of this and a related work (I-26), the authors showed a direct relation between electrical resistivity, thermal conductivity and tensile modulus of carbon fibres. The experimental results obtained on ex-pitch carbon fibres indicate an exponential dependence of the electrical resistivity and thermal conductivity on tensile modulus (I-25). The strong relation between thermal conductivity and electrical resistivity was explained by similar fibre structural effects dominating these properties. Such a dependence would make the existence of the same relation for other carbon fibres quite reasonable. This, in combination with the previously mentioned relation between fibre structure and tensile modulus (I-6), could, at a later stage, lead to the prediction of the properties directly from fibre structural considerations.

## VAPOUR GROWN CARBON FIBRE COMPOSITES

Recently, there has been a growing interest in the applications of VGCF, namely in carbon and polymer matrix composites. As the research on VGCF has mainly been concerned with the growth and properties of the fibres and the investigation of their applications only recently commenced, the number of publications on this subject is limited. Nonetheless, the works reviewed cover a wide range of applications.

Dasch, Baxter and Tibbetts (I-27) reported the first thermoplastic submicron-size VGCF composites, using polycarbonate and nylon as a matrix. They measured increasing mechanical and thermal properties with fibre volume fraction, although this increase is less than could be theoretically expected. The composites were compression moulded using a simple set-up resulting in a fibre alignment that was assumed to be random in three dimensions. The authors predicted higher properties if a process like injection moulding was used to induce fibre alignment. Dutta et al. (I-28) investigated the processability of submicron VGCFs in thermoplastic matrices. They extruded polycarbonate-VGCF composites in a single screw extruder and subsequently melt-drew the composites to induce fibre orientation. They concluded that the dispersion of the fibres in the matrix was very poor at 2 vol.% fibre fraction and became even poorer when the fibre content was increased to 5 vol.%. It was suggested that grinding or melt-blending the fibre with the polymer before extrusion may result in better dispersion.

Hudnut and Chung (I-29) studied the use of submicron VGCFs as random layers between layers of continuous conventional carbon fibres in an epoxy matrix. They found the VGCFs improve significantly the damping capacity of the composites at fibre fractions as low as 0.6 vol.%. Guth et al. (I-30) investigated the use of VGCFs for fabricating thin paper where they successfully replaced the traditionally used commercial chopped ex-PAN and ex-pitch fibres to obtain planar isotropy.

Fu and Chung utilised submicron VGCFs in cement-matrix composites, an application in which they may be extremely useful, due to the relative low cost and easy processability (I-31). With a fibre load of only 1.5 vol.%, they attained the highest electromagnetic interference (EMI) shielding effectiveness ever attained for a cement-matrix composite.

No work can be found in literature on the characterisation of the interface between VGCFs and different matrices. Some indirect evidence can be obtained from studies of submicron VGCF in polymer-matrix composites (I-27,I-28,I-29). This evidence, nevertheless, is inconclusive, and derives mainly from SEM observations of fracture surfaces.

Ting and Lake (I-32) studied the thermal properties of VGCF-carbon composites. Composites based on VGCF-mats were made and heat-treated at 2800°C and their thermal conductivity studied. It was found that the 36 vol.% composite exhibited a room-temperature thermal conductivity of 564 W/mK. This value, somewhat higher than that of copper (+/- 450 W/mK), was attributed to the highly graphitic nature of the VGCF mats. In a similar work, Ting et al. (I-33) fabricated and compared aluminium matrix and carbon-carbon composites based on VGCFs. For the aluminium-VGCF composites at 36.5 vol.% they found a thermal conductivity of 642 W/mK. The properties of the VGCF-carbon composites were comparable to the previous work. An exceptional value of 910 W/mK was observed for a 70 vol.% carbon-VGCF composite, twice the value of copper. However, this value is not as high as could be expected from theoretical considerations. In addition Ting and Guth (I-34) investigated the mechanical properties of VGCF-carbon composites. They arrived at the conclusion that the tensile properties of these composites are lower than expected. It was suggested that the thermal properties of VGCFs are better translated into composites than are the mechanical properties.

## MICROMECHANICAL MODELLING

### Introduction

Although VGCFs can be produced in a variety of dimensions, the submicron VGCFs are certainly those with greater economic potential. They can also be produced in the large quantities needed for current thermoplastics processing technologies, and are therefore of interest for the present investigation. However, the minute dimensions make the experimental determination of their mechanical and thermomechanical properties nearly impossible. In this case, modelling may be the sole method to determine those properties. With a working model, the properties of the fibres can be calculated, knowing their orientation and length distribution, as well as the corresponding properties of the composites.

## Fibre orientation

The main difficulty to be solved in modelling the rheological and mechanical behaviour of short fibre composites is the complexity and wide range of their fibre orientation states, which determines the value of the properties. During moulding of short fibre composites, fibres tend to align parallel to the flow direction in converging flow, but in diverging flow they align perpendicular to the flow direction. Different fibre orientation states through thickness are generally observed in moulded parts, also referred to as ‘skin-core’ structure (I-35,I-36). A ‘core’-layer where fibres align perpendicular to the flow direction is normally present in the mid-plane of the moulded parts, bounded by ‘skin’-layers where fibres are preferentially aligned in flow-direction. In some cases, close to the mould wall, layers are observed where the fibres have no preferential direction.

It is clear that in order to be able to model the composite properties, one first needs to have knowledge about the fibre orientation state in the composite. This can be statistically modelled by an orientation distribution function (I-35,I-37) describing the probability of finding fibres with any given orientation. However, for most purposes, describing fibre orientation in this way requires significant computational effort. In their pioneering work, Advani and Tucker introduced a compact tensor description for fibre orientation (I-37). Apart from the general applicability and computational efficiency, this description allows easy integration with conventional rheological and mechanical tensor descriptions. Due to these inherent advantages, it is now widely used in works on short fibre composites and implemented in commercial software packages for flow simulation, such as C-Mold.

Several methods can be found in literature for direct determination of fibre orientation in a composite (for overviews see I-35,I-38), of which reflected light microscopy of polished surfaces is the most widely used. Although this method has its limitations in that it requires the assumption of certain symmetries in fibre orientation, it is applicable to most fibre-matrix combinations and overcomes many of the experimental complications associated with other methods. The method extracts data on fibre orientation from the ellipses that are the cross-sections of the fibres in polished surfaces. The experimental set-up, methods for bias correction and error estimates of this method have been extensively described by Bay and Tucker (I-39) and Hine et al. (I-40).

Various models for predicting the fibre orientation states are also available, which are based on the theory of Folgar and Tucker (I-41), which in itself is adapted from the well-known Jeffery's equation (I-42). For computational reasons, these models use the tensor description for fibre orientation. Although the theory allows prediction of fibre orientation, it requires the use of an interaction coefficient to account for fibre-fibre interactions, that influence the fibre orientation during flow. As no analytic relations are available to predict this interaction coefficient, an empirical relation has been forwarded to give an expression for its dependence on fibre volume fraction and aspect ratio (I-35). Models to predict fibre orientation have been successfully applied to short fibre composites and are already implemented in commercial software packages. However, in numerical predictions, the tensor description requires the use of closure approximations to derive the higher order tensors needed to obtain a solution to the orientation problem in flow to calculate the mechanical properties (I-37). Several different closure approximations have been formulated (I-37,I-43), of which the so-called 'hybrid closure' for long has been found to perform best. This is also the closure approximation currently included in the commercial packages. Recently, a new type of closure approximations, 'orthotropic closures', has been proposed (I-44), of which the so-called 'L-version' has already proven to improve accuracy (I-45).

### Property prediction

Several models have been proposed to predict the properties of short fibre composites from the fibre and matrix properties. The more useful and generally applicable use the same underlying assumptions and methods. As a first step, these models derive expressions for the properties of a unidirectionally aligned short fibre composite as a function of fibre length. The models assume that: the fibres and matrix are isotropic and linearly elastic; the fibres are axisymmetric, identical in shape and size and can be characterised by an aspect ratio l/d; the fibres and matrix are well bonded at the interface, and remain that way during deformation. Thus, interfacial slip, fibre-matrix debonding or matrix micro-cracking are not considered. Based on these assumptions, the well-known semi-empirical Halpin-Tsai equations (I-46) have proved to be accurate for prediction of stiffness. Due to its relative simplicity, the Halpin-Tsai equations are widely used, although other refinements or exact theories can be found in literature (I-47,I-48,I-49,I-50). Predictions of the coefficient of thermal expansion (CTE) for short fibre composites are less frequently found. However, they are generally based on the Schapery-equations (I-51), as adapted for short fibre materials by Halpin (I-52). Just as with the Halpin-Tsai equations, their relative simplicity allows wide utilisation.

As a next step, models predicting composite properties usually substitute the average fibre length found in the composite in the previously derived expressions, to obtain the properties of the unidirectional composites. In short fibre composites, however, fibre length distributions exist as a result of processing. A significant decrease and spread in fibre length compared to the initial fibre length is usually observed, which obviously affects the composite's properties. A more accurate solution would therefore be to integrate the expressions over the whole range of fibre lengths. For the case of stiffness-prediction, Doshi and Charrier (I-53) have shown that differences in final property predictions can occur when taking into account a single fibre length as opposed to the full fibre length distribution. In the case of carbon fibres, a further complication arises as also the fibre strength is dependent on fibre length (I-54,I-55). However, as information on the actual fibre length distribution is generally not available, nor can be predicted with existing theories and furthermore requires further computational effort, most works limit themselves to taking only the average fibre length into account.

After accounting for the fibre length, the properties of the final composite are taken as an average of these unidirectional properties over all directions, weighted by the orientation distribution function. This is often referred to as 'orientation averaging'. The unidirectional properties as derived above are used to construct the stiffness and thermal expansion tensors. These tensors can be 'orientation averaged' following the method described by Advani and Tucker (I-37), to derive the final composite properties. In this way, models have been developed to predict elastic moduli and thermal expansion coefficients for arbitrary fibre orientations, showing good agreement with experimental results (I-37,I-45,I-56).

Several models have also been proposed to predict strength of short fibre composites, of which some have shown good agreement with experimental results (I-57,I-58,I-59). However, most models are limited to random two- or three-dimensional fibre orientation and their ability to predict strength of composites with arbitrary fibre orientation is limited. Besides, existing models give an expression for strength in one direction under a single load and are unable to deal with multiple loading conditions. As has been shown above, the complexity of fibre orientation patterns and fibre length distributions and the structural analysis problems require a model that is able to predict strength for any kind of fibre orientation and length distribution, in any direction and under any loading condition. The derivation of one such model, following the same general method used for stiffness- and CTE-prediction, still remains to be done.

## Matrix morphology and internal stresses

As stated before, the theories most commonly used to model the properties of short fibre composites share some basic assumptions namely that the matrix is isotropic and the material free of internal stresses. However, due to the way polymer composites are processed, the matrix always shows a certain level of anisotropy, resulting from the development of semi-crystalline microstructures and/or molecular orientation (I-60,I-61). Furthermore, internal stresses are known to be present in the material (I-62,I-63).

The morphology of injection moulded semi-crystalline polymers (such as polypropylene) consist partly of regions with an organised microstructure (e.g. spherulites) and partly of amorphous regions. The existence of these regions depends on several processing parameters; in general, high shear stresses and low cooling rates promote the growth of spherulites. A typical morphology of an injection moulded semi-crystalline material would therefore consist of an amorphous layer close to the mould wall due to rapid cooling. Next to that a layer, where the spherulites are aligned in the flow direction, due to the high shear forces acting during processing. In the centre, a fine or coarse crystalline structure would occur depending on the cooling rate. As the packing order of the organised microstructures is higher than that of the amorphous regions, the crystallinity of a semi-crystalline polymer can be related to its density. Material properties such as strength and stiffness generally increase with crystallinity, whereas the impact resistance and CTE decrease. Thus, the differences in through-thickness morphology will result in anisotropy of an injection moulded semi-crystalline material.

In amorphous materials (such as polycarbonate) the molecules tend to be randomly organised. However, during processing, the molecules will tend to align in the direction of flow. Upon cooling down, part of this molecular orientation is frozen in, resulting in a certain level of anisotropy, which will be reflected in the material properties. A typical molecular orientation through the thickness of an injection moulded part is shown in Figure I-4. Three maximums in orientation can be observed from mould wall to centre. The first maximum, close to the mould wall, reflects the frozen-in molecular orientation due to the rapid cooling of the material, that is strongly stretched by the fountain flow of the polymer melt. The second maximum is due to the high shear stresses acting close to the mould wall, resulting in high molecular alignment in the flow direction. Finally, a third maximum is observed close to the centre, due to the shear stresses developed in the material by the application of the holding pressure at the end of the injection cycle.

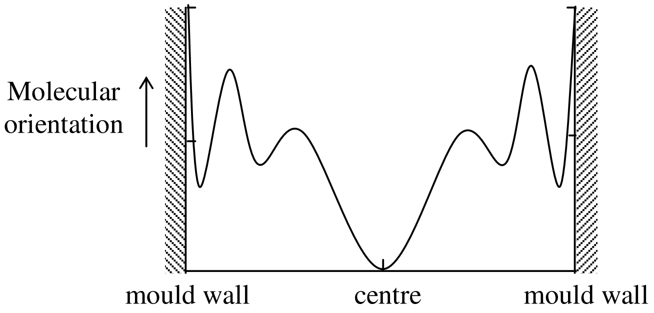

*Figure I-4.* *Molecular orientation through the thickness of an injection moulded part.*

Internal stresses in injection moulded polymers composites are of three types: pressure-induced, flow-induced and thermally-induced stresses (I-63,I-64,I-65).

Pressure-induced stresses result from the fact that in injection moulding each layer solidifies under a different pressure. These pressures are frozen-in, resulting in a stress-distribution through the thickness. A typical profile is shown in Figure I-5: tensile stresses can be observed at the walls and the centre of the part, whereas at intermediate positions, compressive stresses are present.

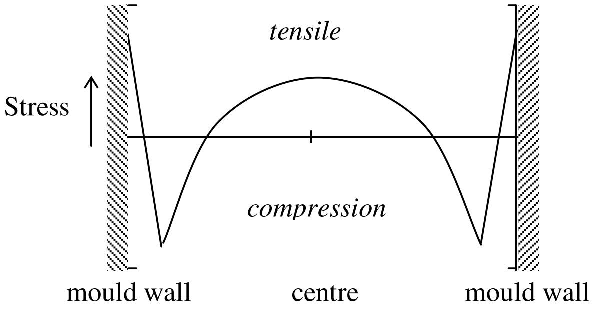

*Figure I-5.* *Pressure induced stresses through the thickness of an injection moulded part (I-62).*

Flow-induced stresses develop as a result of the different flow fields during mould filling. The resulting shear- and elongational stresses are frozen-in during the cooling down of the part. They are generally an order of magnitude smaller than the previously mentioned pressure-induced flows.

A parabolic distribution of internal stresses as a result of inhomogeneous cooling, is normally observed in free quenching experiments (e.g. I-63). During cooling, the surface material will solidify first and is free to shrink. When the core material starts to solidify, shrinkage is prevented by the solidified surface layer and stresses will develop. Generally, compressive stresses are observed at the surface and tensile stresses in the core. However, in injection mouldings the situation is different from the above described free quenching. In fact, the solidifying outer layer is also prevented from shrinking due to the constraint of the mould wall and existing pressures. Hence, the core and outer layers experience the same constraints when solidifying and a constant stress through-thickness is frozen in, which is released when the part is removed from the mould. Thus, thermally-induced stresses due to inhomogeneous cooling are almost absent in injection mouldings. Nevertheless, as a result of the previously mentioned fibre orientation and, to a smaller extent, matrix anisotropy though-thickness, different layers will shrink differently during cooling down. This will lead to a build-up of internal stresses in addition to the mentioned pressure- and flow-induced thermal stresses. Eijpe (I-65) measured internal stresses in polycarbonate reinforced with 30 and 40% short glass fibres by weight. He found a stress-distribution through-thickness similar to that of Figure I-5, with maximum values that reach approximately 8% of the matrix strength.

Although internal stresses can increase material strength when compressive, they can also decrease it when tensile, as they work in addition to the applied stresses under load (I-61). Overall, one should consider that the assumptions of the micromechanical models of an isotropy and absence of internal stresses in the matrix are only an initial estimate. Whether these simplifications are sufficiently accurate to predict the final short fibre composite properties, should be experimentally verified.

## AIM OF THE INVESTIGATION

The research project described in this thesis was initiated as part of a bigger research programme aimed at enhancing the knowledge on production and applications of VGCFs. Taking into account the work already done on VGCFs and VGCF-composites described above, and the areas in which further knowledge is required, three main goals were defined for the current project.

The **first goal** was to investigate the VGCFs, to study systematically the different morphologies in which they can be produced and their effect on the mechanical properties of the fibres. The **second goal** was to develop know-how on the production of thermoplastic matrix composites with VGCFs. The process should use available and unsophisticated technologies in order to be utilised in large production markets. Additionally, the composites should be characterised mechanically, to compare VGCFs as reinforcements of thermoplastics with other fibres. A **final goal** set to this research was to investigate (and where necessary develop) and apply models to predict the more relevant mechanical properties of the composites, namely modulus, tensile strength and CTE. These models can then be used to inversely derive the properties of the submicron VGCF. At the same time such models would be of general use for any short fibre composites.

This thesis is therefore divided in three parts, each covering one of the goals described above.

*Part I* describes a systematical study of VGCFs. An investigation into the diverse shapes in which VGCFs can be produced, and the determination of the mechanical and interfacial properties of one type of VGCFs is described in *Chapter 1*. In *Chapter 2* a second type of VGCFs is investigated in a similar way, and the results combined with those of *Chapter 1* to describe the influence of the morphology of VGCFs on the mechanical properties.

*Part II* deals with the production, processing and characterisation of thermoplastic-VGCF composites. In *Chapter 3* the production and processing of polycarbonate-VGCF composites is described together with their mechanical and rheological characterisation. *Chapter 4* extends this investigation into polypropylene-VGCF composites, describing their production, processing and thermomechanical properties. The results are compared to those of polypropylene-PAN fibre composites and the previously investigated polycarbonate-VGCF composites.

In *Part III* micromechanical models to predict the properties of short fibre reinforced composites are investigated and applied. In *Chapter 5* a new micromechanical model to predict strength of short fibre composites is derived and validated. In *Chapter 6* existing and the newly derived micromechanical model from *Chapter 5*, are applied to inversely derive the properties of the submicron VGCFs from the poplypropylene-VGCF composites.

Finally, in *Chapter 7* the research presented in this thesis is evaluated and the main results discussed. *Chapters 8 and 9* summarise the main conclusions obtained and the more interesting recommendations for future work, respectively.

## REFERENCES

I-1. T. Koyama, *Carbon*, **10**, 757 (1972).

I-2. T. Koyama, and M. Endo, *Ohyo Butsuri*, **42**, 690 (1973).

I-3. A. Oberlin, M. Endo, and T. Koyama, *J. Cryst. Growth*, **32**, 335 (1976).

I-4. M. Endo, and K. Komaki, in *Extended abstracts of 16th Biennial Conference on Carbon*, ed. American Carbon Society, San Diego, CA, 523 (1983).

I-5. M.S. Dresselhaus, G.D. Dresselhaus, K. Sugihara, I.L. Spain, and H.A. Goldberg, *Graphite Fibers and Filaments*, Vol. 5, Springer-Verlag, Berlin (1988).

I-6. G.G. Tibbetts, in *Carbon Fibers, Filaments and Composites*, ed. J.L. Figueiredo, C.A. Bernardo, R.T.K. Baker, and K.J. Huttinger, Kluwer Academic Publishers, Dordrecht, 73 (1990).

I-7. Ph. Serp, and J.L. Figueiredo, *Carbon*, **34**, 1452 (1996).

I-8. G.G. Tibbetts, and C.P. Beetz, Jr., *J. Phys. D: Appl. Phys.*, **20**, 292 (1987).

I-9. G.G. Tibbetts, and M.G. Devour, U.S. Patent No. 4.565.684 (1986).

I-10. G.G. Tibbetts, D.W. Gorkiewicz, and R.L. Alig, *Carbon*, **31**, 809 (1993).

I-11. G.G. Tibbetts, C.A. Bernardo, D.W. Gorkiewicz, and R.L. Alig, *Carbon*, **32**, 569 (1994).

I-12. P. Serp, J.L. Figueiredo, and C.A. Bernardo, in *Carbon and Carbonaceous Composite Materials*, ed. K.R. Palmer, D.T. Marx, and M.A. Wright, World Scientific Publishing, Singapore, 134 (1996).

I-13. A. Madroñero, *Mater.: Sci. Eng.*, A-105, L1 (1994).

I-14. K.J. Chen, and R.J. Diefendorf, in *Extended Abstracts of 17th Biennial Conference on Carbon*, ed. American Carbon Society, Lexington, KY, 387 (1985).

I-15. M. Endo, T. Koyama, and Y.M. Hishiyama, *Jap. J. Appl. Phys.*, **15**, 2073 (1976).

I-16. H. Darmstadt, C. Roy, S. Kaliaguine, J.-M- Ting, and R.L. Alig, *Carbon*, **36**, 1183 (1998).

I-17. Ph. Serp, J.L. Figueiredo, P. Bertrand, and J.-P. Issi, *Carbon*, **36**, 1791 (1998).

I-18. Ph. Serp, and J.L. Figueiredo, *Carbon*, **35**, 675 (1997).

I-19. R.L. Jacobsen, T.M. Tritt, J.R. Guth, A.C. Ehrlich, and D.J. Gillespie, *Carbon*, **33**, 1217 (1995).

I-20. T. Koyama, M. Endo, and Y. Hishiyama, *Jap. J. Appl. Phys.*, **13**, 1933 (1974).

I-21. J.-P. Issi, in *Carbon and Carbonaceous Composite Materials*, ed. K.R. Palmer, D.T. Marx, and M.A. Wright, World Scientific Publishing, Singapore, 51 (1996).

I-22. J. Heremans, *Carbon*, **23**, 431 (1985).

I-23. M.Z. Tahar, M.S. Dresselhaus, and M. Endo, *Carbon*, **24**, 67 (1986).

I-24. J. Heremans, and C.P. Beetz, Jr., *Phys. Rev. B*, **32**, 1981 (1985).

I-25. B. Nysten, L. Piraux, and J.-P. Issi, in *Thermal Conductivity, Proceedings of 19th ITCC*, ed. D.W. Yarbrough, Plenum Press, New York, 341 (1987).

I-26. J.G. Lavin, D.R. Boyington, J. Lahijani, B. Nysten, and J.-P. Issi, *Carbon*, **31**, 1001 (1993).

I-27. C.J. Dasch, W.J. Baxter, and G.G. Tibbetts, in *Extended abstracts of 21st Biennial Conference on Carbon*, ed. American Carbon Society, Buffalo, NY, 82 (1993).

I-28. D. Dutta, M. Husband, D. Ciminelli, and J.W. Hager, in *Extended abstracts of 22nd Biennial Conference on Carbon*, ed. American Carbon Society, San Diego, CA, 292 (1995).

I-29. S.W. Hudnut, and D.D.L. Chung, *Carbon*, **33**, 1627 (1995).

I-30. J.R. Guth, D.W. Hart, and J.-M. Ting, in *Extended abstracts of 22nd Biennial Conference on Carbon*, ed. American Carbon Society, San Diego, CA, 288 (1995).

I-31. Xuli Fu, and D.D.L. Chung, *Carbon*, **36**, 459 (1998).

I-32. J.-M. Ting, and M.L. Lake, *Carbon*, **33**, 663 (1995).

I-33. J.-M. Ting, M.L. Lake, and D.R. Duffy, *J. Mater Res.*, **10**, 1478 (1995).

I-34. J.-M. Ting, and J.R. Guth in, *Extended abstracts of 22nd Biennial Conference on Carbon*, ed. American Carbon Society, San Diego, CA, 296 (1995).

I-35. C.L. Tucker III, and S.G. Advani, in *Flow and Rheology in Polymer Composites Manufacturing*, ed. S.G. Advani, Elsevier, Amsterdam, 147 (1994).

I-36. R.S. Bay, and C.L. Tucker III, *Polym. Compos.*, **13**, 332 (1992).

I-37. S.G. Advani, and C.L. Tucker III, *J. Rheol.*, **31**, 751 (1987).

I-38. M.J. Folkes, *Short Fibre Reinforced Thermoplastics*, Research Studies Press, Chichester, UK (1982).

I-39. R.S. Bay, and C.L. Tucker III, *Polym. Eng. Sci.*, **32**, 240 (1992).

I-40. P.J. Hine, R.A. Duckett, N. Davidson, and A.R. Clarke, *Compos.Sci. Techn.*, **47**, 65 (1993).

I-41. F. Folgar, and C.L. Tucker III, *J. Reinf. Plast. Compos.*, **3**, 98 (1984).

I-42. G.B. Jeffery, *Proc. Roy. Soc.*, **A102**, 161 (1922).

I-43. S.G. Advani, and C.L. Tucker III, *J. Rheol.*, **34**, 367 (1990).

I-44. J.S. Cintra, Jr., and C.L. Tucker III, *J. Rheol.*, **39**, 1095 (1995).

I-45. P.H. Foss, J.P. Harris, J.F. O'Gara, L.P. Inzinna, E.W. Liang, C.M. Dunbar, C.L. Tucker III, and K.F. Heitzman, SPE ANTEC Tech. Papers, **42**, 501 (1996).

I-46. J.C. Halpin, and J.L. Kardos, Polym. Eng. Sci., **16**, 344 (1976).

I-47. H.L. Cox, Brit. J. Appl. Phys., **3**, 72 (1952).

I-48. L.E. Nielsen, J. Appl. Phys., **41**, 4626 (1970).

I-49. G.P. Tandon, and G.J. Weng, Polym. Compos., **5**, 327 (1984).

I-50. M.L. Dunn, and M. Taya, J. Mater. Sci., **29**, 2053 (1994).

I-51. R.A. Schapery, J. Compos. Mater., **2**, 380 (1968).

I-52. J.C. Halpin, J. Compos. Mater., **3**, 732 (1969).

I-53. S.R. Doshi, and J.-M. Charrier, Polym. Compos., **10**, 28 (1989).

I-54. E.G. Stoner, Ph.D. dissertation, Department of Chemical Engineering, Clemson University, Clemson, SC (1991).

I-55. W.J. Padgett, S.D. Durham, and A.M. Mason, J. Compos. Mater., **29**, 1873 (1995).

I-56. C.W. Camacho, C.L. Tucker III, S. Yalvaç, and R.L. McGee, Polym. Compos., **11**, 229 (1990).

I-57. H. Fukuda, and T-W. Chou, J. Mater. Sci., **17**, 1003 (1982).

I-58. W.J. Baxter, Metallurgical Transactions, **23A**, 3045 (1992).

I-59. P.A. Templeton, J. Reinf. Plast. Compos., **9**, 210 (1990).

I-60. Z. Tadmor, and C.G. Gogos, Principles of Polymer Processing, John Wiley & Sons, New York, USA (1979).

I-61. R. Wimberger-Friedl, Polymer Eng. Sci., **30**, 813 (1990).

I-62. J.R. White, Polymer Testing, **4**, 165 (1984).

I-63. K.M.B. Jansen, Int. Polymer Proc., **9**, 82 (1994).

I-64. K.M.B. Jansen, D.J. van Dijk, and M.J.A. Freriksen, Polymer Compos., **19**, 325 (1998).

I-65. M.P.I.M. Eijpe, Ph.D. dissertation, Department of Mechanical Engineering, Twente University, the Netherlands (1997).

# Part I

## *Vapour Grown Carbon Fibres*

# 1 MORPHOLOGICAL, MECHANICAL AND INTERFACIAL ANALYSIS OF VAPOUR GROWN CARBON FIBRES[1]

## 1.1 INTRODUCTION

Recently, there has been a growing interest in the applications of Vapour Grown Carbon Fibres, namely in carbon and polymer matrix composites (1-1,1-2,1-3,1-4). This, in turn, has focused attention on the mechanical properties of these fibres, as they determine the overall properties of the composites (1-5). To measure the mechanical properties it is necessary to know the fibres' dimensions, in particular their cross-sections. In the calculations it is normally assumed that the fibres are perfect cylinders, unequivocally characterised by their diameters. In the case of VGCF, however, it is well known that this is frequently not the case, as they come in different morphologies (1-6,1-7). To a certain extent, these morphologies reflect the fibres' internal structure. From results in the literature (see *Introduction*), it is clear that the modulus and failure mode of VGCFs are linked to their structure. In spite of this information, no systematic study of the morphology of VGCF, or of its effect on the mechanical properties, has ever been reported. Furthermore, it is also clear that the stiffness data of VGCFs depend on the test method used to obtain them. The strength of VGCFs varies less with the test method, but is known to show a great dependence on fibre diameter. However, neither the variation of the strength with fibre length, nor the fact that surface irregularities may be another cause for failure, has been taken into account in earlier research. Furthermore, it is somewhat surprising that no work was ever published on the interface of VGCFs with diameters in the micrometre range, for which mechanical properties' data already exist.

In this chapter we report a systematic analysis of as-grown VGCF, covering their morphologies and mechanical properties. The dependence of the fibres' strength on the length and diameter is discussed. Finally, fragmentation tests were used to obtain information on the failure behaviour of these fibres in monofilament model composites.

---

[1] Reproduced, with adaptations, from: F.W.J. van Hattum, J.M. Benito-Romero, A. Madroñero, and C.A. Bernardo, Carbon, **35**, 1175 (1997).

## 1.2 THEORY

### 1.2.1 Mechanical characterisation

Single filament tensile tests were used to determine the strengths and moduli of VGCFs. To measure the average fibre modulus, the tests were made at different gauge lengths. The total compliance, $C_t$, was calculated by:

$$C_t = \Delta L/F \qquad [1.1]$$

where $\Delta L$ is the total displacement, and $F$ the applied load. If it is assumed that the total compliance can be expressed in terms of the system and fibre compliances, $C_s$ and $C_f$, respectively (1-8), then:

$$C_t = C_f + C_s \qquad [1.2]$$

Finally, expressing $C_f$ as a function of the modulus, $E$, the fibre (gauge) length, $l$, and the cross-section of the fibre, $A$, leads to:

$$C_t = \frac{l}{AE} + C_s \qquad [1.3]$$

Thus, linear regression of $C_t$ on $l/A$ will yield a slope corresponding to the reciprocal of the average fibre modulus and an intercept corresponding to $C_s$ (1-8).

As the tensile strength of carbon fibres depends significantly on the existence of fatal flaws in the tested length, a statistical model must be applied to deal with the data variability. In this work a three-parameter Weibull distribution function was used, to describe the variation of fibre strength with gauge length, which method is described in detail elsewhere (1-9).

The mean tensile strength, $\overline{\sigma}$, and the variance of the Weibull distribution, $\beta_v$, functions of the gauge length, are defined as:

$$\overline{\sigma} = \sigma_0(l).\Gamma(1+ 1/m); \qquad \beta_v = [\sigma_0(l)]^2.[\Gamma(1+ 2/m) - \Gamma^2 (1+1/m)] \qquad [1.4]$$

where $\Gamma$ represents the gamma function, $m$ is the Weibull distribution shape parameter, and $\sigma_0(l)$ the Weibull scale parameter, which is also dependent on the gauge length. Various equations that express this dependence can be found in the literature (1-9). One of the more useful is of the type:

$$ln\sigma_0(l) = (-\gamma/m).ln\ l + ln\sigma_0 \qquad [1.5]$$

In the present work, we estimated the shape and scale parameters using a pooled efficiency method usually utilised for predicting fatigue life in composites (1-10). By fitting a function of the type of equation [1.5], on a plot of the estimated $\sigma_0 (l)$ against the gauge length, using a least-squares method, the parameters $\gamma$ and $\sigma_0$ can be obtained.

### 1.2.2 Fragmentation tests

Fragmentation tests are often used to assess the interfacial characteristics of carbon fibres in a given polymeric matrix. For that, composites with a single, aligned, fibre are prepared and then subjected to uniaxial tensile testing. The stress is applied in the direction of the fibre, and the load is transferred from the matrix through the interface, causing the fibre to break. The fragmentation continues until a minimum length of fibre fragments is achieved. The process stops at this moment, either because the available fibre surface is too small to transmit a load big enough to break the fibre, or due to interfacial rupture (1-11). The critical length of the fibre, $l_c$, i.e., the length below which the transfer of stress from the matrix to the fibre is not enough to cause a new rupture, may be obtained by measuring the average length of the fragments, $l_{aver}$. From there, the interfacial shear stress can be calculated by a balance of the forces that act on a fibre fragment of length $l_c$. The smaller the critical length of the fibre in a given matrix, the bigger the interfacial shear stress, or the stronger the interface.

## 1.3 EXPERIMENTAL

### 1.3.1 Fibre production

The fibres analysed in the present work were produced in catalyst seeded substrates by the decomposition of a hydrocarbon source, using a procedure based on the VLS (Vapour-Liquid-Solid) process described by Wagner and Ellis (1-12). Fibres with a very regular morphology can be obtained with this procedure, which makes it of potential industrial interest. The details of the process have been described elsewhere (1-13,1-14).

### 1.3.2 Fibre shape characterisation

To assess the geometry of the fibres, a laser diffraction technique was used. The system consists of a He-Ne laser (Uniphase®, model 1508-0) that produces a laser beam of 623.8 nm wavelength. A single fibre was glued onto a paper frame, as described in ASTM Standard D3379-75, and subjected to the laser beam. In this way, diffraction dots can be observed on a screen, aligned perpendicularly to the direction of the projection of the fibre (Figure 1-1). From the distance between the dots with maximum intensity, the fibre diameter can be derived.

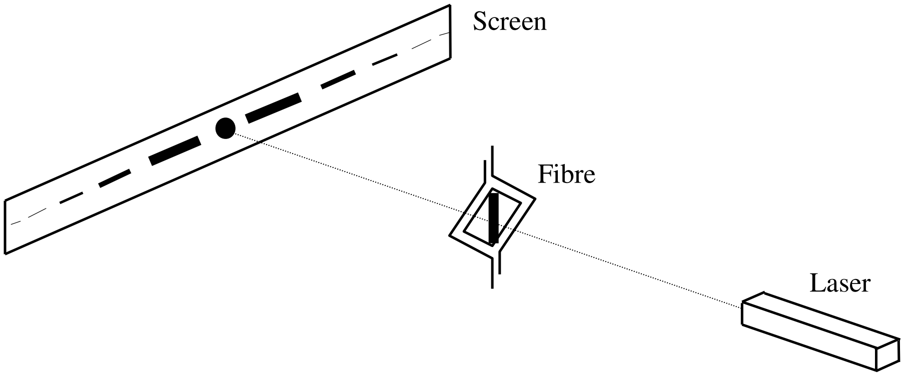

*Figure 1-1. Schematic representation of the laser diffraction system.*

### 1.3.3 Mechanical and interfacial characterisation

The VGCFs were tested according to ASTM D 3379-89, at room temperature, in an Instron 1122 universal testing machine with a 5 N load cell. Using a cross-head speed of 0.5 mm/min, 4 different gauge lengths (15.33, 20.43, 30.29 and 40.24 mm) were tested, 15 samples at each gauge length. The slope of the stress-strain curves increased with the strain, as observed in other VGCF studies (1-6). Considering the non-linear behaviour of the fibres, the compliance was derived from the slope of the part of the force-deflection curve from 1/4 $F_{max}$ to $F_{max}$ , where $F_{max}$ is the maximum applied force. From the same batch of fibres, single fibres were selected for fragmentation testing. Monofilament composites were prepared by compression moulding using a polycarbonate matrix (Makrolon 2805, from Bayer). The composites were then subjected to tensile testing in an Instron 4505 universal testing machine, at a cross-head speed of 0.5 mm/min. After testing, the tension was maintained and the specimen, clamped in a frame, was released from the tensile machine and observed under an optical microscope. As the matrix is transparent, the fragment lengths can be visualised and measured directly (1-15).

## 1.4 RESULTS AND DISCUSSION

### 1.4.1 Fibre shape characterisation

Figure 1-2a through g depict SEM micrographs of different types of VGCF grown, for a number of years, in the laboratories of the Centro Nacional de Investigaciones Metalúrgicas (CENIM) in Madrid, Spain. We believe that this set of photographs portrays the most representative morphologies in which VGCF can be observed.

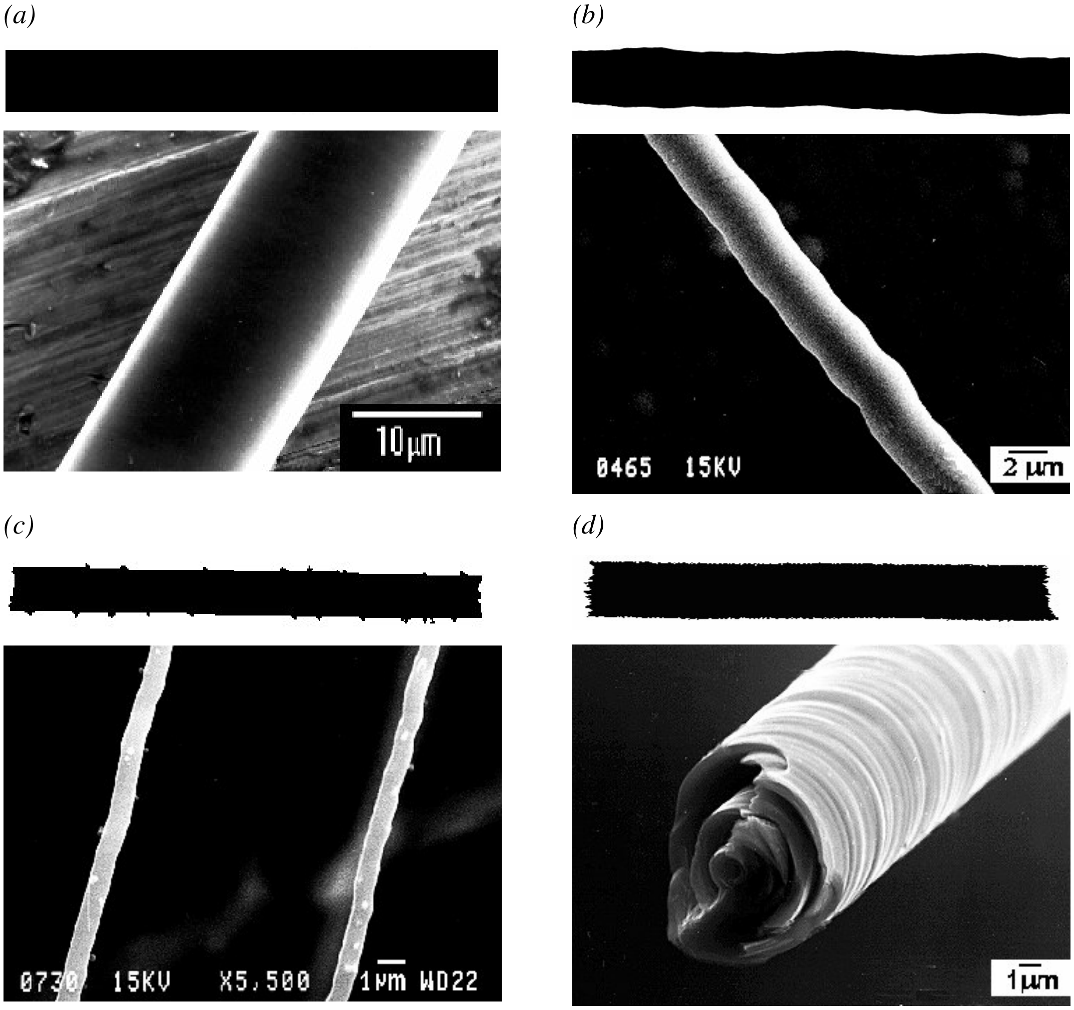

*Figure 1-2. Different morphologies in which VGCF can be produced. (a)"Perfect cylinder"; (b)"Quasi-perfect cylinder"; (c)"Cylinder with debris"; (d)"Finely-screwed thread".*

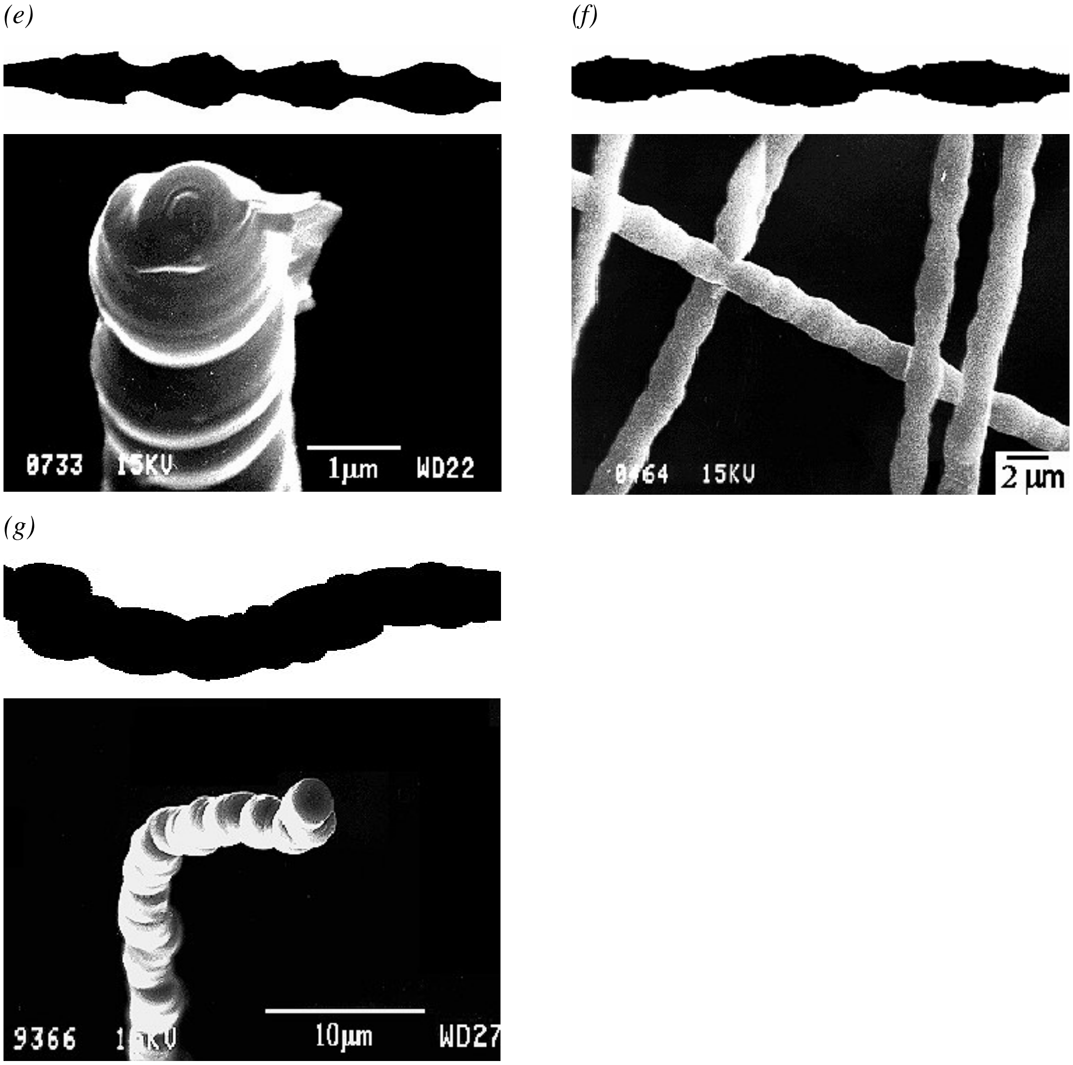

*Figure 1-2. (Continued) Different morphologies in which VGCF can be produced. (e)"Palm tree trunk"; (f)"Lathe shaped"; (g)"Crenulated".*

The characteristic patterns of each of these morphologies, derived from their profiles, are also shown in Figure 1-2. It is clear that for many of these morphologies it is impossible to assign a diameter to the fibres.

### 1.4.2 Mechanical characterisation

The fibres used in the tensile tests correspond to a batch in which "perfect cylinders" predominated. The diameters of the fibres were measured with the laser diffraction technique, at three positions along each fibre's length. The average of the 3 values was considered to be the *average* fibre's diameter. A variation in the values of the diameters was detected over all fibres, as well as along each fibre, although they looked perfectly cylindrical when observed by SEM. The difference between the average diameter and the minimum and maximum diameter found along a fibre's length was typically about +/- 14%. The importance of the diameter chosen for the calculations of the mechanical properties is evident. As the fibres were assumed to break at the cross-section with the smallest area, the minimum diameter of a given fibre was used to calculate its tensile strength. On the other hand, the average diameter was taken for the calculation of its modulus. Table 1-1 summarises the results of the measurements made on more than 60 fibres. The mean of the average diameters of all fibres and the corresponding standard deviation are presented, as well as the maximum and the minimum diameters measured in the whole batch.

*Table 1-1. Diameters determined on 'perfect cylinder' VGCF.*

| Fibre diameter (μm) | | | |
|---|---|---|---|
| Mean | St. dev. | Max. | Min. |
| 11.7 | 3.2 | 20.7 | 4.4 |

In Figure 1-3 a plot of the total compliance as a function of *l/A* (equation [1.3]), as well as the least-squares line used to calculate the average tensile modulus are presented. From the intercept and the slope, values of 875 μm/N and 140 GPa, for the system compliance and the modulus, respectively, were obtained.

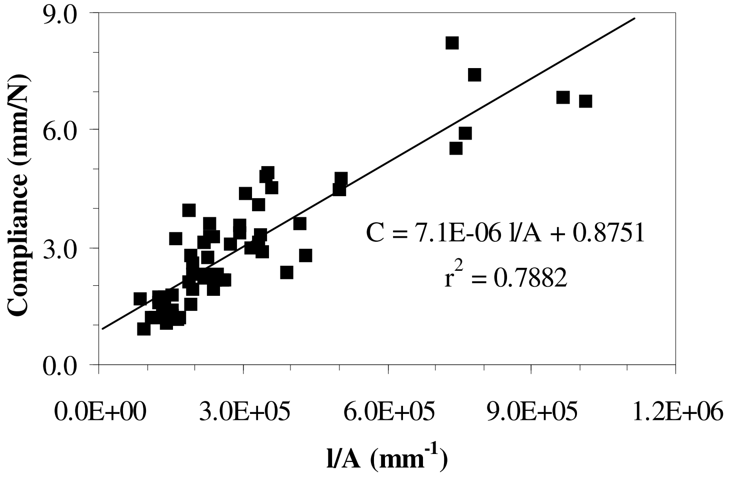

*Figure 1-3. Total compliance $C_t$ as a function of l/A.*

In the above calculation, the average modulus was supposed to be constant for all fibres, irrespective of their diameter. However, as mentioned before, the tensile modulus of VGCF is reported to be dependent on the fibre's diameter (1-6,1-16). In order to check this effect, the fibres were separated in two sets: one corresponding to the fibres with an average diameter below 10 μm and the other to those with a diameter above 10 μm. The mean, maximum and minimum diameters for the two sets are given in Table 1-2.

*Table 1-2. Diameters determined on 2 sets of 'perfect cylinder' VGCF.*

| Set of fibres | Fibre diameter (μm) | | | |
|---|---|---|---|---|
| | Mean | St. dev. | Max. | Min. |
| diameter ≤ 10 μm | 8.6 | 0.9 | 10.0 | 7.1 |
| diameter > 10 μm | 13.7 | 2.3 | 19.0 | 10.1 |

The same procedure used above for the calculation of the average modulus was repeated for the two sets of fibres. Tensile moduli of 165 GPa and 125 GPa for the fibres with diameters below and above 10 μm, respectively, were calculated. It is now clear that the moduli of the fibres decrease as their diameters increase. However, the values of the moduli are lower than those reported by Tibbetts and co-workers, using a test system similar to ours (1-6,1-16). This may be due to a lower degree of graphitic ordering of our fibres or to a more exact measurement of the diameters in the present work.

Using the methodology described in section 1.2.1, the Weibull parameters relevant for the determination of the tensile strength were calculated. The main Weibull parameters are summarised in Table 1-3. In the table, the dependencies on the fibre length are expressed in mm.

*Table 1-3. Parameters of the Weibull distribution.*

| $m$ | $\sigma_0(l)$ (MPa) | $\gamma$ | $\sigma_0$ (MPa) | $\bar{\sigma}$ (MPa) | $\beta_v$ (MPa)$^2$ | St. dev. (MPa) |
|---|---|---|---|---|---|---|
| 4.2293 | $\frac{5828.4}{l^{0.3834}}$ | 1.6215 | 5828.4 | $\frac{5299.8}{l^{0.3834}}$ | $\frac{1997450}{l^{0.7668}}$ | $\frac{1413.3}{l^{0.3834}}$ |

The fibre strength results are plotted against the initial gauge lengths of the tested fibres in Figure 1-4. The mean of the Weibull distribution (Weibull expected values), and the 90% confidence limit, are also shown in the figure.

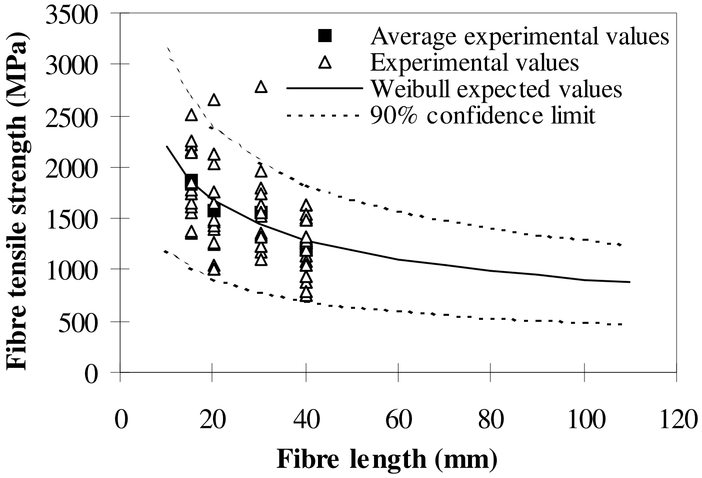

*Figure 1-4.* *Fibre strength data and Weibull confidence limits.*

It is worth noticing that almost all experimental results fall within the 90% confidence limit of the Weibull distribution. As referred to before, a Weibull distribution function was already fitted successfully to the variation of the strength data of VGCF with the diameter (1-6). It is now shown that it is possible to use the same function to describe its dependence on the gauge length. The present results indicate that the Weibull distribution is a good statistical tool to describe the strength data of VGCF. Furthermore it can be noticed that the value for 5 mm gauge length (2.85 GPa, calculated from the relation given in Table 1-3) is comparable to that observed by Tibbetts and Beetz (2.92 GPa) for fibres tested at the same length (1-16).

The average diameter of each individual fibre was determined experimentally, as described above. Hence, it is also possible to represent the fibre tensile strength as a function of the diameter, for each gauge length, as shown in Figure 1-5. From the data in this figure it is apparent that $\sigma$ depends both on the diameter and the length of the fibres.

To get a better idea of the combined effect of diameter and gauge length on the tensile strength, a smoothed weighted average surface fit was performed on the data presented in Figure 1-5. This fit is plotted in 3 dimensions in Figure 1-6. The dual dependence is now clear. From the figure, it can be concluded that the influence of the diameter on $\sigma$ becomes smaller as the tested length of the fibre increases. On the other hand, the variation of $\sigma$ with $l$ is more pronounced for the fibres with smaller diameters. As expected, the highest values of $\sigma$ correspond to the fibres with smaller diameters and smaller lengths. The overall dependence, however, is quite complex.

The conclusions that can be drawn from Figure 1-6 seem reasonable, as the number of potential fatal flaws in the interior of a VGCF should increase with both diameter and length. The relative importance of the flaws' distribution in the axial and radial directions will determine the magnitude of the above variations.

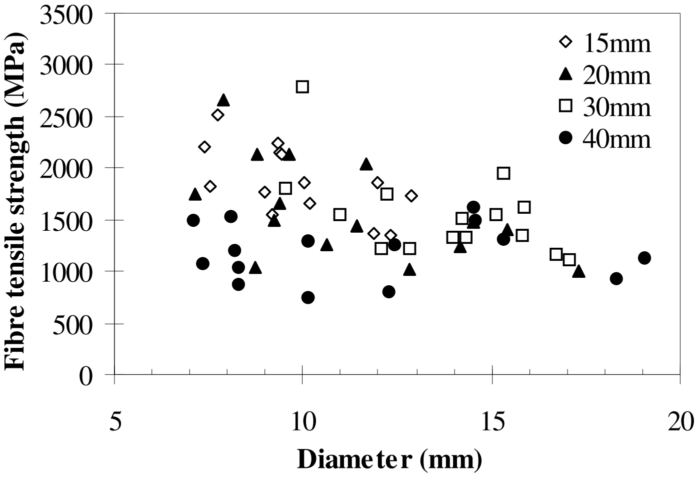

*Figure 1-5. Fibre strength versus average fibre diameter (legend refers to fibre length).*

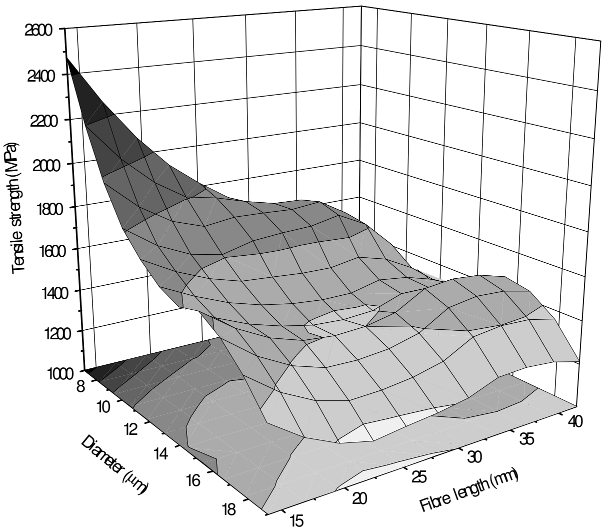

*Figure 1-6. Three-dimensional plot of fibre strength as a function of gauge length and average fibre diameter.*

In this chapter, we have studied the influence of diameter and the length of the fibres on the tensile properties. It was shown that it is possible to treat the VGCF tensile data using the same methodologies that are standard for the ex-PAN and ex-pitch fibres. The effect of the fibre morphology, however, remains an open question. It is obvious that it should be important. In fact, not only the shape of the fibres can make the determination of a "diameter" meaningless, but the surface irregularities may also act as failure initiators. A study to this effect will be described in Chapter 2.

### 1.4.3 Fragmentation test

Monofilament composites were prepared with VGCFs, and subjected to uniaxial tensile testing. The stretched specimens, clamped in a frame, were observed under the microscope to measure the fragment lengths inside the matrix. It was, however, impossible to distinguish the fibre's fragments from each other. To further clarify the problem, the matrix was dissolved in chloroform and the resulting solution carefully filtered. The remaining carbon fibres were then observed by SEM. The results are shown in the micrographs presented in Figure 1-7a through c.

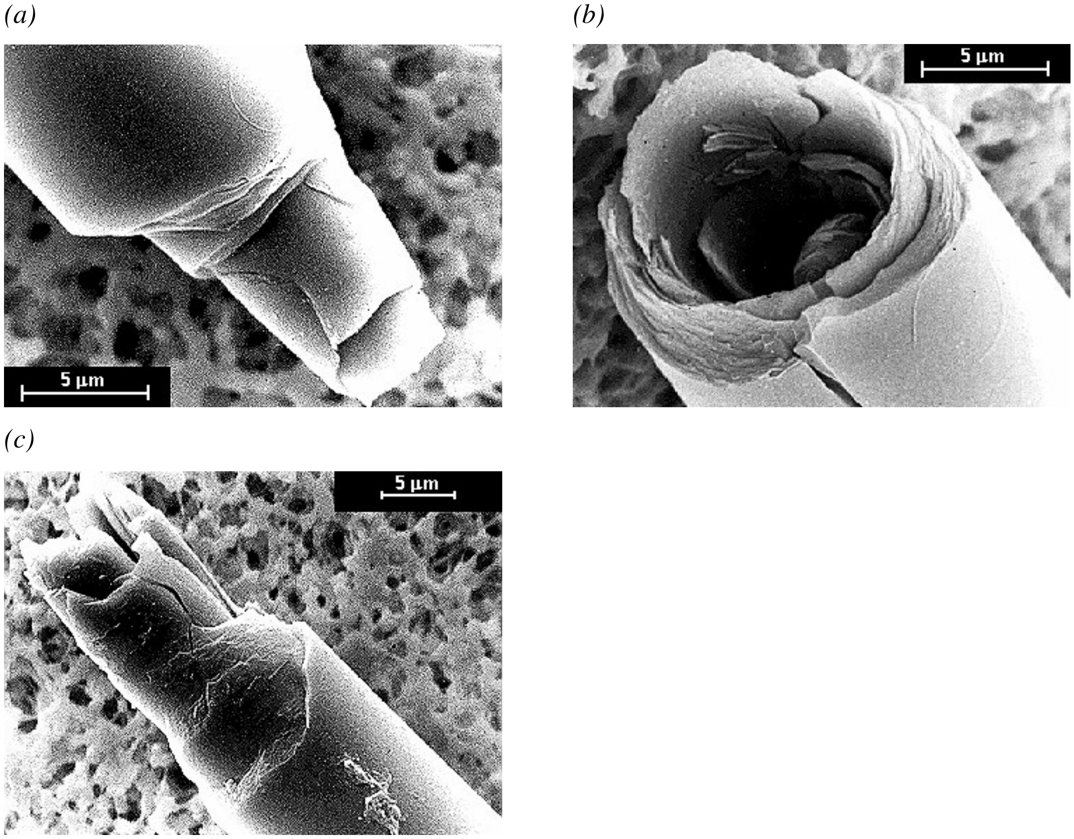

*Figure 1-7. SEM micrographs of VGCF fragments after dissolution of the matrix of monofilament composites.*

It is evident that the impossibility of measuring the fragments is a consequence of the VGCF layered structure and failure mode, referred to before as "sword in sheath" (1-6). With "normal" ex-PAN or ex-pitch fibres, breakages would occur during the test over the whole diameter of the fibre, perpendicularly to the fibre-matrix interface. Under microscopic observation a hole would be visible in the polymer matrix between two adjacent fibre fragments, left after local fibre pull-out (1-15). However, in the case of VGCF, breakage occurs in a different way, the core of the fibre being pulled out of the outer layer like a sword from its sheath. As a consequence, it is impossible to visualise the hole under the microscope.

This can be clearly observed in Figure 1-7. In Figure 1-7a the "sword" part of the breakage is seen, as it was pulled out of the "sheath" part, observed in Figure 1-7b. The micrographs also evidence the layered structure of VGCF: a good indication of the complexity of the fibre breakage is shown in Figure 1-7c.

It seems evident that the fragmentation test cannot be used to determine the quality of the interface of VGCFs in polymeric matrices.

In fact, even if the fragmentation sequence could be followed using a different technique, it would still be impossible to correctly interpret the results. The theory assumes that the force transmission between the fibre and the matrix occurs at the fibre-matrix interface. In the case of VGCFs, the shear-effects (and failure) between the different layers, and the resulting effect on the force transmission, are impossible to quantify. This would make the definition of any interfacial parameters meaningless. It is also evident that the intrinsic failure mode of VGCF makes them particularly interesting for comparative studies of the failure behaviour of unidirectional composites.

## 1.5 CONCLUSION

In this chapter a comprehensive survey of the different morphologies in which VGCFs can be produced is presented. One of the more common morphologies was mechanically characterised by tensile testing, and a Weibull distribution function was used to model the variation of the tensile strength with the gauge length. The Weibull distribution seems to be a good statistical tool to describe the tensile data of VGCFs. It was also possible to analyse in detail the combined effects of both fibre diameter and gauge length on the tensile strength. Finally, it was shown that, because of their failure mode, the interfacial characteristics of VGCF in a polymeric matrix cannot be assessed using the fragmentation method.

## 1.6 REFERENCES

1-1. D. Dutta, M. Husband, D. Ciminelli, and J.W. Hager, in *Extended abstracts of 22nd Biennial Conference on Carbon*, ed. American Carbon Society, San Diego, CA, 292 (1995).

1-2. J.-M. Ting, and M.L. Lake, *Carbon*, **33**, 663 (1995).

1-3. S.W. Hudnut, and D.D.L. Chung, *Carbon*, **33**, 1627 (1995).

1-4. Xiaoping Shui, and D.D.L. Chung, *Carbon*, **34**, 811 (1996).

1-5. R.L. Jacobsen, T.M. Tritt, J.R. Guth, A.C. Ehrlich, and D.J. Gillespie, *Carbon*, **33**, 1217 (1995).

1-6. G.G. Tibbetts, in *Carbon Fibers, Filaments and Composites*, ed. J.L. Figueiredo, C.A. Bernardo, R.T.K. Baker, and K.J. Huttinger, Kluwer Academic Publishers, Dordrecht, 73 (1990).

1-7. A. Madroñero, *Mat: Sci. Eng.*, A-105, L1 (1994).

1-8. E.G. Stoner, Ph.D. dissertation, Department of Chemical Engineering, Clemson University, Clemson, SC (1991).

1-9. W.J. Padgett, S.D. Durham, and A.M. Mason, *J. Compos. Mater.*, **29**, 1873 (1995).

1-10. J.P. Nunes, C.A. Bernardo, A.S. Pouzada, and D.D. Edie, *J. Compos. Mater.*, **31**, 1758 (1997).

1-11. A. Kelly, and W.R. Tyson, *J. Mech. Phys. Solids*, **13**, 229 (1965).

1-12. R.S. Wagner, and W.C. Ellis, *Transactions of the Metallurgical Society of AIME*, **233**, 1053 (1965).

1-13. A. Madroñero, E. Ariza, and M. Verdu, *J. Mat. Chem.*, **6**, 1059 (1996).

1-14. A. Madroñero, *A Reactor for the Production of Short Ceramic Fibres from Gas*, Int. Publication number WO 93/17159 (02.09.93 93/21).

1-15. M.C. Paiva, M. Nardin, C.A. Bernardo, and J. Schultz, *Compos. Sci. Tech.*, **57**, 839 (1997).

1-16. G.G. Tibbetts, and C.P. Beetz, Jr., *J. Phys. D: Appl. Phys.*, **20**, 292 (1987).

# 2 THE EFFECT OF THE MORPHOLOGY ON THE PROPERTIES OF VAPOUR-GROWN CARBON FIBRES[2]

## 2.1 INTRODUCTION

In the previous chapter, the seven different morphologies in which VGCF can be produced were identified. The tensile properties of fibres with one of these morphologies, smooth, nearly straight cylinders with no visible surface irregularities, were measured, and their dependence on both the length and the diameter determined. A SEM micrograph of such a 'perfect cylinder' fibre is presented in Figure 2-1a, together with its characteristic profile.

However, to assess the effect of the fibre shape on the mechanical properties requires the testing of other morphologies. Therefore, in addition, in this chapter a batch of VGCFs, in which two of the other morphologies predominated, has been studied. These were the 'quasi-perfect cylinder' (straight fibres with some surface irregularities, not very pronounced) and the related 'crenulated' (curved fibres with more pronounced surface irregularities). These fibre shapes are shown in Figure 2-1b and c. The reactor used in this work was a vertical, 1 metre long mullite tube, 25 mm in diameter, which was externally heated by an electric furnace connected to a temperature programmer. The fibres were grown on a graphite substrate, pre-impregnated by spraying a solution of the iron precursor and dried in an oven before placement in the reactor. Reactants used were hydrogen and methane as the carbon source. The support was heated to 950°C in an atmosphere of 70% hydrogen and 30% methane, at a flow rate of 150 $cm^3$/min. The temperature was then raised to 1150°C, leading to the production of very thin fibres (diameter $\leq 1\ \mu m$), which can reach several centimetres in length. Subsequent thickening of these fibres took place at a temperature of 1150°C. Further experimental details on the production of these VGCFs can be found in reference (2-1). Although a precise determination of their relative proportion in the batch is impossible, a statistical analysis based on detailed SEM observations led to approximate values of 50% and

---

[2] Reproduced, with adaptations, from: F.W.J. van Hattum, Ph. Serp, J.L. Figueiredo, and C.A. Bernardo, Carbon, **35**, 860 (1997).

45% for the ‘quasi-perfect’ and ‘crenulated’ fibres, respectively. Other VGCF morphologies were also observed, but in minor proportions, being only an estimated 5% of the totality of the fibres.

## 2.2 RESULTS AND DISCUSSION

The diameters and tensile properties of the VGCF with these two shapes were determined using the same methodology and gauge lengths previously used with the ‘perfect cylinders’ (see Chapter 1, section 1.3.).

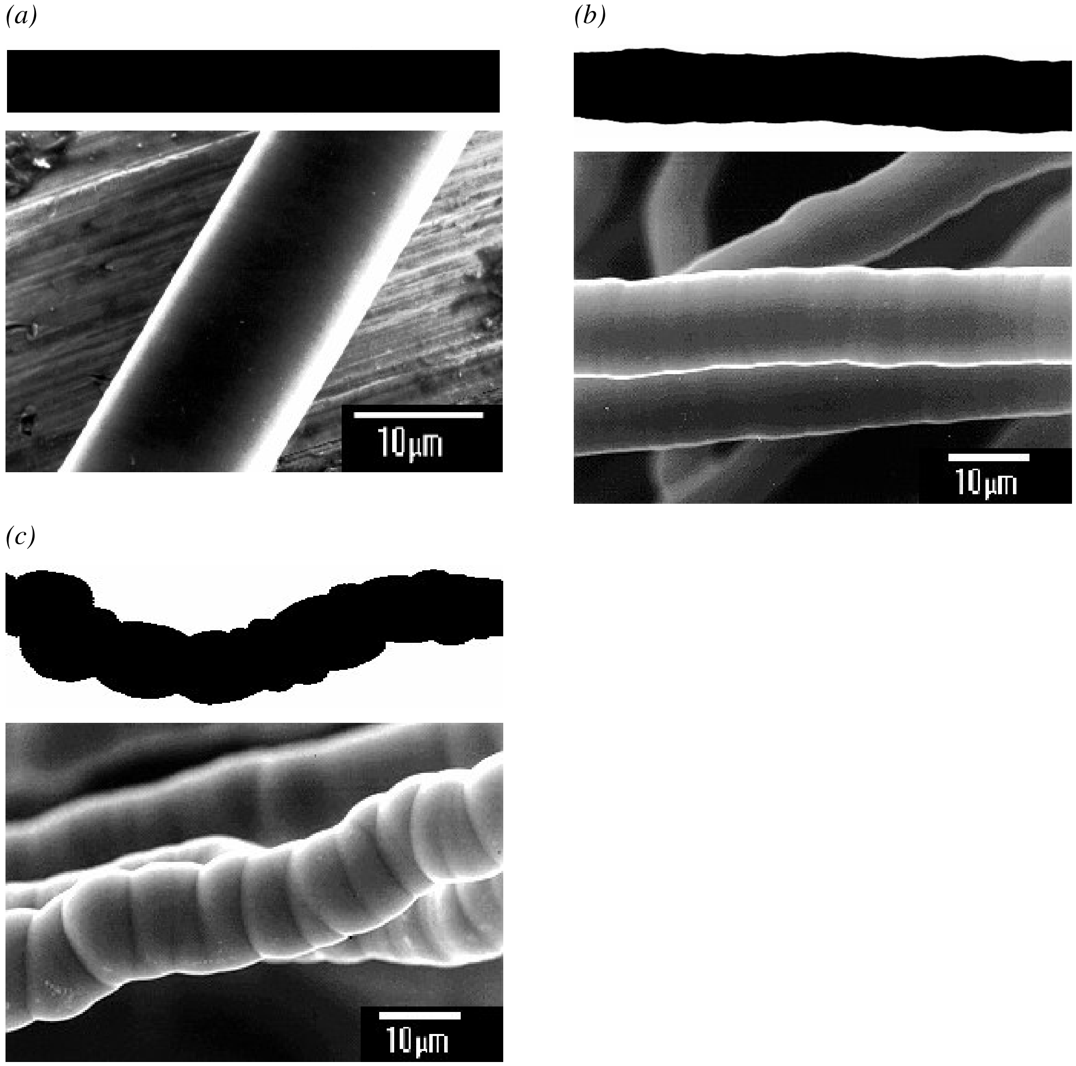

*Figure 2-1. Different shapes of VGCFs. (a)’Perfect cylinder’; (b)’Quasi-perfect cylinder’; (c) ‘Crenulated’.*

As the fibres are very fragile, it is very difficult to separate the two morphologies prior to testing. It was thus decided to test them together. The aggregated values of the diameters and the tensile modulus determined for the two shapes are given in Table 2-1, together with the same values for the 'perfect cylinders'.

A decrease in tensile modulus from 'perfect cylinder' to 'quasi-perfect cylinder/crenulated' of 140 GPa to 110 GPa (21%) can be observed. However, the differences in the ranges of the diameters of the two batches of fibres should be taken into account, as they influence the value of the modulus. As referred to in the previous chapter, it is already known that the moduli decrease with increasing fibre diameter (2-2, 2-3). The dependence of the tensile modulus on fibre diameter in the present set of fibres was verified by dividing it into two sets: one corresponding to the fibres with an average diameter below 15 μm and the other to those with a diameter above 15 μm. Values for the tensile modulus of 112 GPa and 101 GPa, for the fibres with diameters below and above 15 μm, respectively, were determined. This shows that the tensile modulus of 'non-perfect cylinder' fibres also decreases with increasing fibre diameter. Using the data reported by Tibbetts (2-2), a decrease in modulus comparable to that found in the present work can be obtained when the diameter increases 35 %. It is, thus, quite probable that the present difference in the moduli between 'perfect cylinder' and 'quasi-perfect cylinder/crenulated' can be attributed to the difference in the mean diameter of the fibres between the two batches. This means that the tensile modulus is not significantly affected by the fibre morphology.

*Table 2-1. Diameters of 2 batches of VGCF with different shapes.*

| Fibre morphology | Fibre Diameter (μm) | | | | Modulus |
|---|---|---|---|---|---|
| | Mean | St. dev. | Max. | Min. | (GPa) |
| 'Perfect cylinder'* | 11.7 | 3.2 | 20.7 | 4.4 | 140 |
| 'Quasi-perfect cylinder/crenulated' | 18.3 | 2.0 | 24.8 | 10.7 | 110 |

**see Chapter 1*

Using the methodology described in Chapter 1, the Weibull parameters relevant for the determination of the tensile strength were calculated. The fibre strength results are plotted against the initial gauge lengths of the tested fibres in Figure 2-2. The expected Weibull values, with the corresponding confidence limits, are also shown in this figure. The conclusion from Chapter 1 that the Weibull distribution is a good statistical tool to describe the strength of VGCF is also confirmed for fibres with ‘quasi-perfect cylinders/crenulated’ shapes. In fact, as can be seen in Figure 2-2, almost all the experimental results fall within the 95% confidence limit of the distribution. Although the same distribution function, with different parameters, can be successfully used to describe the tensile strength data for both ‘perfect cylinder’ and ‘quasi-perfect cylinder/crenulated’ fibres, the strength values for the latter are significantly lower.

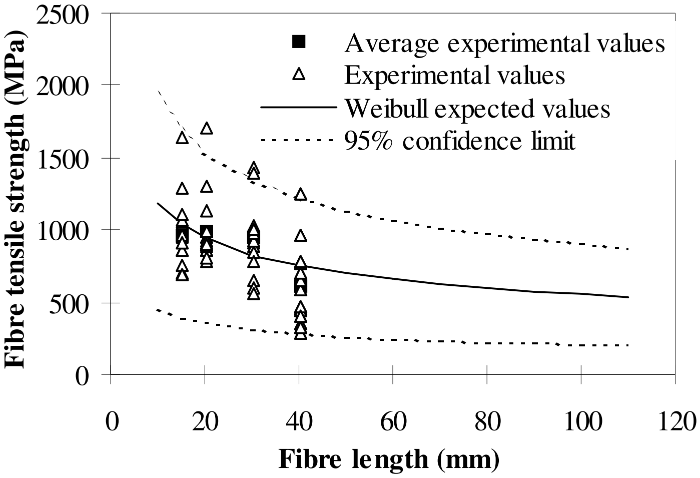

*Figure 2-2. Fibre strength data and Weibull confidence limits for ‘quasi-perfect cylinder / crenulated’ fibres.*

*Table 2-2. Calculated tensile strength for the 2 batches of VGCF.*

| | ‘Perfect cylinder’* | | ‘Quasi-perfect cylinder/crenulated’ | |
|---|---|---|---|---|
| Fibre length (mm) | Tensile Strength (GPa) | | Tensile Strength (GPa) | |
| | Mean ($\bar{\sigma}$) | St. dev. | Mean ($\bar{\sigma}$) | St. dev. |
| 5 | 2.9 | 0.76 | 1.5 | 0.48 |
| 10 | 2.2 | 0.58 | 1.2 | 0.38 |
| 15 | 1.9 | 0.50 | 1.0 | 0.34 |
| 20 | 1.7 | 0.45 | 0.94 | 0.31 |
| 30 | 1.4 | 0.38 | 0.83 | 0.27 |
| 40 | 1.3 | 0.34 | 0.75 | 0.24 |

*see Chapter 1*

This can be seen in Table 2-2, where the values of the tensile strength determined for the present batch at different gauge lengths, are compared with those of the ‘perfect cylinders’. Over the whole range of gauge lengths a decrease in tensile strength from ‘perfect cylinders’ to ‘quasi-perfect cylinders/crenulated’ of approximately 45% can be observed.

This effect can not be attributed to the difference in diameter range between the two batches of fibres, as clarified in Figure 2-3. The figure shows the combined effect of both diameter and gauge length on the strength, evidentiated through a smoothed weighted average surface fit on the tensile data. The fit of the ‘perfect cylinder’ data from Chapter 1, corresponds to the upper surface and that of the ‘quasi-perfect cylinder/crenulated’ to the lower surface.

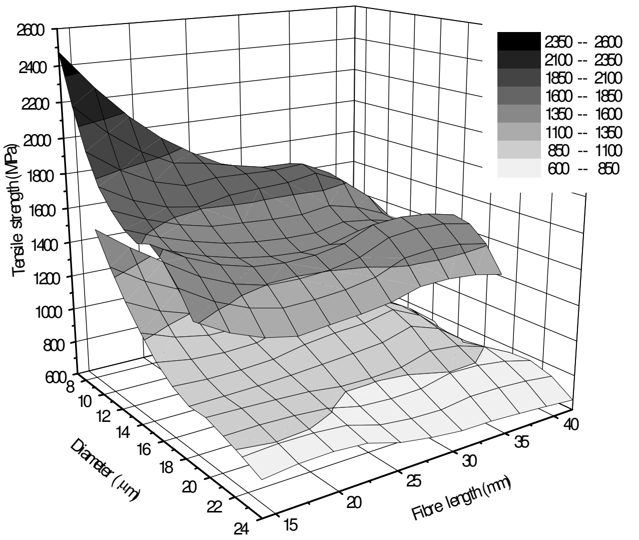

*Figure 2-3.* *Three-dimensional plot of the fibre strength as a function of gauge length and average fibre diameter for both ‘Perfect cylinder’ and ‘Quasi-perfect cylinder / crenulated’ fibres.*

It can be seen that over the whole range of fibre diameters and lengths, the tensile strength values of the ‘quasi-perfect cylinder/crenulated’ fibres are lower than those of the ‘perfect cylinder’ fibres. From these results it can be concluded that the shape of the fibres has a significant decreasing effect on the tensile strength. It can also be concluded that the influence of the diameter on the tensile strength becomes smaller as the tested length of the fibre increases. Identically, the variation of the tensile strength with the tested length becomes more pronounced for fibres with smaller diameters. This agrees with what was observed in the previous chapter for ‘perfect cylinders’. A plausible conclusion is that the overall dependence of tensile strength on both fibre diameter and length is qualitatively similar for all the fibre shapes, albeit quantitatively dependent on the fibre morphology.

One problem, already pointed out in Chapter 1, still remains: which diameter is actually measured? Although the current batch of fibres has a morphology that results in large ‘local’ diameter variations over the fibre length, the laser diffraction technique used is unable to distinguish these diameter variations. Instead, it measures an averaged ‘global’ diameter over a certain part of a fibre, although in this part various sharp ‘necks’ might exist with a resulting smaller diameter. However, the fibre is most likely to break at this neck, due to, for instance, stress concentrations. Using the ‘global’ diameter will lead to a diminished fibre tensile strength, as a result of an incorrectly overestimated fibre area. On the other hand, the calculation of the fibre tensile strength using the appropriate ‘local’ diameter at the point of actual breakage (neck) could have led to a higher value. Thus, it is possible that VGCFs containing pronounced surface irregularities, although showing a lower ‘global’ tensile strength, might actually have no significantly lower ‘local’ tensile strength. This means that the measured decrease in tensile strength may result from pure geometrical considerations and not from differences in the internal structure of VGCF with different morphologies.

In the previous chapter we showed the difficulties associated with assessing the interfacial characteristics of VGCF in a polymeric matrix using the fragmentation method. In the case of smooth-surface, cylindrical fibres, it was impossible to distinguish the fragments from each other after testing. With "normal" ex-PAN or ex-pitch fibres, breaks would occur during the test over the whole diameter of the fibre, perpendicularly to the fibre-matrix interface. If the samples are kept stretched at the end of the rupture events, and observed under an optical microscope, a hole would be visible in the polymer matrix between two adjacent fibre fragments left after local fibre pull-out. However, in the case of VGCFs, due to the layered structure and inherent failure mode, known as "sword in sheath" (2-2), breakage occurs in a different way. The core of the fibre is pulled out of the outer layer like a sword from its sheath. As a consequence, it is impossible to find the hole under the microscope. In the current batch of VGCF, it was expected that, due to the surface irregularities, enhanced mechanical interlocking between the fibre and the matrix could overcome some of the difficulties reported before. To test this hypothesis, fragmentation tests were performed according to a technique previously described (2-4,2-5 and Chapter 1, section 1.3.3.). No significant improvements were observed, however, as it was still impossible to detect the fibre fragments at the end of the fragmentation experiments.

It is again confirmed that the fragmentation test cannot be used to determine the quality of the interface of VGCFs in polymeric matrices. In fact, even if the fragmentation sequence could be followed using a different technique, it would still be impossible to interpret correctly the results. The theory assumes that the force transmission between the fibre and the matrix occurs at the fibre-matrix interface (2-5), which is not the case with VGCF.

## 2.3 CONCLUSION

From the work presented in this chapter, it can be concluded that the shape of VGCFs has a small influence on the value of the tensile modulus. However, fibres with shapes different from perfect cylinders, have a lower apparent tensile strength. This may result from pure geometrical considerations, and not from differences in the inner structure of the fibres. The fragmentation test cannot be used to assess the interfacial properties of VGCF in polymeric matrices, irrespective of the morphology.

## 2.4 REFERENCES

2-1. Ph. Serp, and J.L. Figueiredo, *Carbon*, **34**, 1452 (1996).

2-2. G.G. Tibbetts, in *Carbon Fibers, Filaments and Composites*, ed. J.L. Figueiredo, C.A. Bernardo, R.T.K. Baker and K.J. Huttinger. Kluwer Academic Publishers, Dordrecht, 73 (1990).

2-3. G.G. Tibbetts, and C.P. Beetz, Jr., *J. Phys. D: Appl. Phys.*, **20**, 292 (1987).

2-4. A. Kelly, and W.R. Tyson, *J. Mech. Phys. Solids*, **13**, 229 (1965).

2-5. M.C. Paiva, M. Nardin, C.A. Bernardo, and J. Schultz, *Compos. Sci. Tech.*, **57**, 839 (1997).

# Part II

## *Vapour Grown Carbon Fibre Thermoplastic Composites*

# 3 PRODUCTION AND ASSESSMENT OF VAPOUR GROWN CARBON FIBRE-POLYCARBONATE COMPOSITES[3]

## 3.1 INTRODUCTION

Carbon fibres are widely used as reinforcements for polymeric matrices in many high technology applications, due to their high specific tensile modulus and strength and excellent electrical and thermal properties. VGCFs seem to be quite adequate to reinforce high consumption thermoplastics using conventional processing technologies. However, they are yet to realise their potential in commercially important applications.

As explained in the *Introduction*, VGCFs are prepared via the catalytic decomposition of a gaseous carbon source. The fibres investigated in Chapters 1 and 2 have been produced on catalyst-seeded substrates, in two independent sequential stages. In this way, fibres with diameters up to 100 μm and several centimetres in length have been produced in batch conditions (see also reference 3-1).

An alternative method of preparing VGCF uses a gas phase catalyst that stays unsupported inside a continuous flow reactor (3-2). In this technique, the fibres are produced in just one stage, that incorporates both lengthening and thickening, at much higher rates and lower costs. This makes them commercially more interesting for application in for instance short fibre reinforced (thermoplastic) composites. However, as the residence times are short, the lengths of the fibres are usually below 100 μm and their diameters below 200 nm. Because of this, they are sometimes called submicron (diameter) fibres.

Since the original work of Koyama and Endo, on the production and structure of VGCF (3-3,3-4), a large number of publications has described their growth methods and properties. Topics related to the graphitisability, morphology, structure and physical properties of the longer, batch produced, fibres were covered in two comprehensive reviews (3-5,3-6). Fewer works, however, were dedicated to the applications of these fibres, namely of the shorter ones (3-7,3-8,3-9).

---

[3] Reproduced, with adaptations, from: O.S. Carneiro, J.A. Covas, C.A. Bernardo, G. Caldeira, F.W.J. van Hattum, J.-M. Ting, R.L. Alig, and M.L. Lake, *Compos. Sci. Techn.*, **58**, 401 (1998).

The study presented in this chapter was induced by the balance between the cost and processability of the "short" (submicron diameter) VGCF´s and the expected properties of the resulting composites. Various problems related to the industrial use of these fibres in the production and processing of composites can be anticipated. Amongst these are: i) laborious manipulation, due to their very low apparent density; ii) difficult incorporation into highly viscous matrices; iii) poor composite´s properties, resulting from the dimensions of the fibres. Therefore, the objectives of the present work include the assessment of the practical feasibility of using submicron VGCF to manufacture thermoplastic composites, the investigation of the processability of the composites and the analysis of the VGCF's reinforcing capabilities. Although the complete characterisation of the composites would require measurements of fibre aspect ratio, degree of fibre orientation and fibre properties, among others, the (submicron) size of the VGCF does not allow direct measurement of these parameters. Alternative ways to derive these properties, by 'inversing' micromechanical modelling of the composites, will be presented in Chapter 6 of this thesis.

The work in this chapter was carried out according to the following protocol: first, polycarbonate-VGCF (PC-VGCF) composites with 5, 10, 20 and 30% fraction by weight of VGCF, were produced and characterised. The 30 wt.% composite was not used in subsequent steps, as its brittleness caused difficulties in the injection moulding operation. Next, 20 wt.% composites were prepared with oxygen plasma treated fibres, in order to assess the influence of the fibre-polymer adhesion in the composites´ mechanical performance. Finally, composites with 20 wt.% of as-grown (untreated) VGCF were processed using SCORIM (Shear Controlled ORientation Injection Moulding), in an attempt to maximise the alignment of the fibres in the flow direction. In this process, developed at the University of Brunel, England, this is done by submitting the melt in the mould to a controlled shear force induced by reciprocating pistons acting during the cooling stage of the injection moulding (3-10).

## 3.2 EXPERIMENTAL

### 3.2.1 Materials

The VGCFs used in the present work were produced through a proprietary process based on a patent by G.G. Tibbetts and co-workers (3-2). These fibres, supplied by Applied Sciences, Inc., Cedarville, Ohio, USA, and known commercially as Pyrograf III®, were made in a reactor consisting of a horizontal mullite tube, 244 cm long and with an internal diameter of 13.5 cm, at a minimum temperature of 1100 °C. The feedstock was a mixture of 99.99 % pure methane ($25.35x10^3$ cc/min), 99.99% pure amonia ($3.45x10^3$ cc/min), hydrogen sulfide ($5.86x10^3$ cc/min) and helium ($1.05x10^3$ cc/min), bubbled through 99.5% pure iron pentacarbonyl at room temperature. The fibres were grown for 2 minutes, then the process was stopped for 1.5 minutes, while the fibres were expelled and collected and the operating temperature of the reactor re-established. These two steps were repeated in successive cycles. A considerable amount of fibres can be produced with this semi-continuous process in a relatively short time. This feature is obviously vital for large scale industrial applications.

The as-grown VGCF were analysed by Scanning Electron Microscopy (SEM) and by Electron Spectroscopy for Chemical Analysis (ESCA). Since the area analysed by ESCA is larger than the geometrical surface area of the individual carbon fibres, each analysis provided averaged information on the surface chemistry of a set of VGCFs. The fibres were subsequently de-bulked (densified) with a surfactant to facilitate handling and incorporation into the polymeric matrix.

Some of the VGCFs produced were surface treated using cold oxygen plasma. The treatment was carried out in a Technics Plasma 200-G reactor, activated by microwaves at 2.45 GHz, under 101 Pa oxygen pressure, during 3 minutes, with a power of 75 W. Polycarbonate (PC) is often used as a polymeric matrix in high consumption technological applications, as it combines good engineering properties with a moderate price. Previous studies on the interfacial characteristics of plasma treated ex-pitch carbon fibres-PC composites have shown that the adhesion between these materials is satisfactory (3-11). An injection moulding grade was selected for the present work. It has a MFI of 7-10 (DIN 53735, 300/1.2) and values of $M_n$ and weight $M_w$, determined by GPC, equal to 16000 and 32000, respectively.

### 3.2.2 Manufacture of the composites

Composites in pellet form were manufactured in a co-rotating intermeshing modular Leistritz LSM 30.34 twin-screw extruder, coupled to the relevant downstream equipment. Due to the limited amount of fibres available, ca. 3 kg, preliminary experiments were done to select the operating conditions and the configuration of the screws, using carbon black (CB) with an average particle size of 28-32 nm. The influence of the feed rate, barrel temperature, and geometrical configuration and speed of the screws on the head pressure, melt temperature and mixing quality was ascertained. This resulted in adopting a feed rate of 6 kg/h, a temperature profile reaching 270°C in the extrusion head, and screws with right elements separated by three mixing zones, with kneading blocks, and a venting zone, rotating at 110 rpm.

Processing of PC with the various percentages of VGCF did not raise any special difficulties. Table 3-1 shows the values of operational parameters measured during the extrusion of PC, PC plus VGCF (untreated) and PC plus CB. The incorporation of the fibres into the PC matrix decreases both the power consumption and melt pressure in the extrusion head, thus suggesting a melt lubricating effect. The extrusion of PC with different fractions of CB exhibited a similar behaviour, the effect increasing with the additive content. In contrast, the addition of treated fibres produced a slight increase in power consumption, which can be an indication of better fibre to polymer adhesion.

*Table 3-1. Operational parameters determined in the extrusion experiments.*

| | PC | PC-20%VGCF | PC-2%CB | PC-20%CB |
|---|---|---|---|---|
| Power consumption (A) | 16.5 | 15.5 | 16.5 | 13.5 |
| Melt pressure (MPa) | 2.65 | 1.75 | 1.90 | 1.60 |
| Melt temperature (°C) | 268 | 269 | 265 | 265 |

### 3.2.3 Injection moulding of the composites

The materials used in this chapter were all injection moulded to obtain test specimens: no machining down to required sizes was required. Details of the specimens used can be found in Appendix A. All specimens (apart from the SCORIM specimens) were produced on a 20 Ton Klockner Ferromatic injection moulding machine at the University of Minho. The machine was set with the highest possible values of back pressure (during the plastication stage) and injection moulding speed, to maximise melt homogeneity and degree of fibre orientation, respectively. The injection temperature was set at 305°C and the moulds were maintained at 90°C.

The specimens produced by SCORIM at the Wolfson Centre for Materials Processing at the University of Brunel, England, were obtained both with and without (under conventional conditions) the reciprocating pistons acting during the cooling stage. A low injection pressure had to be used, due to problems in filling the mould.

In this chapter, several different moulds, specimens and manufacturing methods are used. This leads to different fibre orientation states, different matrix morphologies and internal stresses in the tested specimens (see *Introduction*), thus effecting the material properties. Although these parameters have not been measured separately, and sometimes have been altered on purpose (e.g. SCORIM), it was assured that, whenever comparisons between different composites are made, only one of these variables was changed, and the resulting effect on composite properties taken into account. In this way, although the work described in this chapter does cover a range of mould and specimen geometries and processing conditions, valid comparisons are made, thus allowing straightforward conclusions.

### 3.2.4 Mechanical and rheological characterisation

For all specimens (Appendix A, type 1, 3 and 4), tensile tests were carried out at room temperature, according to ASTM D638M, at a testing speed of 5 mm/min, in an Instron 4505 universal testing machine. Up to 1% the deformation was measured using an extensometer, which was removed at higher deformations. The crosshead displacement was then used to calculate the deformation. The elastic modulus was determined for 1% deformation. Charpy-notched type impact tests (Appendix A, specimen type 2 and 4 notched), derived from ASTM D256, were performed at room temperature on a Rosand IFW5 instrumented falling weight machine, using a 25 kg weight and an impact speed of 2 m/s.

The rheological characterisation encompassed capillary (Rosand RH7-2C) and rotational (Weissenberg rheogoniometer) rheometries, at different temperatures. Bagley and Rabinowitsch corrections were applied to the capillary data. Dies of different diameters (0.5, 1.0 and 2.0 mm) were used to cover a wide range of shear rates. The rotational measurements, under steady conditions, were performed on compression moulded specimens, using the parallel-plate geometry (∅40 mm; gap=1500 μm).

## 3.3 RESULTS AND DISCUSSION

### 3.3.1 Characterisation of the fibres

A micrograph showing typical fibres is presented in Figure 3-1. Their geometrical characteristics and density are shown in Table 3-2.

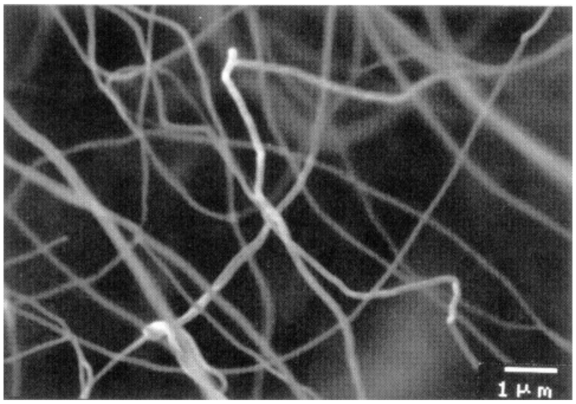

*Figure 3-1. SEM micrograph of the Pyrograf III®.*

The ESCA survey spectra showed peaks of carbon ($C_{1s}$), oxygen ($O_{1s}$), sulphur ($S_{2p}$) and nitrogen ($N_{1s}$) and a peak that may be due to adsorbed water and/or oxygen ($O_2$). The elemental surface composition of the carbon fibre sample is shown in Table 3-3.

*Table 3-2. Geometrical characteristics and density of VGCF.*

| Average diameter (μm) | Aspect ratio | Length (μm) | Density |
|---|---|---|---|
| 0.2 | 250-500 | 50-100 | 1.95 |

*Table 3-3. Elemental composition of the carbon fibre surface.*

| Element | C | O | N | S |
|---|---|---|---|---|
| atomic % | 98.3 | 1.0 | 0.4 | 0.3 |

The most intense peak in the $C_{1s}$ spectra of the carbon fibre samples was the graphite peak. Its presence and the plasmon peak showed that graphite-like structures were present on the surface of the carbon fibres. The spectra also showed pronounced $C_1$ peaks. The $O_{1s}$ spectra showed two peaks for most samples: a peak for oxygen with two bonds due to carbon or to sulphur ($O_1$) and, as referred, a peak which may be due to adsorbed water and/or oxygen ($O_2$).

After being de-bulked with the surfactant, the oxygen concentration on the surface of the fibre increased to 7.8 atomic %, with a concomitant increase of the peak corresponding to adsorbed water and/or oxygen. The more likely explanation is that oxygen-containing groups, originating from the surfactant, remain adsorbed on the surface.

Only de-bulked fibres were subjected to cold oxygen plasma. As a result of the treatment, the oxygen content on the surface of the fibres was increased to 12.6 %.

### 3.3.2 Properties of composites made with as-grown VGCF

The relative mechanical properties of the different PC-VGCF composites (tensile specimen type 1 and impact type 2, Appendix A) shown in Figure 3-2, are represented using PC as a reference. The incorporation of the fibres increases both the tensile strength and the modulus, the effect being proportional to the amount of fibres incorporated. The PC-20%VGCF composite exhibits an improvement of about 39% for the modulus and of 17% for the yield stress, relative to PC. Thus, VGCF have some reinforcing capacity, although not very large. Furthermore, there is a major decrease in impact properties with the incorporation of fibres, suggesting poor adhesion to the PC matrix.

This was confirmed by scanning electron microscopy of fractured surfaces. As shown in the micrograph of Figure 3-3, free fibres, apparently not wetted by the polymer, can be easily observed.

The overall mechanical properties of these composites were compared with those obtained using a chemically similar additive, CB. As shown in Figure 3-4, VGCFs are only marginally better reinforcements than CB.

In a later set of experiments the processing conditions, as well as the geometry of the mould cavity (tensile specimen type 3 instead of 1, Appendix A), were changed, in an attempt to optimise the mechanical properties. These were checked for the 20 wt.% composite. It was possible to improve the tensile properties relatively to the unreinforced PC (+72% for the modulus and 19% for the strength), but the impact properties remained unchanged.

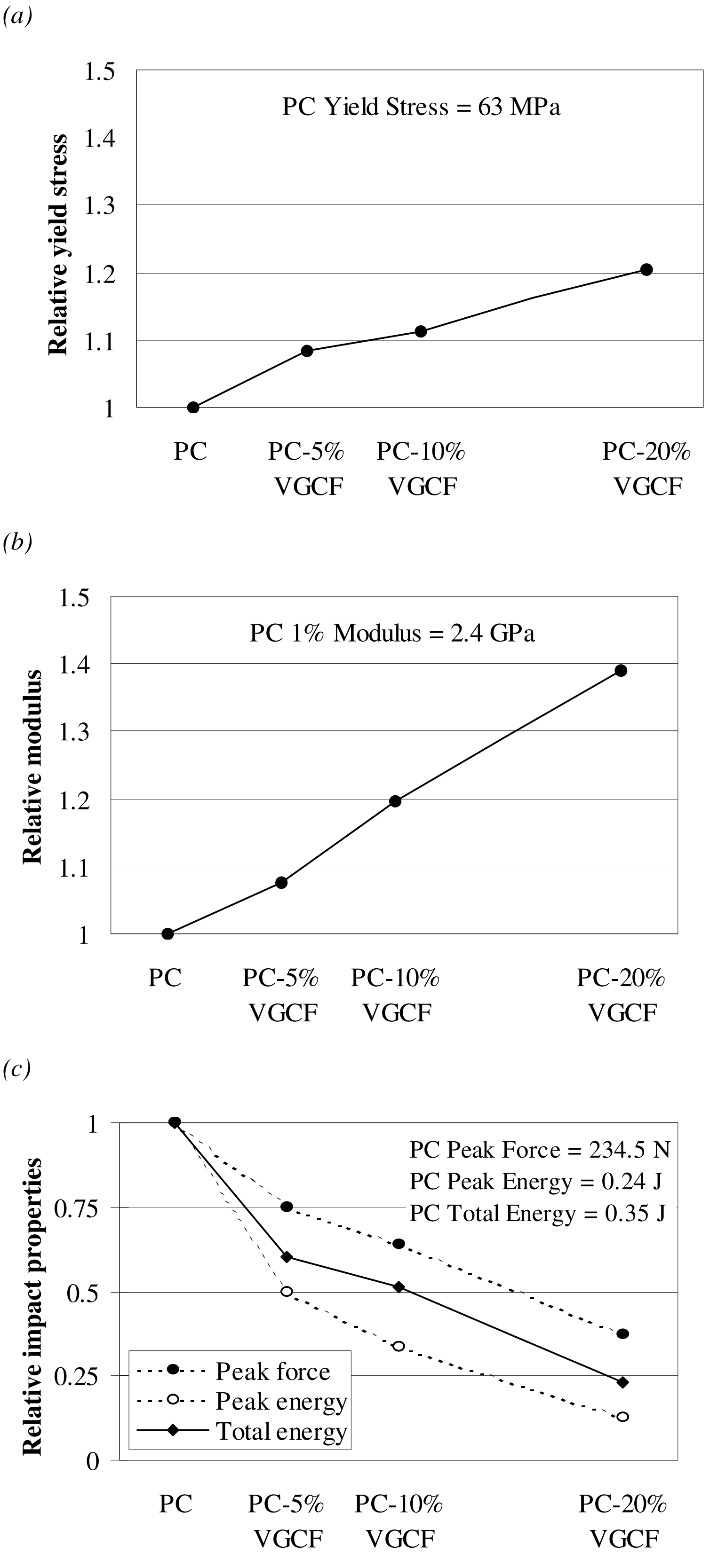

*Figure 3-2. Relative mechanical properties of PC-VGCF composites. (a) Yield stress; (b) Modulus at 1% strain; (c) Impact properties.*

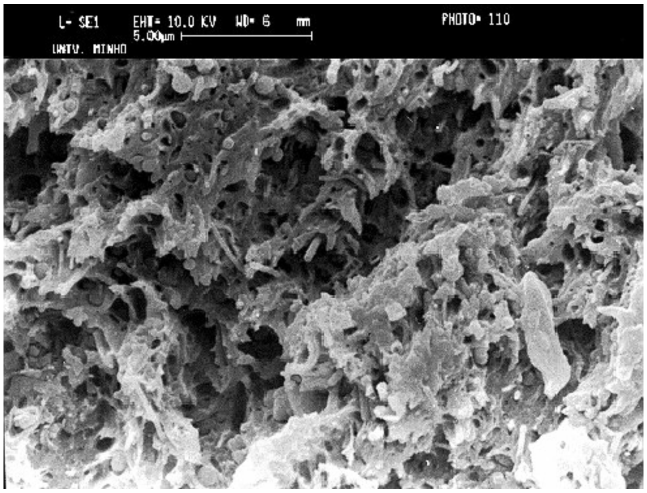
L- SE1 EHT= 10.0 KV WD= 6 mm
5.00µm
PHOTO= 110
UNIV. MINHO

*Figure 3-3. SEM micrograph of a fractured surface.*

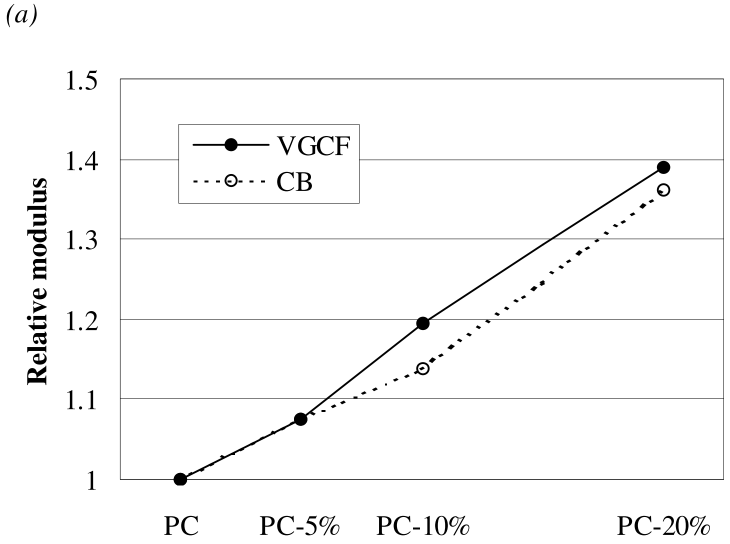

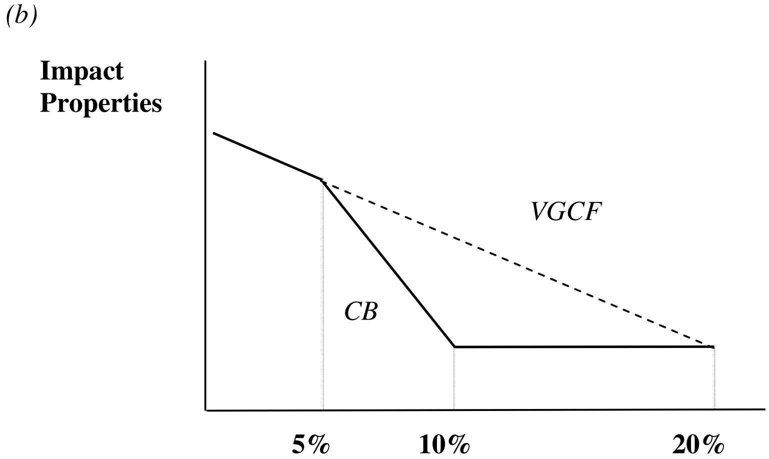

*Figure 3-4. Comparison of the relative properties of PC-VGCF and PC-CB composites: (a) Modulus at 1% strain; (b) Impact properties.*

The shear flow properties of PC and of the PC-VGCF composites are presented in Figure 3-5. PC displays a Newtonian plateau at low shear rates ($3x10^{-2}$ to 2 $s^{-1}$) and a pseudoplastic behaviour at higher deformation rates (2 to $7x10^{3}$ $s^{-1}$). This response is adequately described by a Carreau type equation (3-12).

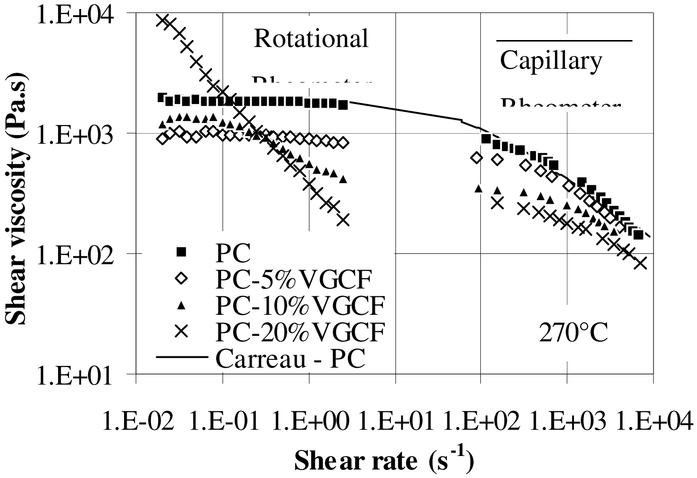

*Figure 3-5. Shear viscosity of the PC and the PC-VGCF composites.*

The viscosity of the composites in the typical shear rate processing range (1 to $10^{3}$ $s^{-1}$) decreases with increasing content of VGCF, which explains the lower power consumption observed during the extrusion of reinforced PC. This feature may be promoted by fluid wall slip, or be related to the eventual fibre orientation in the flow direction (supported by the development of normal stresses in the melt (3-13)), resulting in a layered stream (3-14). This would produce local shear rates in the PC higher than those imposed macroscopically, the effect being more pronounced with increasing fibre content and melt pseudoplasticity. The flow curves seem to converge at higher shear rates, thus evidencing a progressively smaller dependence on fibre concentration. As fibres become more oriented, the probability of fibre-fibre collisions is reduced (3-15).

However, at low shear rates ($3x10^{-2}$ to $2x10^{-1}$ $s^{-1}$), the viscosity of the composites is higher than that of PC. This could be due to the development of weak structures of non-aligned fibres (3-16), or from fibre-fibre collisions, especially at higher concentrations. Also, the Newtonian plateau shortens with increasing fibre content.

Figure 3-6 depicts the changes in rheology observed upon manufacturing and injection moulding PC-VGCF composites. The lower viscosity levels of the injected composite are not related to the eventual degradation of PC, as no significant variation of the average molecular weight, determined by GPC using fresh, extruded, and injected samples of unreinforced PC, could be detected.

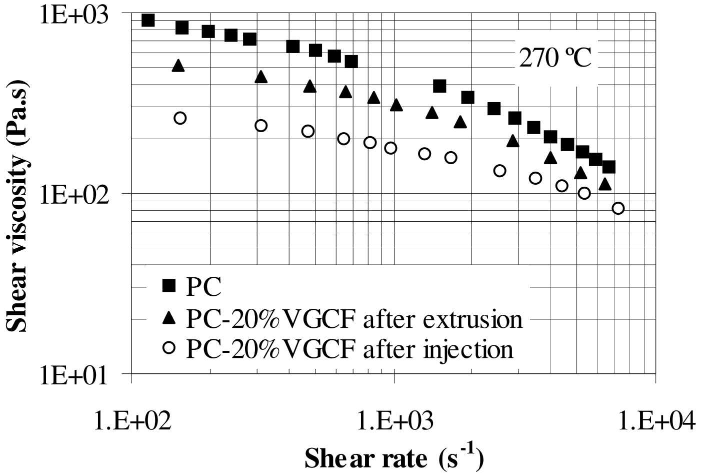

*Figure 3-6. Shear viscosity of the PC and the PC-20%VGCF composite after extrusion and after injection.*

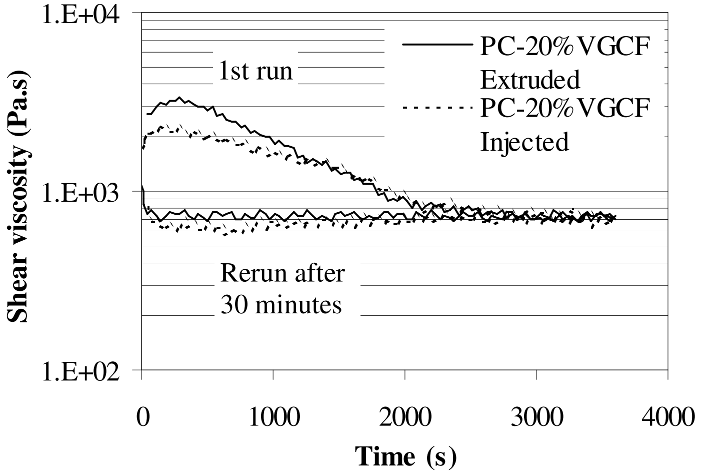

*Figure 3-7. Time sweep for PC-20%VGCF composite after extrusion and after injection.*

Again, fibre orientation is a plausible explanation for the differences shown, since the injection moulded composites were subjected to higher shear rates. This effect could be confirmed from time sweep data obtained in the rotational rheometer, at a constant shear rate of 0.2 $s^{-1}$. This is shown in Figure 3-7. During the first run, the viscosity decreases progressively with time and stabilises after circa 33 minutes. A second identical run, 30 minutes later, shows that the previous orientation is irreversible.

### 3.3.3 Properties of composites made with plasma treated VGCF

The relative mechanical properties of the 20% VGCF composites (tensile specimen type 3 and impact specimen type 2, Appendix A), produced with treated and untreated fibres, are compared in Table 3-4. The reported values of the latter correspond to the optimised conditions, as referred to in section 3.3.2. Representative stress-strain curves from the tensile tests on the composites with untreated fibres are given in Appendix B, Figure B-1. Apparently, as shown in the last column of the table, the fibre treatment has little influence on the mechanical performance of the composites. Although the impact resistance increases, it remains significantly lower than that of PC.

*Table 3-4. Relative differences (%) in tensile and impact properties, resulting from fibre treatment.*

| | | PC-20%VGCF (treated) vs. Unreinforced PC | PC-20%VGCF (untreated) vs. Unreinforced PC | PC-20%VGCF (treated) vs. PC-20%VGCF (untreated) |
|---|---|---|---|---|
| Tensile tests | 1% Modulus | +63 | +72 | -5 |
| | Yield strain | -30 | -43 | +23 |
| | Yield stress | +22 | +19 | +3 |
| Impact tests | Peak force | -43 | -57 | +32 |
| | Peak energy | -89 | -92 | +43 |
| | Total energy | -88 | -92 | +56 |

As shown in Figure 3-8, fibre treatment increases the viscosity levels of the composites beyond those of PC. This may be a consequence of greater fibre-polymer melt interaction. However, this effect is not quite apparent from SEM micrographs of fractured surfaces of composites, made with plasma treated VGCF. Finally, and as discussed previously for Figure 3-6, Figure 3-8 also evidences differences in the viscosity of extruded and injection moulded composites.

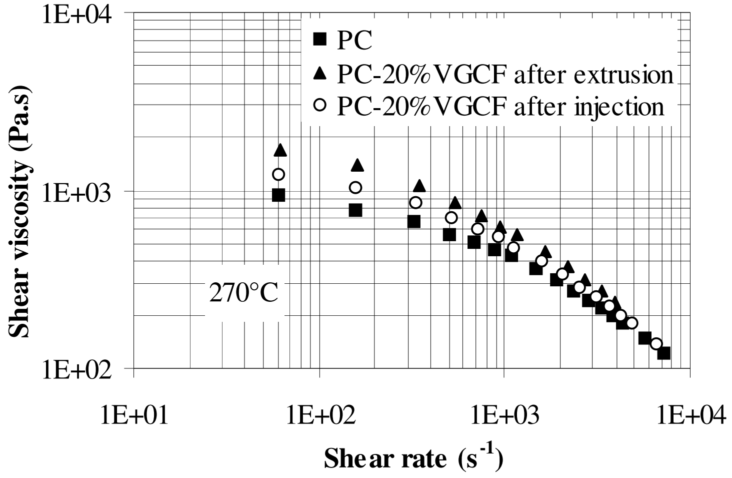

*Figure 3-8. Shear viscosity of PC and PC-20%VGCF composites made with treated fibres, after extrusion and after injection.*

### 3.3.4 Properties of composites made with as-grown VGCF and processed by SCORIM

Table 3-5 presents the relative tensile and impact properties of the PC-20% (as-grown) VGCF composite, obtained using both SCORIM and conventional injection moulding (specimen type 4, Appendix A), in order to show the effect of fibre orientation on the mechanical performance of the composites, expected from that process. The benefit of SCORIM is not particularly impressive, since the tensile properties are little affected and, although the impact resistance is higher, it remains much lower than that of PC.

*Table 3-5. Relative differences (%) in tensile and impact properties as a result of SCORIM.*

| | | PC-20%VGCF (SCORIM) vs. Unreinforced PC (SCORIM) | PC-20%VGCF (SCORIM) vs. PC-20%VGCF (conventional)* |
|---|---|---|---|
| Tensile tests | 1% Modulus | +53 | +1 |
| | Yield strain | -53 | -3 |
| | Yield stress | -8 | -8 |
| Impact tests | Peak force | -29 | +26 |
| | Peak energy | -86 | +96 |
| | Total energy | -90 | +84 |

*same machine as SCORIM, but without inducing shear during processing*

The overall results (presented in Table 3-4 and Table 3-5) may be explained by the presence of polynuclear aromatic hydrocarbons (PAH) on the surface of the fibres. In fact, preliminary findings at General Motors R&D Center, based on gas chromatography/mass spectroscopy/secondary ion mass spectroscopy analyses of extracts from these fibres, were able to detect a substantial amount of PAH, with molecular weights up to 400 (3-17). The PAH may react with the PC, lessening the impact resistance by chemical stress cracking.

## 3.4 CONCLUSION

In this chapter, a comprehensive study is presented of VGCF-PC composites, produced using conventional thermoplastics processing technologies. Both the mechanical and rheological properties of the composites were determined. Structural changes occur during melt flow, affecting irreversibly the viscosity of the system.

Short VGCFs, either as-grown or plasma treated, have some tensile reinforcing capacity, but their incorporation in a PC matrix significantly reduces its impact strength.

SCORIM has no effect on the tensile properties of the composites and, although the impact resistance is improved, it remains much smaller than that of unreinforced PC. The use of a semi-crystaline polymer, such as polypropylene (PP), which has a surface energy closer to that of VGCF and is less prone to chemical stress cracking, may improve this situation. Therefore, a new study using PP and VGCFs with clean surfaces will be presented in the next chapter.

## 3.5 REFERENCES

3-1. G.G. Tibbetts, and M.G. Devour, U.S. Patent No. 4.565.684 (1986).

3-2. G.G. Tibbetts, D.W. Gorkiewicz, and R.L. Alig, *Carbon*, **31**, 809 (1993).

3-3. T. Koyama, *Carbon*, **10**, 757 (1972).

3-4. T. Koyama, and M. Endo, *Ohyo Butsuri*, **42**, 690 (1973).

3-5. M.S. Dresselhaus, G.D. Dresselhaus, K. Sugihara, I.L. Spain, and H.A. Goldberg, *Graphite Fibers and Filaments*, Vol. 5, Springer-Verlag, Berlin (1988).

3-6. G.G. Tibbetts, in *Carbon Fibers, Filaments and Composites*, ed. J.L. Figueiredo, C.A. Bernardo, R.T.K. Baker, and K.J. Huttinger, Kluwer Academic Publishers, Dordrecht, 73 (1990).

3-7. C.J. Dasch, W.J. Baxter, and G.G. Tibbetts, in *Extended abstracts of 21st Biennial Conference on Carbon*, ed. American Carbon Society, Buffalo, NY, 82 (1993).

3-8. D. Dutta, M. Husband, D. Ciminelli, and J.W. Hager, in *Extended abstracts of 22nd Biennial Conference on Carbon*, ed. American Carbon Society, San Diego, CA, 292 (1995).

3-9. S.W. Hudnut, and D.D.L. Chung, *Carbon*, **33**, 1627 (1995).

3-10. P.S. Allan, and M.J. Bevis, Br. Patent 2170-140-B (1987).

3-11. M.C. Paiva, M. Nardin, C.A. Bernardo, and J. Schultz, *Compos. Sci. Tech.*, **57**, 839 (1997).

3-12. M. Gahleitner, and R. Sobczak, *Kunststoffe*, **79**, 1213 (1989).

3-13. H.M. Laun, *Coll. Polym. Sci.*, **262**, 257 (1984).

3-14. Y.G. Yanovsky, *Polymer Rheology: Theory and Practice*, Chapman & Hall (1993).

3-15. R.J. Crowson, and M.J. Folkes, *Polym. Eng. Sci.*, **20**, 934 (1980).

3-16. N.J. Mills, *J. Appl. Polym. Sci.*, **15**, 2791 (1971).

3-17. T.C. Pederson, *Analysis of Polycyclic Aromatics Hidrocarbons Extracted from Pyrograf Fiber Samples*, General Motors R&D Center, internal report (1996).

# 4 A STUDY OF THE THERMOMECHANICAL PROPERTIES OF CARBON FIBRE-POLYPROPYLENE COMPOSITES[4]

## 4.1 INTRODUCTION

In the previous chapter, the production and mechanical characterisation of PC thermoplastic composites reinforced with submicron VGCFs was described. Although this type of VGCFs is commercially attractive, their use poses new problems, as the existing expertise on composite production may in some cases no longer be applied. It was shown, however, that the production of these composites is straightforward using conventional processing technologies. Although the incorporation of the VGCFs in the polymeric matrix led to better mechanical properties, the improvement was only marginal.

The objective of the work presented in this chapter is therefore to produce VGCF-thermoplastic composites with thermomechanical properties significantly better than those of the unreinforced polymer and to compare them with 'conventional' composites. In the previous chapter, it was concluded that the presence of polycyclic aromatic hydrocarbons (PAHs) on the surface of the fibres could cause chemical stress cracking in the PC matrix. As a consequence, in the work described below the fibres were heated to drive off the PAH's before incorporation in the matrix. PP was chosen as a matrix, as this polymer has relatively good mechanical properties at a moderate price and is not very sensitive to chemical stress cracking. For comparison, PP reinforced with PAN-based carbon fibres were also produced and investigated.

---

[4] Reproduced, with adaptations, from: F.W.J. van Hattum, C.A. Bernardo, J.C. Finegan, G.G. Tibbetts, R.L. Alig, and M.L. Lake, *Polym. Compos.*, accepted for publication (1999).

## 4.2 EXPERIMENTAL

### 4.2.1 Materials and sample preparation

The production of the VGCFs, Applied Science's Pyrograf III®, using the method developed by Tibbetts *et al.* (4-1), is described in Chapter 3, section 3.2.1. Montell's Moplen F30G polypropylene, TENAX' PAN-based HTA 5131 carbon fibres and the VGCFs were processed in a Leistritz LSM 30.34 twin-screw extruder to obtain composites with a fibre volume fraction of 15%. The VGCFs were kept in an oven at 200°C for 2 hours prior to processing, to ensure that any PAHs remaining on the fibres' surface had vanished. The extrudate was granulated to obtain composite granules with a length of some millimetres. Prior to further processing, batches with fibre volume fractions of 10% and 5% were obtained by mixing the granulate with unreinforced PP. Tensile bars (Appendix A, type 3), were subsequently injection moulded using a Klockner Ferromatic FM20 injection moulding machine. The processing conditions were kept constant for the different materials, however higher injection pressure and melt temperature had to be used for the PP-VGCF composites. In this way, PP-PAN-fibre and PP-VGCF composite tensile bars were obtained with fibre volume fractions of 5, 10 and 15% respectively. Tensile bars of unreinforced PP were similarly produced. The processing conditions are given in Table 4-1.

*Table 4-1. Operational conditions used in the injection moulding.*

| | PP-PAN | PP-VGCF |
|---|---|---|
| Injection pressure (bar) | 25 | 40 |
| Hold pressure (bar) | 20 | 30 |
| Hold Time (s) | 6 | 4 |
| Cool time (s) | 20 | 20 |
| Mould temperature (°C) | 60 | 60 |
| Melt temperature (°C) | 230 | 250 |

*note: the pressures are those of the hydraulic system*

### 4.2.2 Material characterisation

In order to obtain the mechanical properties of the composites and the virgin material, tensile tests were performed according to the ASTM D638M standard, as described in section 3.2.4. Tensile bars were tested at a crosshead speed of 5 mm/min using an extensometer, and the elastic modulus determined for 1% deformation. In the present work, the longitudinal coefficient of thermal expansion (CTE) of the composites was also determined. This results from the fact that a low CTE is a prerequisite for many applications, and as a result of fibre orientation, the longitudinal CTE is usually lower than the transverse CTE. The CTE in the longitudinal direction was measured with a Thermal Mechanical Analyzer 2940, fabricated by TA Instruments, which is capable of heating or cooling samples while applying a predetermined force. A quartz probe, placed in contact with the sample, is used to determine linear or volumetric changes, at any selected temperature. Samples of material having a maximum height of 25 mm and maximum diameter of 10 mm were cut with parallel faces, and the CTE's were measured from –30°C to 120°C. The fibre volume fractions for each sample were determined by density measurements.

## 4.3 RESULTS AND DISCUSSION

The properties of the composites are given in Table 4-2. Typical tensile stress-strain curves for the PP-PAN and PP-VGCF composites are given in Appendix B, Figures B-2 and B-3, respectively.

*Table 4-2. Composite's test results.*

| Fibre fraction | | 0% | 5% | 10% | 15% |
|---|---|---|---|---|---|
| Tensile modulus at 1% strain (MPa) | *PP-PAN* | 1343 | 2821 | 4294 | 4591 |
| | *PP-VGCF* | 1646 | 2584 | 3466 | 3685 |
| Tensile Strength (MPa) | *PP-PAN* | 30.4 | 36.6 | 42.6 | 49.7 |
| | *PP-VGCF* | 32.9 | 40.3 | 46.5 | 48.5 |
| CTE ($10^{-6}$/°C) | *PP-PAN* | 114.0 | 31.5 | 20.8 | 16.9 |
| | *PP-VGCF* | 111.3 | 57.4 | 39.8 | 26.2 |

It should be noted that the properties for the unreinforced polymer differ for the PP-PAN and PP-VGCF composites. This is due to the differences in processing conditions used, as mentioned in section 4.2.1 (see also Table 4-1). The higher pressures and temperatures used for PP-VGCF result in higher shear stresses and the material staying longer at higher temperatures, respectively. As polypropylene is a semi-crystalline material, both effects will promote spherulite growth in the polymer matrix (see *Introduction*), thus increasing stiffness and strength and decreasing CTE, as reflected in the different properties for the unreinforced polymers in Table 4-2.

For the fibre reinforced materials, the effect of the presence of the carbon fibres on the matrix morphology can play an additional role. However, considering the differences in properties caused by matrix morphology (see differences between PP-PAN and PP-VGCF, at 0%) and the effect of the presence of fibres, one can reasonably assume that the latter is dominant.

As the differences in properties occurring from morphology are partly accounted for by considering the different unreinforced polymer properties, not taking into account the effect of the presence of fibres on the morphology may be negligible. As the fibre orientation is related to the flow, which is greatly determined by mould geometry and on which the current change in processing parameters will have a minor effect, it is assumed equal.

For ease of comparison and to account for the above mentioned difference in matrix properties, Figures 4-1 through 4-3 depict therefore the normalised (that is, divided by the matrix value) stiffness, strength and CTE, respectively.

In these figures, the normalised properties of the PC-VGCF composites (from Chapter 3) are also shown. A major improvement over these previous results on PC-VGCF composites is observed. The current PP-VGCF properties are also better than those found in literature (4-2).

From the table and the figures it is easily observed that the VGCF-composites show strength properties comparable to those of the PP-PAN composites. Stiffness-values are lower, whereas the CTE's are slightly higher. Recent work (4-3), however, has shown that 16 vol.% PP-VGCF composites can be 300% stiffer than the matrix. This increase compared to the present work can possibly be attributed to higher fibre alignment and less fibre length degradation. The dependence of the properties on fibre volume fraction is similar for both PP-VGCF and PP-PAN composites. From the figures it is clear that the strength and CTE (and possibly stiffness) of the VGCF-composites have become competitive with properties of composites based on PAN-fibres.

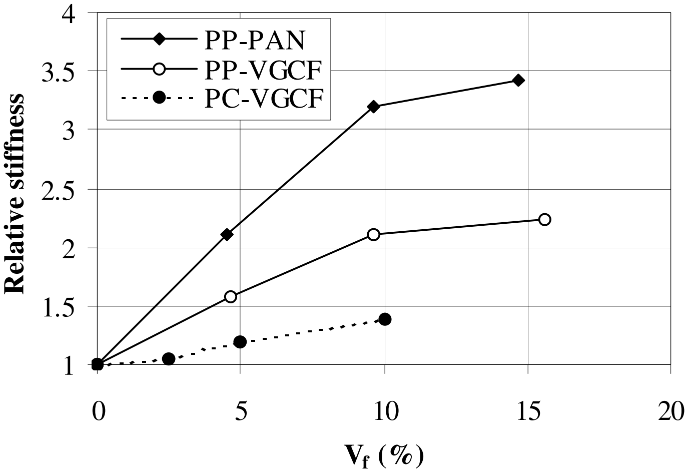

*Figure 4-1. Normalised experimental modulus at 1% strain.*

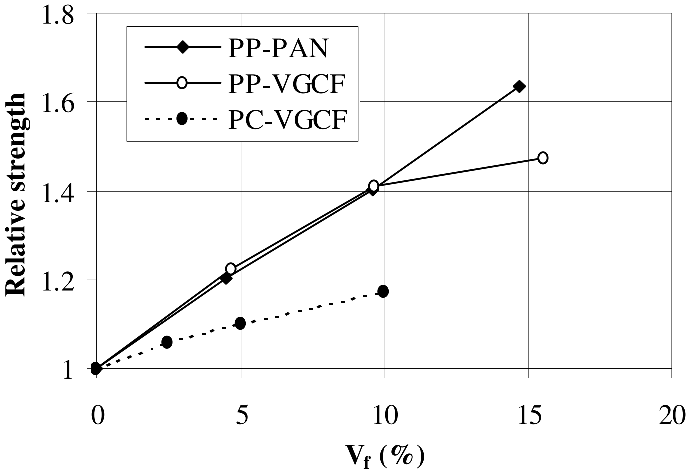

*Figure 4-2. Normalised experimental strength.*

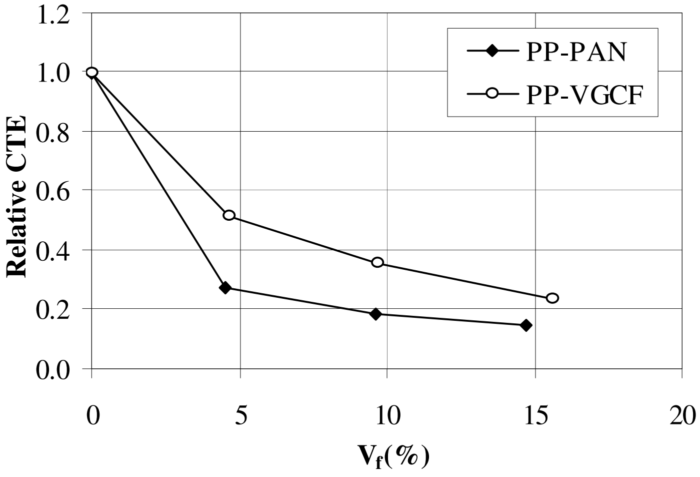

*Figure 4-3. Normalised experimental CTE.*

## 4.4 CONCLUSION

In this chapter it has been shown that VGCF-thermoplastic composites can be produced, with strength and CTE that are competitive to those of ‘conventional’ PAN-fibre composites. Stiffness is still somewhat lower. These properties are a significant improvement over the earlier work on PC-VGCF composites.

## 4.5 REFERENCES

4-1. G.G. Tibbetts, D.W. Gorkiewicz, and R.L. Alig, Carbon, **31**, 809 (1993).

4-2. C.J. Dasch, W.J. Baxter, and G.G. Tibbetts, in *Extended abstracts of 21st Biennial Conference on Carbon*, ed. American Carbon Society, Buffalo, NY, 82 (1993).

4-3. J.-M. Ting, D.J. Burton, R.L. Alig, and P. Flem, in *Extended Abstracts of 23rd Biennial Conference on Carbon*, ed. American Carbon Society, State College, PA, 294 (1997).

# Part III

## *Micromechanical Modelling*

# 5 A MODEL TO PREDICT THE STRENGTH OF SHORT FIBRE COMPOSITES[5]

## 5.1 INTRODUCTION

In Part I of this thesis, the properties of one type of VGCF, long fibres grown on a substrate, have been investigated. In Part II, thermoplastic composites made of a second type of VGCFs, submicron-size, grown in a continuous process, were also investigated. However, as indicated in the *Introduction*, these submicron VGCFs do not allow direct determination of their properties. The sole way of determining these properties might be by inversely applying micromechanical models to derive them from the composite properties.

Several models to predict the properties of short fibre composites, namely stiffness and CTE, already exist (see *Introduction*) and have been successfully applied, all using the same general assumptions and methods. However, no generally applicable model to predict the strength of short fibre composites is available. The complexity of fibre orientation patterns and fibre length distributions and the structural analysis of the composites require a model that is able to predict strength for any kind of fibre orientation and length distribution, in any direction and under any loading condition. The derivation of one such model, following the same general assumptions (e.g. fibre and matrix isotropic and linearly elastic -see *Introduction*- with the exception of fibre-matrix debonding, which is on of the failure modes) and methods used for stiffness- and CTE-prediction, is described in this chapter.

---

[5] Reproduced, with adaptations, from: F.W.J. van Hattum, and C.A. Bernardo, *Polym. Compos.*, in press (1999).

## 5.2 THEORY

### 5.2.1 Strength of unidirectional composites

The derivation of a model to predict the strength of a short fibre composite can begin by considering the strength of a composite with unidirectional microstructure: all fibres aligned in one direction. In that situation, the strength of a unidirectional composite in the direction of the (continuous) fibres is given by the rule of mixtures:

$$\sigma_{cL} = \sigma_f \; V_f + \sigma'_m \; (1 - V_f) \qquad [5.1]$$

where $V_f$ is the fibre volume fraction and $\sigma_f$ and $\sigma'_m$ are, respectively, the fibre strength and the stress developed in the matrix. Although the exact value of $\sigma'_m$ is subject to debate, as an initial approximation it can be taken to be equal to the stress developed in the matrix at fibre failure strain. The transverse strength of such a composite, for a strong interfacial bond, is given by:

$$\sigma_{cT} = \sigma_m \qquad [5.2]$$

When, instead of continuous fibres, short fibres are used, the strength of the unidirectional composite will be diminished. Of the many models dealing with the stress distribution along a (short) fibre found in the literature (5-1,5-2,5-3), the simplest one, proposed by Kelly and Tyson (5-3), was chosen for the present work. In this model the applied load is assumed to be transferred to the fibres by means of a shear force at the fibre-matrix interface. A critical minimum fibre length, $l_c$, is thus needed to build up sufficient stress to fracture the fibre. This critical length is given by

$$l_c = \frac{\sigma_f \, d}{2\tau} \qquad [5.3]$$

where $d$ is the fibre's diameter and $\tau$ the interfacial shear strength between fibre and matrix. In the case of a strong interfacial bond, $\tau$ is limited by the shear strength of the matrix, $\tau_m$. Assuming isotropy of the matrix this results in

$$\tau = \frac{\sigma_m}{\sqrt{3}} \qquad [5.4]$$

Then, assuming no interaction between fibre segments and stress concentrations at the fibre ends, the longitudinal strength of the composite will be given by

$$\sigma_{cL} = V_f \sigma_f \frac{l}{2l_c} + \sigma'_m(1-V_f) = V_f \frac{\tau l}{d} + \sigma'_m(1-V_f) \qquad \textit{for } l < l_c \qquad [5.5a]$$

or

$$\sigma_{cL} = V_f \sigma_f (1-\frac{l_c}{2l}) + \sigma'_m(1-V_f) \qquad \textit{for } l \geq l_c \qquad [5.5b]$$

where $l$ is the length of the fibre.

Thus, equations [5.5a] and [5.5b] give an expression for the tensile strength of a unidirectional composite with uniform fibre length in its principal directions.

### 5.2.2 Single fibre strength

In the above the fibre strength is considered to be constant. However, it is known that the tensile strength of (carbon) fibres depends significantly on the existence of fatal flaws in the tested length. Hence, the fibre strength is not just a constant: a statistical model must be applied to deal with the data variability. The variation of fibre strength with gauge length is well described using a Weibull distribution function, which method is described in detail elsewhere (reference 5-4 and Chapter 1). Applying a three-parameter Weibull distribution function, the mean tensile strength, $\bar{\sigma}$, and the variance of the Weibull distribution, $\beta_v$, functions of the gauge length $l$, are defined as:

$$\bar{\sigma} = \sigma_0(l)\,\Gamma(1+1/m) \qquad \beta_v = \sigma_0{}^2(l)\left[\Gamma(1+2/m) - \Gamma^2(1+1/m)\right] \qquad [5.6]$$

where Γ represents the gamma function, $m$ is the Weibull distribution shape parameter, and $\sigma_0(l)$ the Weibull scale parameter, which is also dependent on the gauge length. Various equations that express this dependence can be found in the literature (5-4,5-5,5-6). One of the more useful is of the type:

$$\ln \sigma_0(l) = (-\gamma/m)\ln l + \ln \sigma_0 \qquad [5.7]$$

where $\gamma$ and $\sigma_0$ are constants. Combining equations [5.6] and [5.7], an expression for the fibre strength as a function of gauge length can be obtained:

$$\sigma_f(l) = \sigma_0\ \Gamma(1+1/m)\ l^{-\gamma/m} \qquad [5.8]$$

Finally, the expression of the longitudinal tensile strength of a unidirectional composite with varying fibre strength can be obtained by combination of equations [5.8] and [5.5]:

$$\sigma_{cL}(l) = V_f \frac{\tau l}{d} + \sigma'_m (1 - V_f) \qquad \textit{for } l < l_c \qquad \textit{[5.9a]}$$

or

$$\begin{aligned} \sigma_{cL}(l) &= V_f \sigma_f(l_c)\,(1 - \frac{l_c}{2l}) + \sigma'_m (1 - V_f) \\ &= V_f \sigma_0 \;\Gamma(1 + 1/m)\; l_c^{-\gamma/m}\,(1 - \frac{l_c}{2l}) + \sigma'_m (1 - V_f) \qquad \textit{for } l \geq l_c \end{aligned} \qquad \textit{[5.9b]}$$

The critical length, $l_c$, can be obtained from:

$$l_c = \frac{\sigma_f(l_c)\, d}{2\tau} \qquad \textit{[5.10]}$$

It should be noted that the expression for the longitudinal tensile strength for fibre lengths below $l_c$ is unaffected by the introduction of $\sigma_f(l)$. For this case, the difference is in the change of the actual value of $l_c$, that is, in the range of fibre lengths for which this expression is valid.

### 5.2.3 Fibre length distribution

Next, instead of taking an average fibre length, the effect of the fibre length distribution on the composite properties should be taken into account. It is well known that the fibre length distribution in a moulded part can be represented by a log-normal distribution function (5-7). Then, a probability density function describing fibre length, $\psi_l$, can be defined in such a way that the probability of a fibre having a length within the range $l$ and ($l$+d$l$) equals $\psi_l(l)\mathrm{d}l$. The function $\psi_l$ is given by:

$$\psi_l(l) = \frac{1}{\sqrt{2\pi}\beta} l^{-1}\, e^{-(\ln l - \alpha)^2 / 2\beta^2} \qquad \textit{[5.11]}$$

where $\alpha$ and $\beta$ are related to the conventional mean, $\bar{l}$, and standard deviation, $sl$, of the length distribution by (5-7, 5-8):

$$\alpha = \ln \frac{\bar{l}}{\sqrt{1 + \left(\frac{sl}{\bar{l}}\right)^2}} \qquad \beta = \sqrt{\ln\left[1 + \left(\frac{sl}{\bar{l}}\right)^2\right]} \qquad \textit{[5.12]}$$

To account for the effect of the fibre length distribution, the properties of the unidirectional composite are weighted over the whole range of fibre lengths, by means of equation [5.11]. The length averaged longitudinal strength, $\overline{\sigma}_{cL}$, of the unidirectional composite can now be expressed using equations [5.9a], [5.9b] and [5.11]:

$$\overline{\sigma}_{cL} = \int_{l=0}^{l_c} \sigma_{cL}(l)\, \psi_l(l)\, dl + \int_{l=l_c}^{l_{\max}} \sigma_{cL}(l) \psi_l(l)\, dl \qquad [5.13]$$

where $l_{max}$ is the maximum fibre length in the composite. The transverse strength, $\sigma_{cT}$, and the interfacial shear strength, $\tau$, remain according to equations [5.2] and [5.4] respectively.

### 5.2.4 Failure criterion

In composite materials, the Tsai-Hill failure criterion is widely used to predict failure under simultaneous loads in the principal directions or off-axis. For instance, Baxter (5-9) successfully applied this criterion to predict strength of short fibre composites having random two-dimensional or three-dimensional fibre distributions. However, to account for arbitrary fibre orientation a failure criterion is needed that is not limited to in-plane stresses. Tsai and Wu (5-10) developed a relatively simple strength criterion for anisotropic materials from a scalar function of two strength tensors. The criterion has the general form

$$F_i \sigma_i + F_{ij} \sigma_i \sigma_j = 1 \qquad [5.14]$$

where the contracted notation is used. The $\sigma_i$'s are the applied stresses and $F_i$ and $F_{ij}$ are strength tensors of the second and fourth order, respectively. Failure will occur when the equality of equation [5.14] is met. In composites it is common practice to deal with a failure criterion in terms of strain. Equation [5.14] can be rewritten in terms of strain as follows (5-10):

$$G_i \varepsilon_i - G_{ij} \varepsilon_i \varepsilon_j = 1 \qquad [5.15]$$

where

$$\begin{aligned} G_i &= F_m C_{mi} \\ G_{ij} &= F_{mn} C_{mi} C_{nj} \end{aligned} \qquad [5.16]$$

In equation [5.16], $F_i$ and $F_{ij}$ are the strength tensors from equation [5.14], $G_i$ and $G_{ij}$ are the strength tensors in terms of strain and $C_{ij}$ is the elastic stiffness tensor. For a short fibre unidirectional composite, it is interesting to define an orthogonal axis system with the 1-axis along the fibre direction, the 2-axis transverse to this direction and the 3-axis perpendicular to the 1-2-plane. With this system, the material will be transversely isotropic, with the 1-axis being axis of symmetry and isotropy in the 2-3-plane. For this material, the strength tensors of equation [5.14] have the general forms

$$F_i = \begin{pmatrix} F_1 \\ F_2 \\ F_2 \\ 0 \\ 0 \\ 0 \end{pmatrix} \qquad F_{ij} = \begin{pmatrix} F_{11} & F_{12} & F_{12} & 0 & 0 & 0 \\ F_{12} & F_{22} & F_{23} & 0 & 0 & 0 \\ F_{12} & F_{23} & F_{22} & 0 & 0 & 0 \\ 0 & 0 & 0 & 2(F_{22}-F_{23}) & 0 & 0 \\ 0 & 0 & 0 & 0 & F_{66} & 0 \\ 0 & 0 & 0 & 0 & 0 & F_{66} \end{pmatrix} \qquad [5.17]$$

Both strength tensors are symmetric. The second and fourth order strength tensors, $F_i$ and $F_{ij}$, have 2 and 5 independent components respectively, that are directly related to the engineering strengths of the transversely isotropic material as derived in the preceding paragraphs. Thus, the Hill criterion, from which the widely applied Tsai-Hill criterion may be considered a specialisation to in-plane stresses, can be expressed for the case of a unidirectional short fibre composite as (5-10):

$$F_i \equiv \{0\} \qquad F_{ij} = \begin{pmatrix} \frac{1}{\bar{\sigma}_{cL}^{2}} & \frac{-1}{2\bar{\sigma}_{cL}^{2}} & \frac{-1}{2\bar{\sigma}_{cL}^{2}} & 0 & 0 & 0 \\ \frac{-1}{2\bar{\sigma}_{cL}^{2}} & \frac{1}{\sigma_{cT}^{2}} & -\frac{1}{2}\left(\frac{2}{\sigma_{cT}^{2}}-\frac{1}{\bar{\sigma}_{cL}^{2}}\right) & 0 & 0 & 0 \\ \frac{-1}{2\bar{\sigma}_{cL}^{2}} & -\frac{1}{2}\left(\frac{2}{\sigma_{cT}^{2}}-\frac{1}{\bar{\sigma}_{cL}^{2}}\right) & \frac{1}{\sigma_{cT}^{2}} & 0 & 0 & 0 \\ 0 & 0 & 0 & \left(\frac{4}{\sigma_{cT}^{2}}-\frac{1}{\bar{\sigma}_{cL}^{2}}\right) & 0 & 0 \\ 0 & 0 & 0 & 0 & \frac{1}{\tau^{2}} & 0 \\ 0 & 0 & 0 & 0 & 0 & \frac{1}{\tau^{2}} \end{pmatrix} \qquad [5.18]$$

where $\bar{\sigma}_{cL}$, $\sigma_{cT}$ and $\tau$ are according to equations [5.13], [5.2] and [5.4], respectively. Note that the relation between engineering strengths and the strength tensor $F_{ij}$ from equation [5.18] is similar to that between engineering constants and the components of the elastic compliance tensor.

The strength tensor $F_{ij}$ can now be rewritten from equation [5.18] to the strength tensor $G_{ij}$, in terms of strain, using equation [5.16]. The elastic stiffness tensor $C_{ij}$, used in this equation for unidirectional short-fibre composites, can be derived using the well-known Halpin-Tsai equations (5-11,5-12,5-13 and Appendix C).

The above derivation provides a strength criterion for any unidirectionally aligned short fibre composite in terms of stresses ($F_{ij}$) or strains ($G_{ij}$). The criterion can be generalised to study off-axis properties in any direction by rotating the material axes. The transformed strength tensors $F_{ij}'$ or $G_{ij}'$ can be calculated from $F_{ij}$ and $G_{ij}$, respectively, using known tensor transformation relations. Subsequently equations [5.14] or [5.15] can be applied to $F_{ij}'$ or $G_{ij}'$, respectively.

### 5.2.5 Fibre orientation distribution

After deriving an expression for the strength in any direction of a unidirectional short fibre composite with arbitrary fibre length distribution, it is necessary to consider the fibre orientation distribution. This will be done in the same way as the fibre length distribution was accounted for. Thus, properties of the final composite are taken as an average of the unidirectional properties over all directions weighted by a fibre orientation distribution function. Following the methodology used by Advani and Tucker (5-11), the orientation of a single fibre in a short fibre composite is defined by the angles $\phi$ and $\theta$, or by a unit vector **p** directed along the fibre axis, as depicted in Figure 5-1. The elements of **p** are given by:

$$p_1 = \sin\theta\cos\phi \quad p_2 = \sin\theta\sin\phi \quad p_3 = \cos\theta \qquad [5.19]$$

The 1-axis is chosen as the direction of main fibre orientation (flow-direction), the 2-axis perpendicular to this direction, and the 3-axis perpendicular to the 1-2-plane (the through-thickness direction).

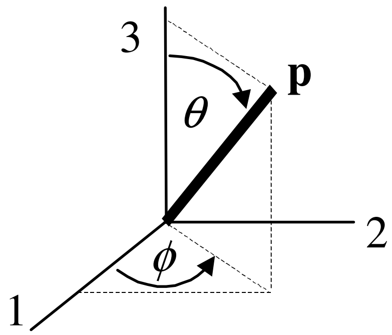

*Figure 5-1. Definition of the fibre angles $\phi$ and $\theta$ and the unit vector **p**.*

Let $\psi_p$ be a probability density function describing fibre orientation. $\psi_p$ is defined in such a way that the probability of a fibre lying within the range **p** and (**p**+d**p**) equals $\psi_p(\mathbf{p})d\mathbf{p}$. Using these descriptions of **p** and $\psi_p$ , Advani and Tucker (5-11) introduced a compact tensor description for fibre orientation. They define a second and fourth order fibre orientation tensor such that

$$a_{ij} = \oint p_i p_j \psi(\mathbf{p}) d\mathbf{p} = < p_i p_j >; \qquad a_{ijkl} = \oint p_i p_j p_k p_l \psi(\mathbf{p}) d\mathbf{p} = < p_i p_j p_k p_l > \qquad [5.20]$$

where the brackets denote the orientation average. The second order tensor, $a_{ij}$, describes the fibre orientation state at any point in the material. The fourth order tensor, $a_{ijkl}$, is, among others, needed to calculate material properties such as stiffness and strength (5-11). The orientation averaging methodology can now be applied to calculate composite strength in much the same way as it is used in calculation of short fibre composites moduli (5-11,5-12, see also Appendix D). The strength tensor $G_{ij}$ of equation [5.16] is a fourth order tensor property, associated with a unidirectional microstructure and it has all the symmetries of an elasticity tensor. Taking **p** as its axis of symmetry, the tensor $G_{ijkl}$ (in index-notation) must have the form (5-11):

$$\begin{aligned} G_{ijkl} = {} & B_1(p_i p_j p_k p_l) \\ & + B_2(p_i p_j \delta_{kl} + p_k p_l \delta_{ij}) \\ & + B_3(p_i p_k \delta_{jl} + p_i p_l \delta_{jk} + p_j p_l \delta_{ik} + p_j p_k \delta_{il}) \\ & + B_4(\delta_{ij}\delta_{kl}) + B_5(\delta_{ik}\delta_{jl} + \delta_{il}\delta_{jk}) \end{aligned} \qquad [5.21]$$

to be transversely isotropic about the direction of **p**. The scalar constants $B_1$ through $B_5$ are related to the components of the (contracted) $G_{ij}$ and the $\delta_{ij}$'s are the Kronecker delta components. Then

$$\begin{aligned} < G_{ijkl} > = {} & B_1(a_{ijkl}) \\ & + B_2(a_{ij}\delta_{kl} + a_{kl}\delta_{ij}) \\ & + B_3(a_{ik}\delta_{jl} + a_{il}\delta_{jk} + a_{jl}\delta_{ik} + a_{jk}\delta_{il}) \\ & + B_4(\delta_{ij}\delta_{kl}) \\ & + B_5(\delta_{ik}\delta_{jl} + \delta_{il}\delta_{jk}) \end{aligned} \qquad [5.22]$$

can be used to calculate the orientation averaged $<G_{ijkl}>$ for any given orientation state, once the orientation tensors are known. Converting $<G_{ijkl}>$ to contracted notation and taking the inverse, the final orientation averaged strength tensor $<F_{ij}>$ can be obtained using:

$$< F_{ij} > = < G_{mn} > < C_{mi} >^{-1} < C_{nj} >^{-1} \qquad [5.23]$$

$<C_{ij}>^{-1}$ is the inverse of the orientation averaged stiffness tensor (or the compliance tensor), calculated by applying the orientation averaging methodology to the elastic stiffness tensor $C_{ij}$ of the underlying unidirectional short fibre composite. From the components of the tensor $F_{ij}$, the engineering strengths of a short fibre composite with arbitrary fibre orientation state and fibre length distribution can be easily calculated. Failure of the composite under any combination of applied strains or stresses can be verified by applying equations [5.14] or [5.15] to $<F_{ij}>$ or $<G_{ij}>$, respectively. The only requirement being that the longitudinal, transverse and shear strength of the underlying unidirectional composite, the orientation tensors $a_{ij}$ and $a_{ijkl}$ and the fibre length distribution function $\psi_l$ are known.

## 5.3 EXPERIMENTAL

### 5.3.1 Material preparation

The theory derived above is of specific interest for short fibre reinforced thermoplastic composites. Injection moulded parts of these composites show complex fibre orientation patterns and fibre length distributions, complicating the prediction of the final properties. In this work, therefore, the results from the tests of the unfilled and carbon fibre filled PP moulded tensile bars (type 3, Appendix A), described in Chapter 4, were used to evaluate the theory. The materials and preparation of the specimens are described in Chapter 4, section 4.2.1. The processing conditions can be found in Table 4-1.

### 5.3.2 Material characterisation

#### *5.3.2.1 Composite and fibre tensile testing*

In order to obtain the mechanical properties of the composites and the virgin material, tensile tests were performed as described in Chapter 3, section 3.2.4 and Chapter 4, section 4.2.2. The single carbon fibres were tested according to ASTM D 3379-89 in an Instron 1122 universal testing machine with a 5 N load cell, in analogy to the tests on VGCFs described in Chapters 1 and 2. Using a crosshead speed of 0.5 mm/min, 5 different gauge lengths (5.28, 10.16, 20.32, 40.28 and 80.48 mm) were tested, 20 samples at each gauge length. Average fibre modulus and fibre strength were obtained as described in Chapter 1, section 1.2.1. The diameters of the fibres were measured prior to testing using a laser diffraction technique.

#### *5.3.2.2 Fibre orientation measurement*

Fibre orientation measurements were made on polished cross sections cut parallel to flow at the centre of the composite tensile bars, using the method described by Bay and Tucker (5-14). From the polished cross-sections, pictures were taken under an optical microscope for 11 layers through-thickness, 3 columns of pictures for each sample. The pictures were saved on a computer and using software developed in-house, measurements were made on the ellipsoidal cross-sections, like which the fibres appear on the polished cross-sections. In this way it was assured that for each sample at least 500 fibres were measured. Subsequently, the data obtained were corrected for the 90° angle to flow direction and bias (5-14) with a mathematical computer program. Using these data, the second order and fourth order fibre orientation tensors were constructed.

#### *5.3.2.3 Fibre length distribution and volume fraction*

Some of the composite tensile bars were oxidised in air at 400°C for 4 hours to remove the matrix. The fibres were then spread on a glass slide and fibre lengths measured under an optical microscope using an Image Analysis system. In this way, a total number of approximately 1000 fibres was measured for each sample. The fibre volume fractions for each sample were determined by density measurements. Assuming no voids to be present, differences in weight before and after submerging in a liquid of known density were used to derive the fibre volume fractions.

## 5.4 RESULTS AND DISCUSSION

### 5.4.1 Material characterisation

The results of the tensile tests done on the composites and on the virgin PP, the fibre length measurements and the fibre volume fractions are summarised in Table 5-1. Representative tensile stress-strain curves for the different materials are given in Appendix B, Figure B-2. The parameters of the Weibull distribution (equations [5.6] through [5.8]), calculated for the 100 fibres tested at different gauge lengths are given in Table 5-2. The resulting plot of the estimated Weibull strength as a function of fibre length is given in Figure 5-2, together with its 95% confidence limits and the measured and average tensile strength data.

*Table 5-1. Composite's test results.*

| | | PP | PP-PAN 5% | PP-PAN 10% | PP-PAN 15% |
|---|---|---|---|---|---|
| Fibre volume fraction (%) | Mean | - | 4.5 | 9.6 | 14.7 |
| | St. dev. | - | 0.5 | 1.0 | 0.1 |
| Fibre length (μm) | Mean | - | 161.7 | 148.3 | 161.3 |
| | St. dev. | - | 106.1 | 96.6 | 103.2 |
| Tensile modulus at 1% strain (MPa) | Mean | 1343 | 2821 | 4294 | 4591 |
| | St. dev. | 40 | 194 | 525 | 86 |
| Tensile strength (MPa) | Mean | 30.4 | 36.6 | 42.6 | 49.7 |
| | St. dev. | 0.2 | 0.5 | 1.4 | 1.1 |

*Table 5-2. Parameters of the Weibull distribution.*

| $m$ | $\sigma_0(l)$ (MPa) | $\gamma$ | $\sigma_0$ (MPa) | $\sigma_f(l)$ (MPa) | $\beta_v$ (MPa)$^2$ | St. dev. (MPa) |
|---|---|---|---|---|---|---|
| 9.7060 | $\frac{5199.4}{l^{0.1554}}$ | 1.5083 | 5199.4 | $\frac{4940.1}{l^{0.1554}}$ | $\frac{373714.6}{l^{0.3108}}$ | $\frac{611.32}{l^{0.1554}}$ |

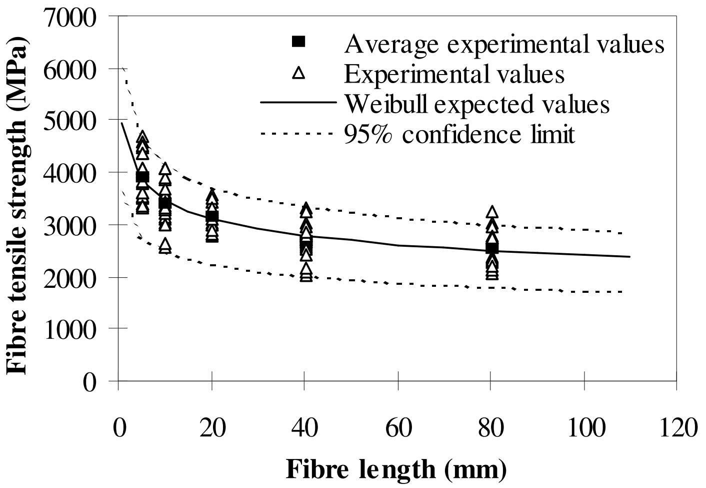

*Figure 5-2. Fibre strength data and Weibull confidence limits.*

As can be seen, most strength data fall within the 95% confidence limits of the estimated Weibull strength. The fibre tensile strengths for different initial gauge lengths are summarised in Table 5-3, together with the values of the modulus and the diameters. For comparison, the data sheet values are also given. The differences between measured and datasheet values for both tensile modulus and fibre diameter are negligible. Although, at low to intermediate lengths, there is also no major difference between data sheet and tested strength values, the rapid increase in fibre tensile strength at smaller gauge lengths should be noted (< 5 mm, see Table 5-3 and extrapolate Figure 5-2). Since this is the relevant range in almost all short fibre composites, the importance of taking into consideration the effect of length on fibres' tensile strength is evident. This effect is relevant both in determining the critical fibre length, $l_c$ (equation [5.10]), as well as in describing the composite's strength, for fibres with lengths above $l_c$ (equation [5.9b]).

*Table 5-3. Fibre properties.*

| Fibre length (mm) | | 1 | 5 | 10 | 20 | 40 | 60 | 80 |
|---|---|---|---|---|---|---|---|---|
| Tensile Strength (GPa) | Mean | 4.9 | 3.8 | 3.5 | 3.1 | 2.8 | 2.6 | 2.5 |
| | St. dev. | 0.61 | 0.48 | 0.43 | 0.38 | 0.34 | 0.32 | 0.31 |
| | Datasheet | | | | 3.95 | | | |
| Tensile Modulus (GPa) | Mean | | | | 218 | | | |
| | Datasheet | | | | 238 | | | |
| Fibre Diameter (μm) | Mean | | | | 7.2 | | | |
| | St. dev. | | | | 0.22 | | | |
| | Datasheet | | | | 7 | | | |

### 5.4.2 Predictions versus experiment

The data obtained from the tests, that were used to evaluate the theoretical model described in section 5.2 are summarised in Table 5-4. Comparison of $\bar{l}$ and $l_c$ shows that the lengths of the fibres in the composites are mostly below the critical one.

Typical fibre length-distribution and fibre orientation through-thickness are shown Figure 5-3a and b, respectively, for the case of the composite with 15% fibre volume fraction. As can be seen from Figure 5-3a, the fibre length can be well described by a log-normal distribution. In Figure 5-3b, $a_{11}$ and $a_{22}$ represent the well-known 2nd order orientation tensor components from equation [5.20], giving the relative orientation of the fibres around the 1-axis (flow-direction) and 2-axis (cross-flow direction), respectively. The so-called 'skin-core' structure, reported for many injection moulded short fibre composites, is readily observed in this figure.

*Table 5-4. Material parameters used for the evaluation of the model.*

| Material parameters | PP | PP-PAN 5% | PP-PAN 10% | PP-PAN 15% | PAN |
|---|---|---|---|---|---|
| Matrix modulus, $E_m$ (GPa) | 1.343 | | | | |
| Matrix Poisson ratio, $\nu_m$ | 0.40[1] | | | | |
| Matrix yield stress, $\sigma_m$ (MPa) | 30.4 | | | | |
| Matrix stress at fibre failure strain, $\sigma'_m$ (MPa) | 20.8[2] | | | | |
| Fibre modulus, $E_f$ (GPa) | | | | | 218 |
| Fibre diameter, $d$ (μm) | | | | | 7.2 |
| Fibre Poisson ratio, $\nu_f$ | | | | | 0.26[1] |
| Fibre tensile strength, $\sigma_f(l)$ (MPa) | | | | | $\frac{4940.1}{l^{0.1554}}$ |
| Fibre failure strain (%) | | | | | 1.55[1] |
| Critical fibre length, $l_c$ (μm) | | | | | 1012 |
| Fibre volume fraction, $V_f$ (%) | | 4.5 | 9.6 | 14.7 | |
| Average fibre length, $\bar{l}$ [St. dev., $sl$] (μm) | | 161.7 [106.1] | 148.3 [96.6] | 161.3 [103.2] | |

[1] *datasheet value*

[2] *calculated from fibre failure strain and matrix modulus*

From the properties of fibre and matrix shown in Table 5-1, Table 5-2 and Table 5-3, $\tau$ and $l_c$ were calculated using equations [5.4] and [5.10] respectively. Then, the strength properties of the unidirectional composite were calculated following equations [5.2] and [5.9], and the stiffness properties using the Halpin-Tsai equations (5-13 and Appendix C). Next, these properties were length averaged, using the function $\psi_l$ computed from equations [5.11] and [5.12]. The length averaged unidirectional strength properties are substituted in the strength tensor $F_{ij}$ from equation [5.18] and the stiffness properties used to calculate the elastic stiffness tensor $C_{ij}$ (see Appendices C and D). Subsequently, the tensor $G_{ij}$ was obtained from $F_{ij}$ and $C_{ij}$ by means of equation [5.16]. Using the orientation tensors, the orientation averaged tensors $<G_{ij}>$ and $<C_{ij}>$ and, subsequently, $<F_{ij}>$ were determined for each layer through-thickness. From $<F_{ij}>$ and $<C_{ij}>$, the engineering strengths and moduli for each layer and later the overall strengths and moduli for the tested specimens in flow direction were calculated.

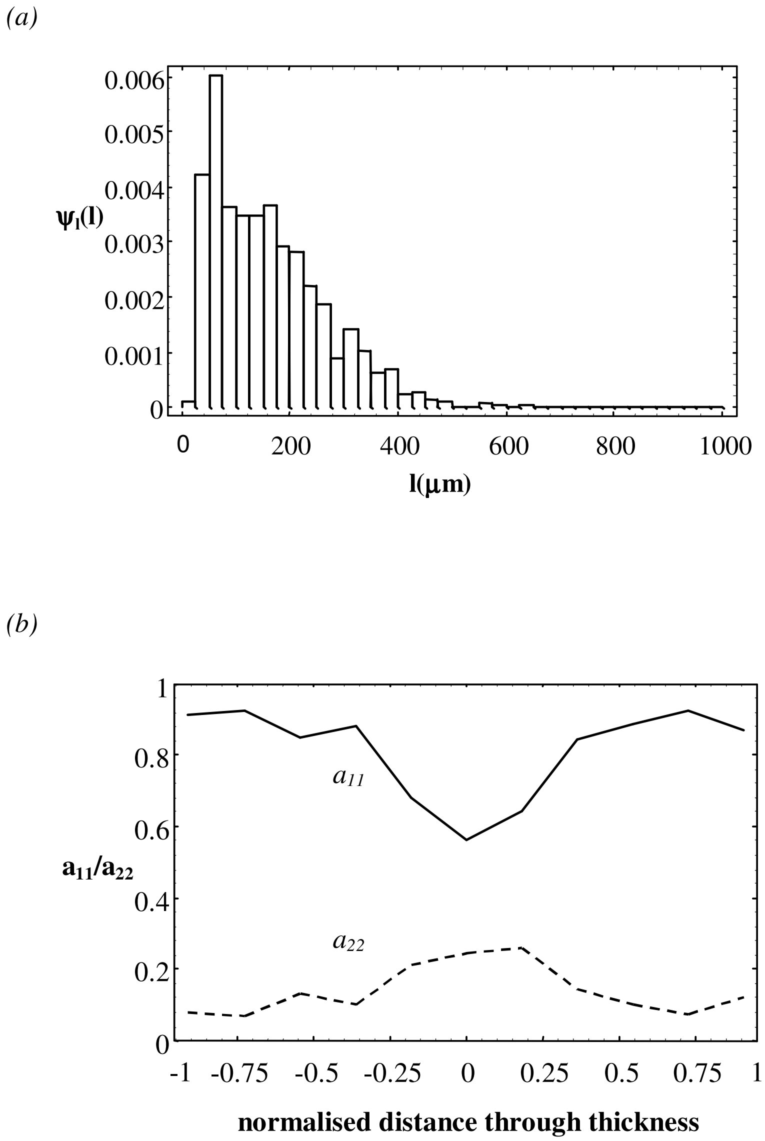

*Figure 5-3. Typical fibre length-distribution (a), and fibre orientation through-thickness (b), for PP-PAN 15%.*

The results, together with the experimentally determined strength and modulus-values, are shown in Table 5-5 (*l* distribution). Since the actual fibre length distribution in a short fibre composite after processing is not easy to predict, in most practical cases, an average fibre length is taken instead. To investigate the effect of this simplification, the model was also evaluated using the same material properties, but substituting the fibre length distribution by the corresponding average fibre length, $\bar{l}$. These results are also given in Table 5-5. As can be seen from Table 5-5, the model predictions are in good agreement with the experimental values for the whole range of fibre volume fractions studied. For the materials tested in this work, the model yields strength predictions that are easily within 10% of the experimental values for the short fibre composites. This level of accuracy is comparable to that observed in the present and earlier predictions of composite stiffness (5-12,5-15). Templeton (5-16) obtained similar accuracy for strength predictions on some of his materials, although in his work the fibre volume fraction was not varied. In spite of the fact that unreinforced PP shows non-linear behaviour up to failure (Figure B-2), the assumption of linear elasticity of the matrix does not seem to affect the accuracy of the models' predictions. This can be related to the dominating effect of the fibres in the composites, as at small strains (up to the fibre failure strain), the unreinforced PP can be approached by a linear elastic material. Furthermore, in the present model the possible effects of matrix anisotropy or internal stresses (see *Introduction*) are not taken into account. Again, this does not seem to affect the final accuracy of the model. Apparently, these factors do not dominate the behaviour of the present materials, thus validating the assumptions made in the model.

*Table 5-5. Experimental and predicted values of the mechanical properties.*

| | | PP-PAN 5% | PP-PAN 10% | PP-PAN 15% |
|---|---|---|---|---|
| Strength (MPa) | *Experimental* | 36.6 | 42.6 | 49.7 |
| | *l distribution* | 35.1 | 45.2 | 51.5 |
| | $\bar{l}$ | 35.0 | 45.2 | 51.4 |
| Modulus (MPa) | *Experimental* | 2821 | 4294 | 4591 |
| | *l distribution* | 2703 | 4010 | 4901 |
| | $\bar{l}$ | 2777 | 4140 | 5043 |

### 5.4.3 The role of the fibre length in the model

The results in Table 5-5 show that simplifying the model by taking the average fibre length instead of the full length distribution yields comparable results, with slightly bigger differences for the stiffness-predictions. In general, taking the average fibre length will result in slightly higher predictions. The effect of this simplification can be explained through a closer look at the unidirectional properties. Since the fibres in the composites after injection moulding are highly aligned, the overall properties will be dominated by the longitudinal properties for the case of a unidirectional composite. As an example, in Figure 5-4a and b, the longitudinal strength $\sigma_{cL}(l)$ from equations [5.9a] and [5.9b] and the longitudinal modulus for the case of a unidirectional composite, are plotted against fibre length. It can be seen that, below $l_c$, $\sigma_{cL}(l)$ is linearly dependent on fibre length.

In the present work, the fibre length distributions of the materials studied are well below the critical length given in Figure 5-4a (compare $l_c$, for instance, to the fibre length distribution given in Figure 5-3a). Therefore, replacing the full distribution by the average fibre length will affect the final strength results only slightly. For the modulus however, the dependence on fibre length is far less linear (Figure 5-4b), thus having a stronger effect on the final properties. Hence, the bigger difference between taking average fibre length or the full length distribution, observed in Table 5-5, for modulus-predictions compared to strength. As the fibre length distribution shifts even more towards the non-linear regions of the curves depicted in Figure 5-4, this effect will become more pronounced.

*(a)*

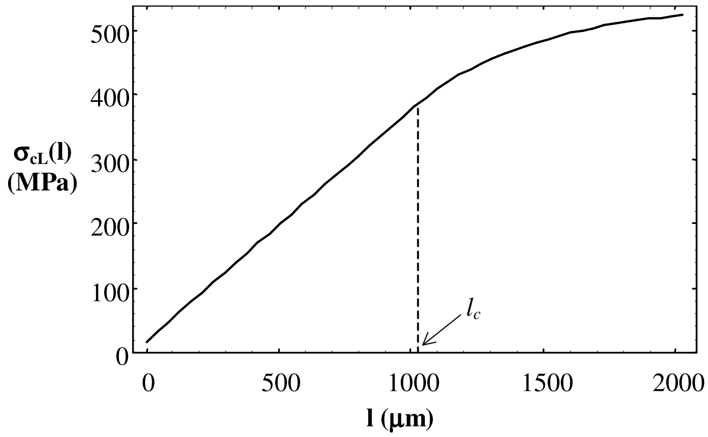

*(b)*

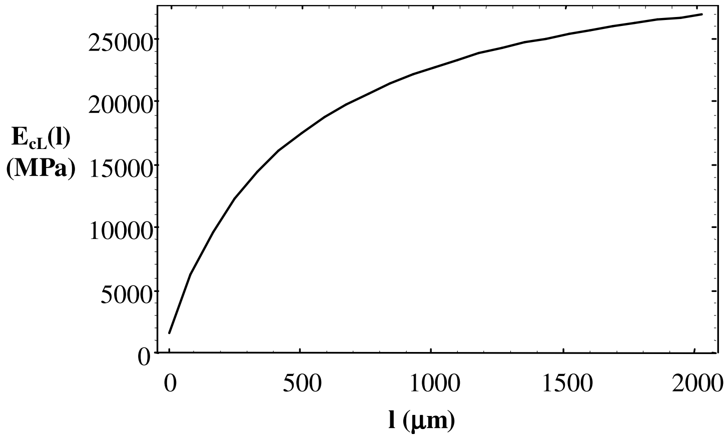

*Figure 5-4. Longitudinal strength (a), and modulus (b) of unidirectional composite as a function of fibre length, for PP-PAN 15%.*

### 5.4.4 The role of the fibre strength in the model

In the above theory the fibre strength is considered $l$-dependent, decreasing with increasing fibre length. As stated before, the range of fibre lengths in the material under investigation is shorter than $l_c$. A rapid increase of fibre strength at these short fibre lengths has been observed (see section 5.4.1). In fact, at the $l_c$ of 1025 μm used in this chapter (see Table 5-4), the fibre strength would equal 4.9 GPa, increasing to a value of 6.6 GPa at 150 μm (the average fibre lengths found in the composites, see Table 5-4).

However, it was also concluded that the overall composite strength is dominated by the longitudinal strength, $\sigma_{cL}(l)$, given by equation [5.9a]. In this equation, the composite strength is not directly dependent on the fibre strength, but on the interfacial shear strength, $\tau$, which is assumed to be related to the matrix strength, $\sigma_m$ (see equation [5.4]). Hence, the high fibre strength at short fibre lengths is not directly translated into composite properties. Instead, the variation of fibre strength only influences the final composite strength by changing the values of $l_c$ (see equation [5.10]). Taking the fibre strength as constant and equal to the datasheet value from Table 5-3, as is common in most practical cases, would, from equation [5.3], lead to a change of the critical fibre length, $l_c$, from 1025 μm to 811μm. As the fibres would still be below this critical length, no change in final composite strength would result.

### 5.4.5 The role of the interfacial shear strength in the model

From the above, it can be concluded that for the present materials, due to their short fibre lengths, the final strength is not so much depending on the actual strength of the fibres as it is on the interfacial shear strength, $\tau$. This will be the case for most injection moulded short fibre composites, as the vast majority of their fibre lengths found will be below $l_c$. Direct measurements of $l_c$ (5-17), allowing calculation of $\tau$ directly from $\sigma_f(l)$ and $d$ (equation [5.10]), alternatively to the $\tau$ currently derived following equation [5.4], would change this situation and could lead to more accurate predictions. However, this is a tedious task to perform, and the results are subject to debate (5-2). Therefore, for most practical fibre-matrix combinations, deriving $\tau$ from $\sigma_m$ as in the theory described above, would be the most versatile solution.

The model proposed in this chapter has a general character, that has been verified using data determined on composites with fibre lengths and contents typical of injection mouldings. However, the model has not been used to its full extent. In fact, it would be desirable to apply it to composites having larger fibre lengths and higher fibre contents. Furthermore, as the model allows prediction of properties in different directions and under combined loading conditions, it would be particularly interesting to use it in structural analysis of moulded parts.

## 5.5 CONCLUSION

In this chapter a model that can predict the strength of short fibre composites with arbitrary fibre orientation and fibre length distribution under any loading condition was derived, based on classical (micro-) mechanical theories. The model was verified using tensile data obtained on short fibre composites with different fibre contents and, for all cases, the predictions show to be within 10% of the measured values. The level of accuracy is therefore comparable to that observed in predictions of composite stiffness. The model can be employed in (3D) structural analysis in a way that is similar to that currently used for stiffness predictions. Due to the small fibre lengths (below $l_c$) of the composites studied in this chapter, the versatility of the model could not be evidentiated to its full extent. Thus, it was shown that the effect on the accuracy of taking into account fibre length distribution or length-dependent fibre strength instead of an average fibre length or constant fibre strength is negligible. Considering the ranges of fibre lengths generally found in injection moulded short fibre composites, this will very likely be the case for most practical situations.

## 5.6 REFERENCES

5-1. H.L. Cox, Brit. J. Appl. Phys., **3**, 72 (1952).

5-2. Th. Lacroix, B. Tilmans, R. Keunings, M. Desaeger, and I. Verpoest, Compos. Sci. Tech., **43**, 379 (1992).

5-3. A. Kelly, and W.R. Tyson, J. Mech. Phys. Solids, **13**, 329 (1965).

5-4. E.G. Stoner, Ph.D. dissertation, Dept. of Chemical Engineering, Clemson University, Clemson, SC (1991).

5-5. W.J. Padgett, S.D. Durham, A.M. Mason, *J. Compos. Mater.*, **29**, 1873 (1995).

5-6. J.P. Nunes, C.A. Bernardo, A.S. Pouzada, D.D. Edie, *J. Compos. Mater.*, **31**, 1758 (1997).

5-7. S.R. Doshi, and J.-M. Charrier, *Polym. Compos.*, **10**, 28 (1989).

5-8. I. Miller, J.E. Freud, and R.A. Johnson, *Probability and Statistics for Engineers*, 4th edition, Prentice-Hall, London, UK (1990).

5-9. W.J. Baxter, *Metallurgical Transactions*, **23A**, 3045 (1992).

5-10. S.W. Tsai, and E.M. Wu, *J. Compos. Mater.*, **5**, 58 (1971).

5-11. S.G. Advani, and C.L. Tucker III, *J. Rheol.*, **31**, 751 (1987).

5-12. P.H. Foss, J.P. Harris, J.F. O'Gara, L.P. Inzinna, E.W. Liang, C.M. Dunbar, C.L. Tucker III, and K.F. Heitzman, *SPE ANTEC Tech. Papers*, **42**, 501 (1996).

5-13. J.C. Halpin, and J.L. Kardos, *Polym. Eng. Sci.*, **16**, 344 (1976).

5-14. R.S. Bay, and C.L. Tucker III, *Polym. Eng. Sci.*, **32**, 240 (1992).

5-15. C.W. Camacho, C.L. Tucker III, S. Yalvaç, and R.L. McGee, *Polym. Compos.*, **11**, 229 (1990).

5-16. P.A. Templeton, *J. Reinf. Plast. Compos.*, **9**, 210 (1990).

5-17. A.T. Di Benedetto, and L. Nicolais, *Plast.*, **10**, 83 (1979).

# 6 MODELLING THE THERMOMECHANICAL PROPERTIES OF CARBON FIBRE-POLYPROPYLENE COMPOSITES[6]

## 6.1 INTRODUCTION

The objective of the present chapter is to derive the thermomechanical properties of the submicron VGCFs from the composite properties through 'inverse modelling', as referred to in Chapter 3, section 3.1. This implies using the micromechanical models that can predict the properties of short fibre composites as presented in the *Introduction* and in the previous chapter. These models are first validated and subsequently used to infer the properties of the fibres from those of the composite. The materials used to validate the models and to infer VGCF-properties are those already described in Chapters 4 and 5. The existing micromechanical models found in the literature (see *Introduction*) were applied to calculate the elastic modulus and CTE of the VGCFs. The newly derived model that predicts the strength of short fibre reinforced composites, described in the previous chapter, was also used in the determination of the fibre properties. The validity of the models was first tested on PP-PAN composites.

## 6.2 EXPERIMENTAL

### 6.2.1 Material characterisation

In Chapter 4 the PP-PAN and PP-VGCF composites had already been thermo-mechanically characterised. In addition also the PAN-fibre properties, fibre orientation distribution, fibre length distribution and fibre volume fractions were determined in Chapter 5.

Due to the small fibre size in the PP-VGCF composites, traditional determination of fibre properties cannot be applied. The work on a different type of longer VGCFs (diameters and lengths in the micrometre and centimetre range, respectively) as described in Chapters 1 and 2, has already revealed the large dependence of the properties on fibre shape, and the occurrence of a large number of fibre shapes. Overall, the properties showed a qualitative dependence similar to that observed with conventional carbon fibres. As processing conditions of the PP-VGCF composites were similar to those of the PP-PAN composites (see Chapter 4, section 4.2.1) and conventional measurement of the fibre orientation state in the PP-VGCF composites was not possible due to the fibre size, their fibre orientation was assumed to be equal to that measured in the PP-PAN composites. Possible errors due to this assumption have to be accounted for at a later stage. The fibre volume fractions of the PP-VGCF composites were determined by density measurements, in analogy to those described for the PP-PAN composites in Chapter 5, section 5.3.2.3. The fibre lengths of the VGCFs were determined by oxidising the composite in air at 400° C. SEM samples were prepared by first squeezing a glue dot onto an aluminium sample stub and then scraping it off with forceps to leave an area of adhesive so thin that fibres could not submerge in it. Next, a small wad of fibres held in a pair of forceps was scraped over the adhesive area to disperse and spread the individual fibres. Gold was then sputter-deposited on the stub to make it conductive. From micrographs of regions where the fibres were well dispersed, the lengths of at least 50 fibres were measured and averaged.

---

[6] Based on: F.W.J. van Hattum, C.A. Bernardo, J.C. Finegan, G.G. Tibbetts, R.L. Alig, and M.L. Lake, Polym. Compos., accepted for publication (1999).

### 6.2.2 Micromechanical modelling

Micromechanical models to predict stiffness and CTE of short fibre composites have already been successfully applied (6-1,6-2 and *Introduction*). In addition, in the previous chapter a model to predict strength in short fibre composites, following the same general method used for stiffness- and CTE-prediction, was derived and successfully applied. In the present work, these micromechanical models are used to predict the properties of the PP-PAN composites. The applicability of the models is verified by comparison with experimental data. Subsequently the models are used to infer the VGCF properties from the PP-VGCF composite properties.

## 6.3 RESULTS AND DISCUSSION

### 6.3.1 Validating the models

The experimental data obtained in Chapters 4 and 5 were used to model the PP-PAN composite properties. The test data used for modelling the properties are those given in Chapter 5, Table 5-4. From the properties of fibre and matrix shown in this table, stiffness, strength and CTE for the PP-PAN specimens in the flow direction were calculated using the methods described in (6-3), Chapter 5, section 5.2, and (6-2), respectively (see Appendices C and D). The predictions, together with the experimental values, are given in Table 6-1. As already shown in Chapter 5, the predicted values for strength and stiffness for the PP-PAN composites are within 10% of the experimental values. The CTE-predictions lead to greater discrepancies. These errors, however, are consistent with results found in work of other authors (6-2). The dependence of all composite properties on fibre volume fraction, as observed experimentally, is well described by the models, as can be seen from Figures 6-1 through 6-3, where the experimental and predicted properties for the PP-PAN composites are depicted.

*Table 6-1. Experimental and predicted values of the composite properties*

| | | PP-PAN 5% | PP-PAN 10% | PP-PAN 15% | PP-VGCF 5% | PP-VGCF 10% | PP-VGCF 15% |
|---|---|---|---|---|---|---|---|
| Strength (MPa) | *Experimental* | 36.6 | 42.6 | 49.7 | 40.3 | 46.5 | 48.5 |
| | *Predicted* | 35.0 | 45.2 | 51.4 | 37.4 | 47.0 | 52.2 |
| Modulus (MPa) | *Experimental* | 2821 | 4294 | 4591 | 2584 | 3466 | 3685 |
| | *Predicted* | 2777 | 4140 | 5043 | 2566 | 3531 | 4322 |
| CTE ($10^{-6}$/°C) | *Experimental* | 31.5 | 20.8 | 16.9 | 57.4 | 39.8 | 26.2 |
| | *Predicted* | 51.3 | 32.3 | 24.1 | 69.1 | 49.2 | 39.4 |
| Fibre volume fraction (%) | | 4.5 | 9.6 | 14.7 | 4.7 | 9.7 | 15.6 |
| Fibre length (μm) | | 161.7 | 148.3 | 161.3 | 3.8 | 3.8 | 3.8 |

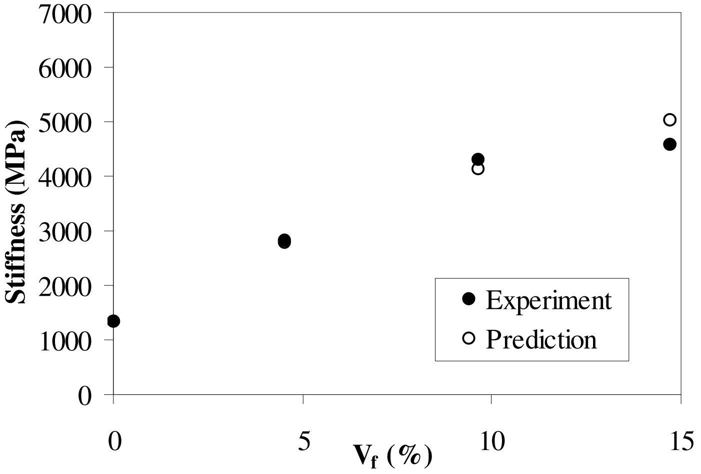

*Figure 6-1. Experimental and predicted modulus for the PP-PAN composites.*

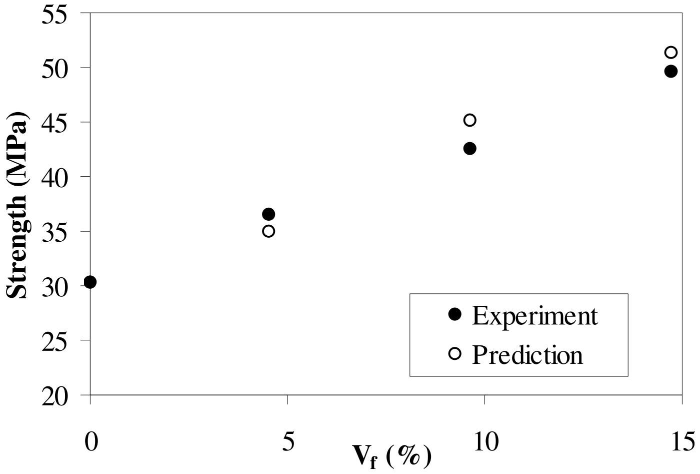

*Figure 6-2. Experimental and predicted strength for the PP-PAN composites.*

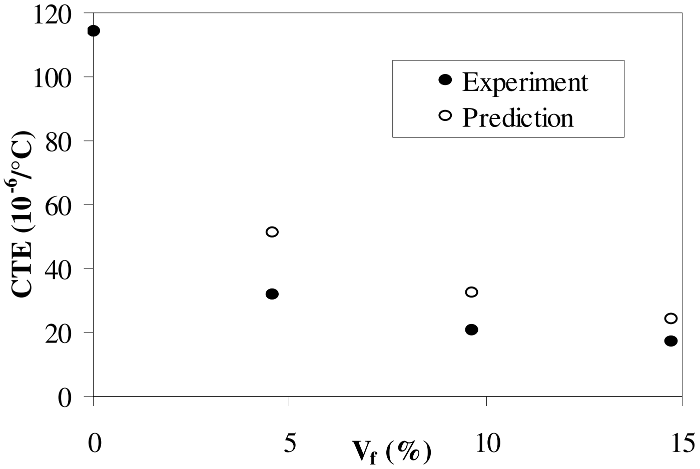

*Figure 6-3. Experimental and predicted CTE for the PP-PAN composites.*

### 6.3.2 Inverse modelling

Maintaining similar differences between experimental and predicted values as found for the predictions of the PP-PAN composite properties, the models are inversely applied to the PP-VGCF composites to derive the apparent stiffness and CTE of the VGCFs. In the previous chapter, it was shown that the interfacial shear strength rather than fibre strength, dominates composite strength, due to the short fibre lengths (see Chapter 5, section 5.4.5). In the PP-VGCF composites this should also be the case, considering the average fibre length found experimentally (see Table 6-1). Therefore it is impossible to derive an actual fibre strength value for the VGCFs. Instead, a normalised value for the apparent interfacial shear strength between VGCF and matrix can be obtained. This value gives the relation between the interfacial shear strength between fibre and matrix and the maximum attainable value for the composite.

It should be noted that, due to the simplifications made in applying the micromechanical models, strict conclusions cannot be drawn using this method. The method does, however, allow the derivation of the properties of a 'model fibre'. This ideal fibre, if used as reinforcement in a PP matrix, would lead to composite properties matching those of the PP-VGCF properties. In this way, the apparent properties of the VGCF can be determined, allowing comparison with conventional fibres.

Predictions as made for the PP-PAN composites, were also made for the PP-VGCF composites, only varying the input properties of the fibres. For each VGCF input property, the predicted results were compared with experimental data for the PP-VGCF composites. When the predictions were within the error margin found in the prediction of the PP-PAN composite properties, the VGCF input property was deemed correct. The experimental and predicted PP-VGCF composite properties are given in Table 6-1. The latter are only presented to indicate the error that is obtained when using the methodology described above. The apparent VGCF properties derived in this way are given in Table 6-2, together with the values for the PAN-fibres. For comparison, experimental values from the longer VGCFs characterised in Chapter 1 are shown, as well as typical values for E-glass fibres (6-4).

It can be observed that the stiffness of the submicron VGCF is significantly lower than that of the PAN-fibres and the longer VGCFs. The differences in stiffness between the two types of VGCFs are greater than could be expected from the simplifications accepted in the models. Two possible explanations can be envisaged: either the inherent stiffness of the submicron

VGCFs is lower, or the models become less accurate at very short (<10 μm) fibre lengths. Lower submicron VGCF properties, compared to PAN-fibres and 'long' VGCFs from Chapter 1 and 2, can be expected from the less ordered structure of these fibres resulting from their rapid growth (see *Introduction*). In addition to the lower stiffness, the calculated value of the CTE is also significantly higher than that of the PAN-fibres. This supports the former hypothesis of inherent lower submicron VGCF properties.

*Table 6-2. Apparent submicron VGCF fibre properties, compared with other fibres*

| | PAN | Submicron VGCF | Glass[1] | VGCF[2] |
|---|---|---|---|---|
| Modulus (GPa) | 218 | 50 | 75 | 140 |
| CTE ($10^{-6}$/°C) | -0.1 | 5 | 5 | - |
| Relative interfacial shear strength | 1 | 0.95 | - | - |

*[1] typical values for E glass fibres, from (6-4)*
*[2] experimental value for 'large' VGCFs, from Chapter 1*

However, it should be noted that the apparent interfacial shear strength derived for the PP-VGCF composites is close to the theoretical upper limit, as it was for the PP-PAN composites, thus implying good interfacial adhesion between VGCF and the PP-matrix.

This outcome is consistent with the trends observed in the comparison of the experimental results of PP-PAN and PP-VGCF, thus implying that the differences between composite properties is mainly a result of different fibre properties.

In spite of the limitations mentioned above, the results of the present work show that VGCFs have properties that are similar to those of the most common polymer reinforcements. In fact, the CTE and stiffness of VGCFs are similar or only slightly lower than that of glass fibres. This means that there is scope for their application as thermoplastic reinforcements, provided the polymer has adequate interfacial characteristics.

## 6.4 CONCLUSION

In the present work it has been shown that VGCF-thermoplastic composites can be produced, with strength and CTE that are competitive to those of 'conventional' PAN-fibre composites. Micromechanical models have been successfully applied to predict the strength and stiffness of PP-PAN composites. Modelling the CTE in the same way yielded slightly worse results.

The models were used to infer the apparent VGCF-properties. It was shown that the VGCFs, have a higher apparent CTE than that of PAN-fibres. The stiffness of the VGCFs is significantly lower. Although the fibre strength could not be calculated, derivation of the interfacial shear strength shows that the interfacial adhesion between VGCF and the PP matrix is comparable to that of PAN-fibres. The apparent properties of submicron-size VGCF are comparable to those of glass fibres. The differences found in the behaviour of the PP-PAN and PP-VGCF composites can probably be attributed to differences in the fibre properties.

## 6.5 REFERENCES

6-1. P.H. Foss, J.P. Harris, J.F. O'Gara, L.P. Inzinna, E.W. Liang, C.M. Dunbar, C.L. Tucker III, and K.F. Heitzman, *SPE ANTEC Tech. Papers*, **42**, 501 (1996).

6-2. C.W. Camacho, C.L. Tucker III, S. Yalvaç, and R.L. McGee, *Polym. Compos.*, **11**, 229 (1990).

6-3. S.G. Advani, and C.L. Tucker III, *J. Rheol.*, **31**, 751 (1987).

6-4. P.C. Powell, *Engineering with fibre-polymer laminates*, Chapman & Hall, London, UK, (1994).

# 7 GENERAL DISCUSSION

The research described in this thesis started with three main goals, as mentioned in the *Introduction*. First, to study systematically the different morphologies in which VGCFs can be produced and to evaluate their effect on the mechanical properties. Second, to develop know-how on the production of thermoplastic-VGCF composites. The determination of the mechanical properties of the composites allowed the assessment of VGCFs as reinforcements of thermoplastics. Finally, to develop micromechanical models to predict the more relevant mechanical properties of the materials produced. By using these models inversely, it was possible to derive the properties of the fibres. In the case of VGCFs with diameters below 1 μm (submicron VGCFs) this is the only way to determine these properties.

In each part of this thesis the investigation towards attaining one of the goals has been described. Therefore, in the text below, the conclusions of each part will be reviewed separately, the results discussed and future focussing areas suggested.

## 7.1 VAPOUR GROWN CARBON FIBRES

In the first part of this thesis the different morphologies in which VGCFs can be grown have been systematically studied and the dependence of the properties on the morphology quantified for the three more common morphologies. The first principal conclusion is that strength of VGCFs, unlike stiffness, is strongly dependent on the morphology of the fibres. Overall it was shown that stiffness and strength of VGCFs are considerably lower than those of conventional carbon fibres. Although the conclusions drawn are based on the three more common morphologies, one can reasonably expect that they will hold for other VGCF morphologies as well, as the different morphologies reflect the internal structure of the fibres which, on its turn, determines the properties of the fibres. This assumption is supported by the work of several authors, relating different properties of VGCFs to their graphitic structure (7-1,7-2). The continuation of the research initiated in this work into the other morphologies can therefore lead to a definite description of mechanical properties as a function of fibre morphology for VGCFs.

As the mechanical properties of the VGCFs are somewhat moderate, this focuses the interest on the thermal and electrical properties of these fibres. Research already done in this area can be found in the literature (see references 7-1, 7-2 and 7-3 and the *Introduction*), indicating that these properties are comparable or superior to ex-pitch carbon fibres, and superior to ex-PAN carbon fibres and glass fibres. Still, as was the case with the mechanical properties, no systematic study of the dependence of these properties on the morphology of VGCFs has been done. As both thermal and electrical properties are directly related to the internal structure of the fibre (7-4,7-5), reflected by their morphology, this research would result in a direct relation between them and the geometrical characteristics of VGCFs.

## 7.2 VAPOUR GROWN CARBON FIBRE THERMOPLASTIC COMPOSITES

In the second part of this thesis it was found that VGCF-thermoplastic composites can be easily produced with conventional technologies, provided the appropriate equipment is used. Furthermore, it was also shown that the processing of the composites was straightforward. This is a major advance towards a wider application of VGCFs in thermoplastic composites. Research into these composites so far has been limited to lab-scale production. As heretofore it had not been shown that these composites could be produced with the equipment available in industry, wider research of these fibres as possible competitors for conventional glass and carbon fibres has been limited (see *Introduction*). The results of the present research, however, open the way to a broader perspective into different applications of VGCFs.

Another conclusion is that the properties of the VGCF-thermoplastic composites produced are competitive with those of composites reinforced with conventional carbon fibres. Both strength and CTE are comparable to those of the conventional composites, whereas stiffness is still lower. The present research, however, has shown an improvement in performance of the VGCF-thermoplastic composites by systematically studying the different factors that determine it. Control of these factors was shown to lead to a significant improvement of the properties of the composites. As also the production of VGCFs is continuously being improved (7-6,7-7), it can reasonably be expected that this line of progress will continue. Although the apparent interfacial strength in the PP-VGCF composites was already adequate, in other fibre-matrix combinations both improved fibre surface treatment and sizing, enhance the mechanical properties. Also further post-treatment of the fibres, like debulking, may allow the production of better VGCF-thermoplastic composites.

Reasonable mechanical properties and potential low-cost production, combined with high thermal and electrical properties, also makes VGCF an interesting competitor to glass-fibres as reinforcement for thermoplastic composites. Very limited research in this area can be found in the literature (7-8,7-9), although possible thermal and electrical applications of these composites are known (7-2,7-9,7-10). The investigation of the thermal and electrical properties of VGCFs and their composites remains, thus, a major challenge for the near future. In fact, as a result of the current research, a new project, focussing on the thermal and electrical properties of VGCF-composites, has already been started in co-operation with the Department of Physics at the University of Minho (7-11).

## 7.3 MICROMECHANICAL MODELLING

In the third part of this thesis it was shown that it is possible to predict, within acceptable limits, the thermomechanical properties of short fibre reinforced plastics (SFRPs). Complementing existing micromechanical models to predict stiffness and CTE, a new, generally applicable model has been developed in the present research, that allows the prediction of strength. Although the models presented herein have the required accuracy, further improvements can be sought in several areas. As explained before, a wider range of composites, having different fibre lengths and fibre-matrix combinations, should be made to further use the models to their full extent. Apart from that, the importance of different ways of length-averaging (7-12), the influence of the various theories for the prediction of unidirectional properties (7-13,7-14) and the performance of different closure approximations for the orientation tensors (7-15) should be investigated. As has been shown, in most SFRPs the interfacial shear strength between fibre and matrix determines to a great extent the final composite strength. As determination of this property is complicated and the results subject to debate, detailed research into this property will be essential.

As indicated above, thermal and electrical properties of VGCF- and other SFRPs are of increasing interest. Furthermore, thermal and mechanical properties of carbon fibres are known to be directly related to their mechanical properties (7-4,7-5) and also the modelling of their composites' mechanical and thermal properties is similar (7-16,7-17,7-18). Extension of the modelling described above to the area of thermal and electrical property prediction is therefore justified. This area will be further investigated as part of the previously mentioned project in co-operation with the Department of Physics.

The general character of the models makes them very useful for application in structural analysis of moulded parts. The modelling work presented herein allows the development of the desired link between property predictions, solely using numerical programs, and practice. Ultimately this would result in an extremely useful design tool, allowing property prediction of injection moulded SFRP parts at a very early stage. This would save time and money by avoiding trial-and-error and allowing the designer to work closer to the material limits. As a result of the present research, a project aimed at the development of such a tool has also been started at the Polymer Engineering Department.

Finally, it was concluded, by inversely applying the micromechancial models discussed above, that the stiffness of submicron VGCFs is lower than that of conventional carbon fibres, whereas the CTE is higher. Although the fibre strength could not be derived, derivation of the interfacial shear strength shows that the interfacial adhesion between VGCF and the thermoplastic matrix is comparable to that of conventional carbon fibres. The difference in properties between the conventional carbon fibre composites and the VGCF-composites can be attributed to the differences in fibre properties. However, the interest of this way of deriving properties could be improved if it was possible to use an accurate way of measuring the fibre orientation of VGCF-thermoplastic composites. Another interesting conclusion is that the properties of submicron-size VGCF are, at least, as good as those of glass fibres. This again emphasises the potential of VGCFs as competitors for glass fibres, given their superior thermal and electrical conductivity.

## 7.4 REFERENCES

7-1. J. Heremans, _Carbon_, **23**, 431 (1985).

7-2. G.G. Tibbetts, in _Carbon Fibers, Filaments and Composites_, ed. J.L. Figueiredo, C.A. Bernardo, R.T.K. Baker and K.J. Huttinger, Kluwer Academic Publishers, Dordrecht, 73 (1990).

7-3. J. Heremans, and C.P. Beetz, Jr., _Phys. Rev. B_, **32**, 1981 (1985).

7-4. J.G. Lavin, D.R. Boyington, J. Lahijani, B. Nysten, and J.-P. Issi, _Carbon_, **31**, 1001 (1993).

7-5. B. Nysten, L. Piraux, and J.-P. Issi, in *Thermal Conductivity, Proceedings of 19th ITCC*, ed. D.W. Yarbrough, Plenum Press, New York, 341 (1987).

7-6. R. Alig, and J. Ting, in *Proceedings European Conference on Carbon*, Newcastle, UK, July 491, 1996.

7-7. H. Darmstadt, C. Roy, S. Kaliaguine, J.-M. Ting, and R.L. Alig, *Carbon*, **36**, 1183 (1998).

7-8. J.-M. Ting, and M.L. Lake, Carbon, **33**, 663 (1995).

7-9. C.J. Dasch, W.J. Baxter, and G.G. Tibbetts, in *Extended abstracts of 21st Biennial Conference on Carbon*, ed. American Carbon Society, Buffalo, NY, 82 (1993).

7-10. B. Miller, in *Plastics World*, 73, Sept. 1996.

7-11. F.J. Macedo, J.A. Ferreira, F.W.J. van Hattum, and C.A. Bernardo, *J. Mat. Proc. Tech.*, accepted for publication (1998).

7-12. S.R. Doshi, and J.-M. Charrier, *Polym. Compos.*, **10**, 28 (1989).

7-13. G.P. Tandon, and G.J. Weng, *Polym. Compos.*, **5**, 327 (1984).

7-14. H.L. Cox, *Brit. J. Appl. Phys.*, **3**, 72 (1952).

7-15. J.S. Cintra, Jr., and C.L. Tucker III, *J. Rheol.*, **39**, 1095 (1995).

7-16. D.M. Bigg, *Polym. Compos.*, **7**, 125 (1986).

7-17. R.C. Progelhof, J.L. Throne, and R.R. Ruetsch, *Polym. Eng. Sci.*, **16**, 615 (1976).

7-18. L.E. Nielsen, *Ind. Eng. Chem. Fundam.*, **13**, 17 (1974).

---

# 8 CONCLUSIONS

---

The conclusions that can be drawn from the research presented in this thesis are summarised below.

## **Part I** *Vapour Grown Carbon Fibres*

The study of the diverse morphologies in which VGCFs can be produced and their effect on the fibre properties led to the following conclusions:

*1)* VGCF tensile data can be obtained and treated using the same methodologies that are standard for the conventional ex-PAN and ex-pitch carbon fibres.

*2)* The Weibull distribution function is a good statistical tool to describe the tensile strength data of VGCFs.

*3)* The fibre tensile modulus decreases with fibre diameter irrespective of the morphology.

*4)* The fibre tensile strength decreases with both fibre diameter and fibre length irrespective of the morphology.

*5)* The fibre tensile modulus is not significantly influenced by the fibre morphology.

*6)* VGCFs with morphologies different from perfect cylinders have a lower tensile strength. This difference may result however from pure geometrical considerations, and not from differences in the inner structure of the fibre.

*7)* Stiffness and strength of VGCFs are considerably lower than those of conventional carbon fibres.

*8)* The fragmentation test cannot be used to assess the interfacial properties of VGCFs, irrespective of the morphology.

## **Part II** *Vapour Grown Carbon Fibre Thermoplastic Composites*

From the study into the production, processing and characterisation of thermoplastic-VGCF composites the following conclusions can be drawn:

*9)* VGCF thermoplastic composites can be produced and processed using conventional thermoplastic processing technologies.

*10)* VGCF-thermoplastic composites can be produced that have strength and CTE comparable with those of conventional PAN-fibre composites; the stiffness, however, is lower.

## **Part III** *Micromechancial Modelling*

The study into micromechanical modelling of the properties of short fibre composites and the 'inverse-modelling' derivation of the submicron VGCF properties has shown that:

*11)* For the present materials, micromechanical models can predict stiffness and strength of short fibre composites within 10% of the experimental values, provided that accurate fibre and matrix material data are available.

*12)* The application of similar models to predict the CTE of short fibre composites leads to greater discrepancies.

*13)* The dependence of stiffness, strength and CTE on fibre volume fraction is well described by the micromechanical models.

*14)* The effect on the accuracy of taking into account fibre length distribution or length-dependent fibre strength instead of an average fibre length or constant fibre strength is negligible when modelling the strength of short fibre composites.

*15)* The strength of injection moulded short fibre composites is dominated not by the fibre tensile strength but by the interfacial shear strength between fibre and matrix.

*16)* The models are accurate enough to infer the apparent submicron VGCF properties from their composites.

*17)* Submicron VGCFs show apparent interfacial shear strength comparable to that of PAN-fibres, lower stiffness and higher CTE.

*18)* The apparent stiffness and CTE of submicron VGCF are comparable to those of glass fibres.

*19)* The difference between conventional carbon fibre- and VGCF-thermoplastic composites can be attributed to difference in fibre properties.

# 9 RECOMMENDATIONS

From the results of the research presented in this thesis and the general discussion presented in Chapter 7, the following future work can be recommended:

*1)* To study the effect of the morphology on VGCF mechanical properties using the morphologies not studied in this work.

*2)* To study the thermal and electrical properties of VGCFs and relate these to the morphologies.

*3)* To continue the study of the application of VGCFs in thermoplastic composites using different matrices.

*4)* To study the thermal and electrical properties of VGCF-thermoplastic composites.

*5)* To study the properties of VGCF-thermoplastic composites, comparatively to those of glass-fibre reinforced composites.

*6)* To extend the use of the micromechanical models for property prediction of short fibre composites to a wider range of composites having different fibre lengths and fibre-matrix combinations.

*7)* To refine micromechanical models by investigating the influence of different ways of length-averaging and different theories for unidirectional property prediction.

*8)* To investigate the performance of different closure approximations for the orientation tensors in micromechanical modelling.

*9)* To develop similar models for prediction of thermal and electrical properties.

*10)* To apply the models in structural analysis of short fibre composites.

*11)* To develop a link between numerical programs for flow-simulation and structural analysis of short fibre composites.

*12)* To investigate possibilities of fibre orientation measurement in submicron VGCF-thermoplastic composites.

# Appendices

# APPENDIX A SPECIMEN GEOMETRY

In Chapter 3 of this thesis, several specimen geometries have been used. The different dimensions of these specimens are described below. Specimens 1 through 3 were moulded on the conventional Klockner injection moulding machine at the University of Minho, specimen 4 on the SCORIM injection moulding machine at Brunel University in England.

### *1. Circular tensile specimen*

The tensile specimens described in section 3.3.2 (both with as-grown VGCF and carbon black (CB), results presented in Figures 3-2 and 3-4), are dogbone-shaped, 60 mm length with a parallel section of 20 mm long and a circular cross-section of 1.5 mm diameter. This small cross-section was used to create high shear stresses during moulding, thus inducing fibre orientation and therefore improving mechanical properties. A schematic of the specimen is given in Figure A-1.

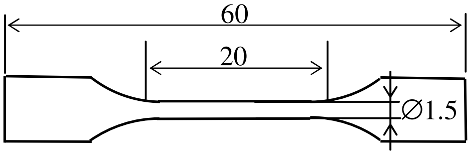

*Figure A-1. Schematic of the circular tensile specimen*

### *2. Impact specimen*

The Charpy notched impact specimens described in section 3.3.2 (both with as-grown VGCF and CB, results presented in Figures 3-2 and 3-4) and section 3.3.3 (both with as-grown and treated VGCF, results presented in Table 3-4) are derived from ASTM standard D256. They have a length of 45 mm, a rectangular cross-section of 6.5 x 4 mm with a 2 mm notch moulded in. A schematic of the specimen is given in Figure A-2.

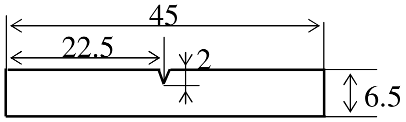

*Figure A-2. Schematic of the impact specimen*

### 3. Square tensile specimen

The tensile specimens described in section 3.3.3 (both with as-grown and treated VGCF, results presented in Table 3-4) are derived from ASTM standard D638M. They are dogbone-shaped with a parallel section of 15 mm and a rectangular cross-section of 2x4 mm. A schematic of the specimen is given in Figure A-3. Only this type of specimen has been used in the experiments described from Chapter 4 onwards.

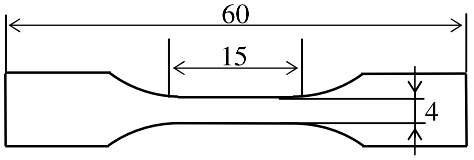

*Figure A-3. Schematic of the square tensile specimen*

### 4. SCORIM specimen

The SCORIM specimens (with as-grown VGCF only) described in section 3.3.4 (results presented in Table 3-5) are dogbone shaped, 80 mm long with a parallel section of 30 mm long and a circular cross-section of 5 mm diameter. For the impact testing, a 2 mm notch was machined in the middle of the specimen. A schematic of the specimen is given in Figure A-4.

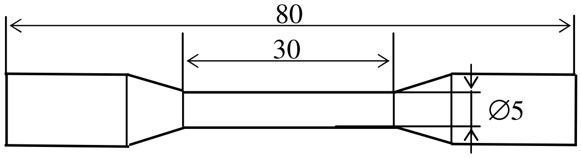

*Figure A-4. Schematic of the SCORIM specimen*

# APPENDIX B CHARACTERISTIC TEST CURVES

For the different composite materials used in this thesis, the characteristic tensile stress-strain curves are plotted below. In Figure B-1, the stress-strain curve for unfilled PC and PC reinforced with 20% VGCFs (Chapter 3) are given. In Figures B-2 and B-3 the stress-strain curves for the PP-matrix composites are given (Chapters 4 through 6). Figure B-2 presents the curves for the PP-PAN composites with 0, 5, 10 and 15 vol.% fibres, respectively. Figure B-3 shows the same curves for the PP-VGCF composites with 0, 5, 10 and 15 vol.% fibres.

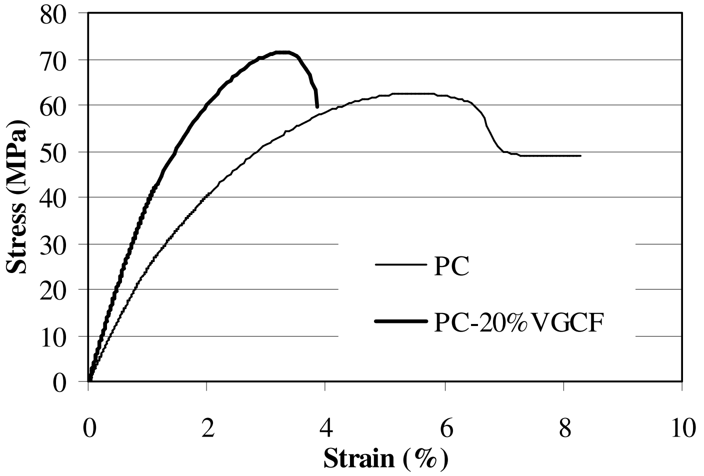

*Figure B-1. PC-VGCF stress-strain curves*

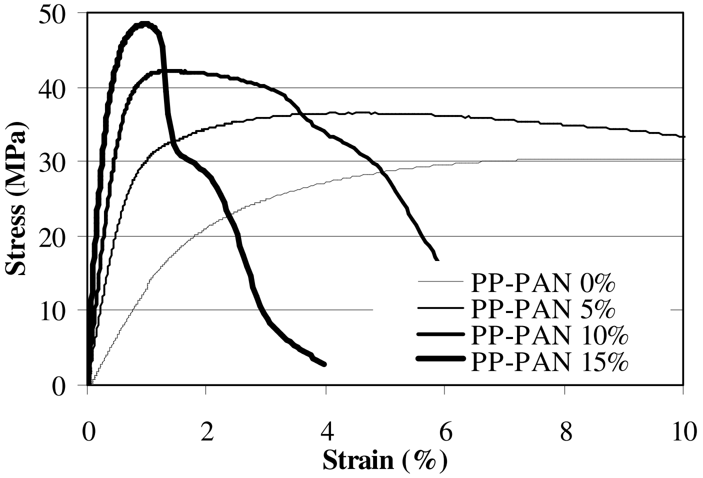

*Figure B-2. PP-PAN stress-strain curves*

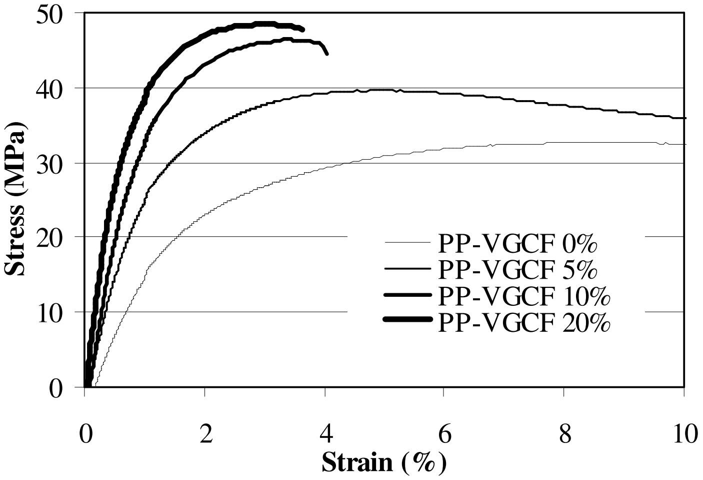

*Figure B-3. PP-VGCF stress-strain curves*

# APPENDIX C HALPIN-TSAI AND HALPIN-SCHAPERY EQUATIONS

## HALPIN-TSAI EQUATIONS

Halpin and Tsai (5-13) derived expressions for the elastic constants of a short-fibre composite. The common form of these expressions is:

$$\frac{P}{P_m} = \frac{1+\zeta\eta V_f}{1-\eta V_f} \qquad \textit{with} \qquad \eta = \frac{(P_f / P_m) - 1}{(P_f / P_m) + \zeta} \tag{C.1}$$

where $P$ is the composite modulus, $P_f$ and $P_m$ are the corresponding moduli of the fibre and matrix, respectively, and $\zeta$ is a parameter that depends on the particular property being considered. The values of the parameters used in equation [C.1] are given in Table C-1 (5-13,I-52).

*Table C-1. Halpin-Tsai parameters used in equation [C.1].*

| $P$ | $P_f$ | $P_m$ | $\zeta$ | Description |
|---|---|---|---|---|
| $E_{11}$ | $E_f$ | $E_m$ | $2(l/d)$ | Longitudinal modulus |
| $E_{22}$ | $E_f$ | $E_m$ | $2$ | Transverse modulus |
| $G_{12}$ | $G_f$ | $G_m$ | $1$ | Longitudinal shear modulus |
| $G_{23}$ | $G_f$ | $G_m$ | $\frac{K_m/G_m}{(K_m/G_m+2)}$ | Transverse shear modulus[1] |
| $\nu_{12}$ | $= \nu_f V_f + \nu_m(1-V_f)$ | | | Poisson ratio |
| $G_{f/m}$ | $= \frac{E_{f/m}}{2(1+\nu_{f/m})}$ | | | Fibre/matrix shear modulus |
| $K_m$ | $= \frac{E_m}{3(1-2\nu_m)}$ | | | Matrix bulk modulus |

[1] *See (5-11)*

The parameters thus calculated can be substituted into the compliance tensor $S_{ij}$ (in contracted form) for a transversely isotropic material with the 1-axis being axis of symmetry and isotropy in the 2-3-plane (i.c. the unidirectionally aligned short fibre composite), given in equation [C.2]:

$$S_{ij} = \begin{pmatrix} \frac{1}{E_{11}} & \frac{-\nu_{12}}{E_{11}} & \frac{-\nu_{12}}{E_{11}} & 0 & 0 & 0 \\ \frac{-\nu_{12}}{E_{11}} & \frac{1}{E_{22}} & \frac{-\nu_{23}}{E_{22}} & 0 & 0 & 0 \\ \frac{-\nu_{12}}{E_{11}} & \frac{-\nu_{23}}{E_{22}} & \frac{1}{E_{22}} & 0 & 0 & 0 \\ 0 & 0 & 0 & \frac{2}{E_{22}}(1+\nu_{23}) & 0 & 0 \\ 0 & 0 & 0 & 0 & \frac{1}{G_{12}} & 0 \\ 0 & 0 & 0 & 0 & 0 & \frac{1}{G_{12}} \end{pmatrix} \quad \textit{[C.2]}$$

where $\nu_{23} = \frac{E_{22}}{2G_{23}} - 1$. $S_{ij}$ can then be inverted to obtain the stiffness tensor $C_{ij}$.

## HALPIN-SCHAPERY EQUATIONS

Using the relations derived by Schapery (I-51), Halpin (I-52) developed expressions for the coefficient of thermal expansion (CTE) in the longitudinal ($\alpha_l$) and transverse direction ($\alpha_2$) of a short fibre composite, that are given by:

$$\alpha_1 = \bar{\alpha} + \left( \frac{\overline{E\alpha}}{\bar{E}} - \bar{\alpha} \right) \frac{\left( \frac{1}{E_L} - \frac{1}{E_{11}} \right)}{\left( \frac{1}{E_L} - \frac{1}{E_V} \right)}$$

$$\alpha_2 = (1+\nu_m)(1-V_f)\alpha_m + (1+\nu_f)V_f\alpha_f - \alpha_1(\nu_f V_f + \nu_m(1-V_f)) \quad \textit{[C.3]}$$

where $1/E_L = V_f/E_f + (1-V_f)/E_m$; $E_V = V_f E_f + (1-V_f)E_m$ with the upper bars representing volume averages: i.e. $\bar{\alpha} = \alpha_f V_f + \alpha_m(1-V_f)$. Here, $E_f$ and $E_m$ are the moduli, $\alpha_f$ and $\alpha_m$ the CTE's and $\nu_f$ and $\nu_m$ the Poisson's ratios of the fibre and matrix respectively. $E_{11}$ is the modulus in the longitudinal direction as given by the Halpin-Tsai equations above. $\alpha_l$, from equation [C.3], is midway between the upper and lower bounds derived by Schapery, wheras $\alpha_2$ is equivalent to Schapery's relation.

The parameters thus calculated can be substituted into the thermal expansion tensor $\alpha_{ij}$ for a transversely isotropic material with the 1-axis being axis of symmetry and isotropy in the 2-3-plane (i.c., the unidirectionally aligned short fibre composite) given in equation [C.4]:

$$\alpha_{ij} = \begin{pmatrix} \alpha_1 & 0 & 0 \\ 0 & \alpha_2 & 0 \\ 0 & 0 & \alpha_2 \end{pmatrix} \qquad [C.4]$$

# APPENDIX D ORIENTATION AVERAGING

Consider the 2nd and 4th order unidirectional property tensors, $T_{ij}$ and $T_{ijkl}$, of a transversely isotropic material with the unit vector **p** (see equation [5.19] and Figure 5-1) as the axis of symmetry. The 2nd and 4th order fibre orientation tensors $a_{ij}$ and $a_{ijkl}$ are defined according to equation [5.20]. Based on these assumptions, Advani and Tucker (5-11) have shown that the orientation averages $<T_{ij}>$ of the 2nd order and $<T_{ijkl}>$ of the 4th order unidirectional property tensors are given by:

$$< T_{ij} >= A_1 a_{ij} + A_2 \delta_{ij}$$

$$\begin{aligned} < T_{ijkl} >= {} & B_1 (a_{ijkl}) \\ & + B_2 (a_{ij} \delta_{kl} + a_{kl} \delta_{ij}) \\ & + B_3 (a_{ik} \delta_{jl} + a_{il} \delta_{jk} + a_{jl} \delta_{ik} + a_{jk} \delta_{il}) \\ & + B_4 (\delta_{ij} \delta_{kl}) \\ & + B_5 (\delta_{ik} \delta_{jl} + \delta_{il} \delta_{jk}) \end{aligned} \qquad [D.1]$$

where the *A*'s and *B*'s are related to the elements of the unidirectional property tensors.

In the case of the unidirectional stiffness tensor $C_{ij}$ (in contracted notation) from equation [C.2], the orientation average $<C_{ij}>$ is given directly by equation [D.1], with the *B*'s related to the elements of $C_{ij}$ according to:

$$\begin{aligned} B_1 &= C_{11} + C_{22} - 2C_{12} - 4C_{66} \\ B_2 &= C_{12} - C_{23} \\ B_3 &= C_{66} + \tfrac{1}{2}(C_{23} - C_{22}) \\ B_4 &= C_{23} \\ B_5 &= \tfrac{1}{2}(C_{22} - C_{23}) \end{aligned} \qquad [D.2]$$

Similarly, for the unidirectional strength tensor $G_{ij}$ from equation [5.16] (see also equation [5.22]), the orientation average $<G_{ij}>$ is determined directly from equation [D.1]. The *B*'s are now given by:

$$\begin{aligned} B_1 &= G_{11} + G_{22} - 2G_{12} - 4G_{66} \\ B_2 &= G_{12} - G_{23} \\ B_3 &= G_{66} + \tfrac{1}{2}(G_{23} - G_{22}) \\ B_4 &= G_{23} \\ B_5 &= \tfrac{1}{2}(G_{22} - G_{23}) \end{aligned} \tag{D.3}$$

In the case of the Coefficient of Thermal Expansion (CTE) the stress $\sigma_{ij}$ in an element oriented in the direction of **p** (5-15) can be obtained from:

$$\sigma_{ij}(\mathbf{p}) = C_{ijkl}(\mathbf{p})\varepsilon_{kl} - C_{ijkl}(\mathbf{p})\alpha_{kl}(\mathbf{p})\Delta T \tag{D.4}$$

where $C_{ijkl}(\boldsymbol{p})$ is the unidirectional stiffness tensor (in index notation) and $\alpha_{kl}(\boldsymbol{p})$ the unidirectional thermal expansion tensor in the direction of $\boldsymbol{p}$. The average stress now is:

$$\begin{aligned} <\sigma_{ij}> &= < C_{ijkl}(\mathbf{p})\varepsilon_{kl}> - < C_{ijkl}(\mathbf{p})\alpha_{kl}(\mathbf{p})\Delta T > \\ &= < C_{ijkl} > \varepsilon_{kl} - < C_{ijkl}\alpha_{kl} > \Delta T \end{aligned} \tag{D.5}$$

It can be shown that the stiffness of the composite is given by the orientation averaged stiffness tensor $<C_{ijkl}>$ (in index notation) and the thermal expansion coefficients of the composite are given by:

$$\alpha_{ij}(composite) = < C_{ijkl}\alpha_{kl} >< C_{ijkl} >^{-1} \tag{D.6}$$

where $<C_{ijkl}>^{-1}$ is the inverse of the orientation averaged stiffness tensor $<C_{ijkl}>$. $<C_{ijkl}>$ can be derived as indicated above by combining equations [D.1] and [D.2]. Furthermore, from equation [D.1]:

$$< C_{ijkl}\alpha_{kl} > = D_1 a_{ij} + D_2\delta_{ij} \tag{D.7}$$

where (I-56):

$$\begin{aligned} D_1 &= A_1(B_1 + B_2 + 4B_3 + 2B_5) + A_2(B_1 + 3B_2 + 4B_3) \\ D_2 &= A_1(B_2 + B_4) + A_2(B_2 + 3B_4 + 2B_5) \end{aligned} \tag{D.8}$$

where the $B$'s are related to the elements of $<C_{ijkl}>$ and thus given by equation [D.2] and the $A$'s can be derived by applying equation [D.1] to the thermal expansion tensor of equation [C.4]:

$$\begin{aligned} A_1 &= \alpha_1 - \alpha_2 \\ A_2 &= \alpha_2 \end{aligned} \tag{D.9}$$

Thus, by substituting equations [D.7] through [D.9] into equation [D.6] the orientation averaged CTE's are obtained.